






<b>Report's title</b>	
Ductility limits of high strength steels	
<b>Customer, contact person, address</b>	<b>Order reference</b>
Digital, Internet, Materials & Engineering Co-Creation (DIMECC)	BSA P2 SP2 Task 4
<b>Project name</b>	<b>Project number/Short name</b>
Virtual testing lab for novel materials and products	104679-1.2.3 / VILMA
<b>Author(s)</b>	<b>Pages</b>
Petr Hradil, Asko Talja	93/
<b>Keywords</b>	<b>Report identification code</b>
steel, FEM, true stress-strain, ductility, diffuse necking	VTT-R-04741-16
<b>Summary</b>	
<p>The research outcomes presented in this report serve as background information for two conference papers attached as Appendix E and Appendix F of this report.</p> <p>The virtual testing tools developed in VILMA project and presented in this report were used to provide insight into the basic questions whether the Eurocode's material requirements are correct or not, could they be eased or not, and how much they could be eased.</p> <p>The automated method of obtaining true stress-strain material model from coupon tests is introduced in this report for the purpose of numerical evaluation of material behaviour in details with high localized strains and possible diffuse necking. The method is validated against experiments.</p> <p>Two parametric studies are presented to evaluate the validity of Eurocode's ductility criteria. The hypothetical material models used in the studies cover wide range of common structural steels, but are focused especially on new high strength grades.</p> <p>Two alternative ductility criteria proposals are also presented and evaluated. One is based on the prescribed minimum "necking capacity" rather than elongation at failure and the second assumes that the load in coupon tests shall decrease at least to the level of yield strength after necking.</p>	
<b>Confidentiality</b>	Public
Espoo 10.3.2017	
<b>Written by</b>	<b>Reviewed by</b>
	
Petr Hradil Senior Scientist	Ludovic Fülöp Principal scientist
<b>Accepted by</b>	
	
Edgar Bohner Research Team Leader	
<b>VTT's contact address</b>	
P.O. Box 1000, FI-02044 VTT, Finland	
<b>Distribution</b>	
Online at FIMECC Research Portal and VTT webpage	
<p><i>The use of the name of the VTT Technical Research Centre of Finland (VTT) in advertising or publication in part of this report is only permissible with written authorisation from the VTT Technical Research Centre of Finland.</i></p>	

## Preface

---

This report is updated public version of the research report VTT-R-02599-15 “Ductility limits of high strength steels” produced for the Finnish Metals and Engineering Competence Cluster (FIMECC) in 2015. FIMECC became part of Digital, Internet, Materials & Engineering Co-Creation (DIMECC) in 2016.

The report is part of DIMECC program BSA - Breakthrough steels and applications (2014-2018) and its project P2: Design beyond present codes – enabling efficient utilisation of new materials. The project is industry-driven and is based on critical future needs of steel end-users (market pull). The overall goal of BSA program is to enable a renewal of the Finnish metal and engineering industries through major improvements in their offerings and global competitiveness brought about by the intelligent use of novel advanced steel products. Key emphasis is on end-users in selected business areas: bionergy, power generation, mining, lifting, handling and transport, offshore and marine, waste recycling, arctic technologies and processing industry

(<http://www.dimecc.com/dimecc-services/bsa-breakthrough-steels-applications/>).

The report belongs to Subproject SP2 Task 4 “BSA P2 SP2 Task 4: Virtual testing lab for novel materials and products”, called VILMA 2014–2016. The main research objective of VILMA is to propose an efficient virtual testing platform for a fast and effective introduction of new steels and steel products to the market. The main practical objective is to use the platform to develop recommendations of the material ductility requirements in the Eurocodes for high strength steels.

The results presented in this report serve as background information for the future studies of ductility requirements in different design situations within VILMA.

BSA P2 SP2 Task 4 (VILMA) task group consist of Jyrki Kesti from Ruukki Construction, Jussi Minkkinen from SSAB, Petri Ongelin from TRY, and Asko Talja, Ludovic Fülöp, Juha Kurkela and Petr Hradil from VTT. The authors wish to thank the industry members who have been active in planning and supervising the work.

Espoo 10.3.2017

Authors

## Contents

---

Symbols .....	4
1. Introduction .....	6
1.1 General objectives of VILMA project .....	6
1.2 Ductility limits in standards .....	7
1.3 Tension properties of structural steels .....	8
1.4 Limit state criteria in FE modelling .....	9
1.5 Ductile Failure Criteria .....	9
1.5.1 Triaxiality .....	10
1.5.2 SMCS fracture model .....	11
1.5.3 Maximal shear stress criterion .....	13
1.5.4 Modified Mohr-Coulomb (MMC) fracture model .....	14
1.6 Plastic strain–triaxiality damage data .....	15
2. Stress-strain characterization .....	19
2.1 Background .....	20
2.2 True stress-strain curves for Abaqus models .....	22
2.3 Verification of true stress-strain material models .....	26
3. Strain limits for FEM modelling .....	30
3.1 Simple limits for equivalent plastic strain .....	30
3.2 Evaluation of proposed strain limits .....	32
3.3 The effect of mesh size .....	36
4. Preliminary numerical study .....	38
4.1 Material model parameters .....	39
4.2 True stress-strain curves .....	40
4.3 Maximum plastic strain and stress triaxiality .....	42
4.4 Evaluation of Eurocode ductility criteria .....	44
4.5 Alternative ductility criteria .....	46
5. Final parametric study .....	49
5.1 Material model parameters .....	49
5.2 Evaluation of Eurocode ductility criteria .....	50
5.3 Alternative ductility criteria .....	57
6. Summary and conclusions .....	59
6.1 Ductility limits .....	59
6.2 Strain limits for FEM modelling .....	59
6.3 Numerical studies .....	60
References .....	62
Annex A: Strain concentration in CHT specimens .....	64
Annex B: Simplified material models .....	67
Annex C: The upper limit of ultimate strain .....	70
Annex D: CHT simulations of simplified material models .....	72
Annex E: True stress-strain relationship for finite element simulations of structural details under diffuse necking .....	76
Annex F: Ductility requirements for structural details with stress concentration and diffuse necking .....	86

## Symbols

---

$A$	cross-sectional area
$A_0$	initial cross-sectional area
$A_g$	percentage of non-proportional elongation at maximum load (also called uniform plastic elongation before necking $\varepsilon_{u,pl}$ )
$A_{gt}$	percentage of total elongation at maximum load (also called ultimate elongation $\varepsilon_u$ )
$A_t$	percentage of total elongation at fracture: total elongation (elastic elongation plus plastic elongation) of the gauge length at the moment of fracture, expressed as a percentage of the original gauge length $L_0$ (also called as total elongation at failure $\varepsilon_f$ )
$A_{xx}$	percentage permanent elongation after fracture: Permanent elongation of the gauge length after fracture ( $L_u - L_0$ ), expressed as a percentage of the original gauge length $L_0$ (also called plastic elongation at failure $\varepsilon_{f,pl}$ ); the value is presented as A5 elongation when gauge length $L_0=5.65 \sqrt{A}$ ; if different gauge length is used, the length is presented by subscript, for example $A_{50}$ means gauge length 50 mm
$A_{pl}$	cross-sectional area based on the assumption of pure plastic deformation
$C$	Hollomon's coefficient
$c_1, c_2$	parameters of MMC model
$e$	Napier's constant ( $\approx 2.7183$ )
$E$	modulus of elasticity (Young's modulus)
$f$	material parameter of Hooputra's model
$f_y$	upper yield strength or 0.2% offset proof stress
$f_u$	ultimate tensile strength corresponding to the maximum force
$K$	Ramberg-Osgood's coefficient
$k_s$	material parameter of Hooputra's model
$L$	gauge length
$\Delta L$	change of the gauge length during the loading (referred as displacement)
$\Delta L_{M(FE)}$	measured (or calculated) displacement
$L_0$	initial gauge length
$L_{pl}$	gauge length based on the assumption of pure plastic deformation
$m$	Hollomon's exponent
$n$	Ramberg-Osgood's exponent
$P$	axial load
$P_{M(FE)}$	measured (or calculated) axial load
$r, r_{lim}$	calculation error and its maximum value
$R$	radius of the notch/hole
$T$	stress triaxiality
$\alpha$	toughness parameter of SMCS fracture model
$\varepsilon$	engineering strain
$\varepsilon_1, \varepsilon_2, \varepsilon_3$	principal plastic (true) strains
$\varepsilon_{cr}$	predicted critical strain (true equivalent plastic)
$\varepsilon_{eq}$	equivalent plastic (true) strain

$\varepsilon_{eq,ed}$	equivalent plastic (true) strain at the outer edge of specimen
$\varepsilon_{eq,f(R,10,15)}$	equivalent strain at failure (or yield load after necking, 10% and 15% elongation)
$\varepsilon_{f(R,10,15)}$	engineering strain at failure (or yield load after necking, 10% and 15% elongation)
$\varepsilon_{pl}$	plastic engineering strain
$\varepsilon_{pl,u}$	ultimate (uniform) plastic engineering strain
$\varepsilon_R$	limit engineering strain at yield load after necking
$\varepsilon_t$	true (logarithmic) strain
$\varepsilon_{t,pl}$	plastic true (logarithmic) strain
$\varepsilon_{t,pl,u}$	ultimate (uniform) plastic true (logarithmic) strain
$\varepsilon_y$	engineering yield strain ( $f_y/E$ )
$\varepsilon_u$	ultimate (uniform) engineering strain
$\nu$	Poisson's ratio
$\sigma$	engineering stress
$\sigma_1, \sigma_2, \sigma_3$	principal (true) stresses
$\sigma_h$	hydrostatic stress
$\sigma_m$	von Mises stress
$\sigma_n$	normal stress
$\sigma_t$	true stress
$\sigma_{t,100}$	true stress at 100% true plastic strain
$\sigma_{t,pl}$	true stress based on the assumption of pure plastic deformation
$\sigma_u$	ultimate (uniform) engineering stress
$\tau$	shear stress
$\theta$	Normalized Lode angle
$\Theta, \Theta^+, \Theta^-$	shear stress parameters of Hooputra model
$\theta_L$	Lode angle



## 1. Introduction

### 1.1 General objectives of VILMA project

The presented studies are part of project “Virtual testing lab for novel materials and products” (VILMA). The project aims to ensure that structural design is not an obstacle to use novel steels in current and in future applications. Structural design codes are lagging behind today’s needs, often unable to follow the advances in computing. The introduction of new materials and semi-finished products requires permanent review of the existing design rules. Usually the validation of the design rules is made by very laborious laboratory tests. This project utilizes cost-effective virtual testing methods, which replace extensive and expensive structural testing. However, also some experiments are needed for validation of the models.

The use of virtual testing in VILMA is focused on statically loaded connections of structural elements. In particular, the study includes the new high strength steels in their applications. Steel grades higher than S460 and up to S700 are covered by Eurocode 3, Parts 1 [1] and 12 [2], but some of requirements ( $f_u \geq 1,05f_y$ ,  $\epsilon_u \geq 15f_y/E$ ,  $A_5 \geq 10\%$ ) are very conservative and hard to fulfil. The grade S960 is not yet implemented in Eurocodes. The requirements are also not completely justified with physical background but they are rather based on the best available engineering judgment at the moment.

The local stresses exceed yield stress  $f_y$  in details of many practical applications (such as plastic design or connections). The strain levels can be even higher than  $\epsilon_u$ , and therefore the knowledge of full stress-strain curve and failure criterion is needed in simulation of tests. It should be noted that the failure can be initiated in lower strains than in coupon tests in some cases, because the failure initiation depends both on stresses and strains.

The main research objective of the project is to propose an efficient virtual testing platform for fast and effective introduction of new structural steels and steel products to the market. The main practical objective is to use the platform to develop recommendation for the material ductility requirements in the Eurocodes for high strength steels (Figure 1).

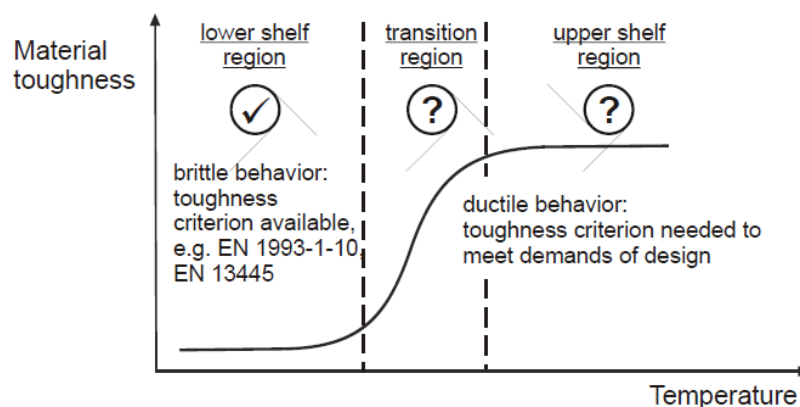


Figure 1. Toughness-temperature-curve of steel and lack of verified assessment criteria [3].

The project aims to give answers to the questions:

- 1) What should be the ductility requirements in Eurocodes for tension parts of the cross-section?
  - Which plastic strains do structural details tolerate?
  - Do the new materials comply with the design equations?
  - How are the ductility criteria related to the design approach?

- 2) What kind of guidance can be given for structural engineer?
- How the failure can be estimated?
  - How the details should be modelled?

## 1.2 Ductility limits in standards

Ductility is defined as a measure of a material's ability to undergo plastic deformation before fracture [4]. It may be expressed as percent elongation or percent area reduction from a tensile test. Ductility is required in the forming process but also needed for plastic redistribution of stress in members and connections, where stress concentration would occur.

Ductility limits (at upper shelf region) are usually in standards based on the ratio  $f_u/f_y$ ,  $\epsilon_u/\epsilon_y$  or the elongation at failure (Table 1, Figure 2). The ductility requirements in Eurocodes are based on gauge length  $L_0=5.65 \sqrt{A}$ , according to EN 10002-1 [5].

Table 1. Ductility limits for structural carbon steel in the design codes.

Standard	$f_u/f_y$	$\epsilon_u$ <sup>1)</sup>	Elongation at failure	Note
EN 1993-1-1	$\geq 1.10$	$\geq 15 \epsilon_y$	$\geq 15\%$	S235-S460
EN 1993-1-12	$\geq 1.05$	$\geq 15 \epsilon_y$	$\geq 10\%$	S460-S700
EN 1992-1-1 [6] (rebar)	$\geq 1.08$ $\geq 1.05$	$\geq 2,5\%$ $\geq 5,0\%$		S400-S600, Class A Class B, no plastic analysis
ANSI/AISC 360-05	$\geq 1.25$			
AISI S100-2007 AS/NZS 4600:2005	$\geq 1.08$		$\geq 10\%$ (50mm gauge) $\geq 7\%$ (200 mm gauge)	Cold-formed steel

<sup>1)</sup>  $\epsilon_y=f_y/E$  ( $15 \epsilon_y = 2.9\%$  for S400 and  $4.3\%$  for S600)

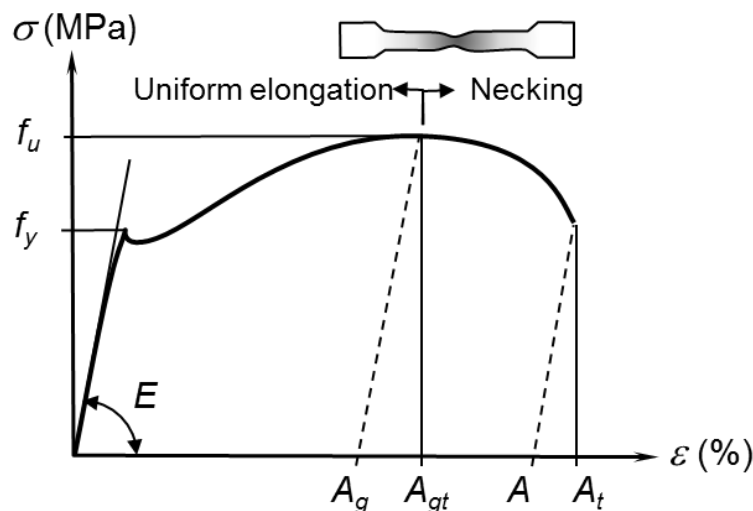


Figure 2. Material testing according to EN 10002-1.

Important is to note that because of the localized deformation at necking, the gauge length used in testing affects the elongation at failure expressed in percent (the measured



engineering strain). The shorter the gauge length is the larger is the percent elongation. Therefore some researchers have proposed different criteria for localized and uniform elongation. For example Dhalla and Winter [7] have suggested that the minimum localized elongation shall be at least 20% in a 12.7 mm gauge length for low-ductility steels in cold-formed members. In addition, the uniform plastic elongation ( $A_g$ ) shall be at least 3% in a 76.2 mm gauge length and  $f_u/f_y$  shall be at least 1.05. They have concluded that these requirements are enough to redistribute the stresses in the plastic range to avoid premature brittle fracture and to achieve full net section strength in a tension member.

### 1.3 Tension properties of structural steels

Material properties shown in Table 2 and Figure 3 illustrate the differences of the material behaviour of normal and high strength steels. High strength steels have lower  $f_u/f_y$  ratio and lower elongation at failure than normal steels. Figure 3 shows also that high strength steels have low uniform plastic elongation at maximum force. It indicates that material strain-hardening is low, therefore necking starts at lower strains and the plastic deformations in necking are more localized. The special care is required in both the control of deformations and detailing to avoid notches and other stress concentrations (EN 1993-1-12).

Table 2. Tension properties of structural steels.

Grade	$f_u/f_y$	Elongation at failure	Note
S235	$\geq 1.53$	$\geq 24\%$ ( $L_0=5.65 \sqrt{A}$ )	EN 10025-2:2004
S275	$\geq 1.49$	$\geq 21\%$ ( $L_0=5.65 \sqrt{A}$ )	EN 10025-2:2004
S355	$\geq 1.32$	$\geq 20\%$ ( $L_0=5.65 \sqrt{A}$ )	EN 10025-2:2004
S460MC	$\geq 1.13$	$\geq 17\%$ ( $L_0=5.65 \sqrt{A}$ )	EN 10149-2:2013
S700MC	$\geq 1.07$	$\geq 12\%$ ( $L_0=5.65 \sqrt{A}$ )	EN 10149-2:2013
S960MC	$\geq 1.02$	$\geq 7\%$ ( $L_0=5.65 \sqrt{A}$ )	EN 10149-2:2013
S960 Q	$\geq 1.02$	$\geq 10\%$ ( $L_0=5.65 \sqrt{A}$ )	EN 10025-6 :2004
ASTM A36	$\geq 1.76$	$\geq 19-23\%$ (50mm gauge) $\geq 20\%$ (200 mm gauge)	$f_y =250$ MPa
ASTM A529	$\geq 1.43$	$\geq 19\%$	$f_y =290$ MPa
ASTM A441		$\geq 21\%$ (50mm gauge) $\geq 18\%$ (200 mm gauge)	$f_y \geq 275$ MPa, HSS
ASTM A588		$\geq 21\%$ (50mm gauge) $\geq 18\%$ (200 mm gauge)	$f_y \geq 435$ MPa, HSS
ASTM A517		$\geq 16-18\%$ (50mm gauge)	$f_y \geq 620$ MPa, QT HSS

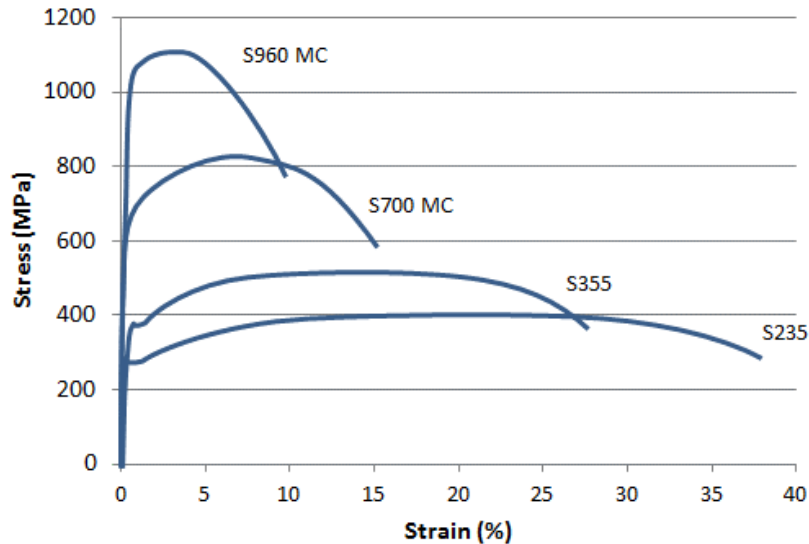


Figure 3. Typical stress strain behaviour of structural steels.

## 1.4 Limit state criteria in FE modelling

Informative Annex C of EN 1993-1-5 (plated structural elements) [8] gives guidance in using non-linear FE-methods for determining elastic-plastic resistance in ULS. There is also given criterion for the ultimate limit state. The principal membrane strain is limited to 5% in regions subjected to tensile stresses. Also other criteria may be used, e.g. attainment of the yielding criterion or limitation of the yielding zone. EN 1993-1-12 [2] mentions that the global analysis using non-linear plastic analysis considering partial plastification of members in plastic zones only, applies for steels of grades than S460 up to S700.

In EN 1993-1-6 [9] (Shell Structures) plastic limit state (LS1) is based on von Mises equivalent plastic strain and the limit is  $\varepsilon_{mps} = 50 (f_y/E)$ . Cyclic plasticity limit state (LS2) the value of the total accumulated von Mises equivalent plastic strain is  $\varepsilon_{p,eq,Ed} = 25 (f_y/E)$ . For example  $25 \times (f_y/E) = 4.2\%$  for S355 and  $5.5\%$  for S460.

In normative Annex B of EN 13445-3 [10] (pressure vessels) the principal structural strains are limited to 5 %.

As a summary it can be concluded that at least for steel strength S460 or less, a usual plastic strain limit in EN standards is about 5%. However, some difference relates to the fact which plastic strains are used in the criterion. The equivalent plastic strain  $\varepsilon_{eq}$  is defined as

$$\varepsilon_{eq} = \frac{\sqrt{2}}{3} \sqrt{(\varepsilon_1 - \varepsilon_2)^2 + (\varepsilon_1 - \varepsilon_3)^2 + (\varepsilon_2 - \varepsilon_3)^2} \quad (1)$$

where  $\varepsilon_1$ ,  $\varepsilon_2$  and  $\varepsilon_3$  denote the principal plastic strains. For example  $\varepsilon_{eq} = 0.67 \varepsilon_1$ , for the case  $\varepsilon_2 = \varepsilon_3 = 0$ , and  $\varepsilon_{eq} = 1.33 \varepsilon_1$  for the case  $\varepsilon_2 = \varepsilon_3 = -\varepsilon_1$ .

## 1.5 Ductile Failure Criteria

Prediction of ductile fracture is important in evaluating performance of structural components and connections, when large local deformations must be accommodated before the design resistance is achieved. Fracture is generally distinguished between brittle and ductile mechanisms, where brittle mechanisms are characterized by transgranular cleavage and ductile mechanisms involve localized yielding and growth of microvoids.

Ductile fracture is usually identified as the fracture initiating event in structural steel members subjected to high plastic strains. The ductile fracture initiation is a multistep and multiscale process. Factors that can influence material failure include, for example, the current states of stress and strain, the loading history, the strain rate, the temperature and the properties of the material.

This study uses macroscopic ductile failure criteria in ductile fracture initiation, and they are describing ductile fracture of crack-free details under large deformations. They are often used for structural details where sharp stress concentrations do not exist, as is the case in stress concentrations around bolt hole, welded connections or localized yielding in steel beams and braces. Traditional fracture mechanics methods, which require indefinitely sharp cracks, are best suitable for cracks due to fatigue or welding.

### 1.5.1 Triaxiality

Fracture initiation depends on the state of stress and hardening properties of the material. The stress state is generally measured by stress triaxiality

$$T = \sigma_h / \sigma_m \quad (2)$$

where  $\sigma_h$  is the hydrostatic stress and  $\sigma_m$  is von Mises stress. Based on principal stresses  $\sigma_1 \geq \sigma_2 \geq \sigma_3$ ,

$$\sigma_h = (\sigma_1 + \sigma_2 + \sigma_3) / 3 \text{ and } \sigma_m = \frac{1}{\sqrt{2}} \sqrt{(\sigma_1 - \sigma_2)^2 + (\sigma_1 - \sigma_3)^2 + (\sigma_2 - \sigma_3)^2} \quad (3)$$

Examples of triaxialities for elastic plane stress conditions are given in Table 3. It should be noted that under plastic deformations triaxiality is usually not constant, and it depends on the shape and size of the material deformations.

Table 3. Triaxialities of different plane stress conditions.

Stress state	Principal stresses	$\sigma_h$	$\sigma_m$	$T$
Uniaxial tension	$\sigma_1 > 0, \sigma_2 = \sigma_3 = 0$	$\sigma_1 / 3$	$\sigma_1$	$1/3$
Plane strain tension	$\sigma_2 = \sigma_1 / 2, \sigma_3 = 0$	$\sigma_1 / 2$	$\sqrt{3} \sigma_1 / 2$	$1/\sqrt{3}$
Equibiaxial tension	$\sigma_2 = \sigma_1, \sigma_3 = 0$	$2 \sigma_1 / 3$	$\sigma_1$	$2/3$
Equibiaxial compression (Pure shear)	$\sigma_2 = -\sigma_1, \sigma_3 = 0$	0	$\sigma_1 / 3$	0
Uniaxial compression	$\sigma_1 < 0, \sigma_2 = \sigma_3 = 0$	$-\sigma_1 / 3$	$ \sigma_1  / 3$	$-1/3$

Based on the results of FEM calculations for structural details [3], it was found that usually  $T < 1.0$  with average value of  $T = 0.5$ . For beam-column connections and stiffened profiles (Figure 4) in bending  $T$  was 0.3–0.5. For plate details the values were more widespread.

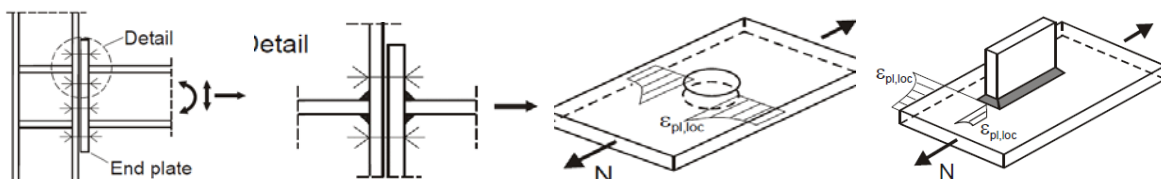


Figure 4. Typical structural details [3].

### 1.5.2 SMCS fracture model

SMCS (Stress Modified Critical Strain model) is the simplest and possibly most used ductile failure criterion. It is a macroscopic failure criterion and assumes that the critical equivalent plastic strain at failure  $\varepsilon_{cr}$  is exponentially dependent on the stress triaxiality  $T$  [11].

$$\varepsilon_{eq} > \varepsilon_{cr} = \alpha \cdot e^{-1.5T} \quad (4)$$

The exponent of 1.5 used commonly in the void growth expression. It is based on theoretical derivations by Rice and Tracey [12]. Researchers have suggested also other values of 1.1–2.3 for steels [11].

The toughness parameter  $\alpha$  is usually calibrated based on tests made for smooth-notched CNT specimens and complementary FEM analyses of the tested specimens. FEM analysis is used for finding the stresses and strains, corresponding to the critical displacement at tested failure (Figure 5). Then the calculated critical equivalent plastic strain  $\varepsilon_p^{critical}$  and stress triaxiality  $T$  are substituted into the SMCS fracture model, from where the critical toughness parameter  $\alpha$  can be backcalculated. Certainly FEM analysis needs also the true stress – true strain curve of the material.

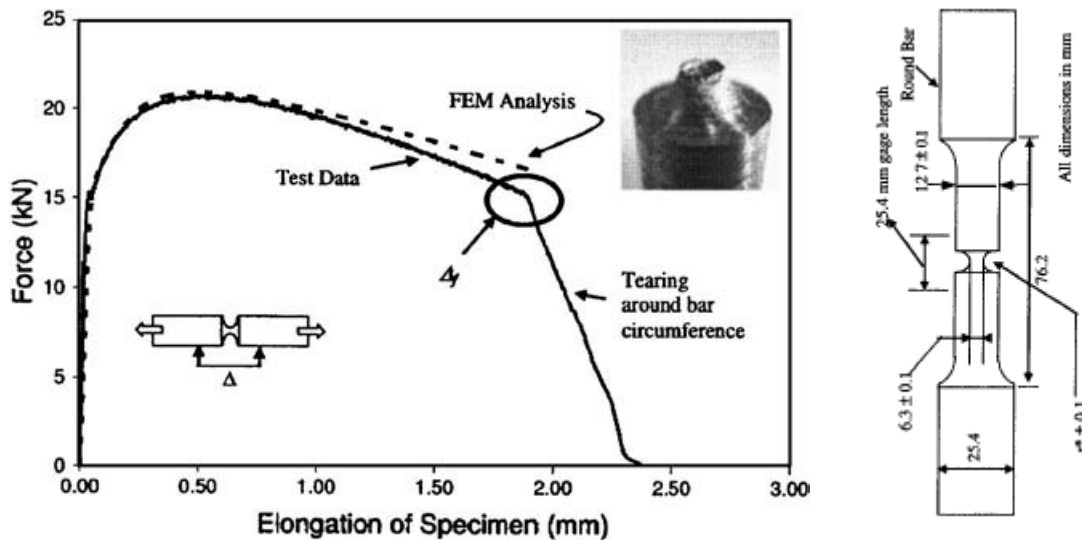


Figure 5. Analytical and experimental load displacement curves for CNT specimens [11].

Often the toughness parameter for steels is in range of 1–5 (Table 4). Then, depending on the material grade, the critical plastic strain can be 25–100%, if the triaxiality is less than 1, (Figure 6). The  $\alpha$  parameter depends on the steel producer and especially on Charpy V impact energy at ductile fracture zone. There strong relationship between  $\alpha$  and ASTM E23 upper-shelf Charpy V impact energy was observed [13] (Figure 7).

Table 4. Examples of measured toughness parameters according to [13].

Steel grade and nominal $f_y$ (MPa)	Measured $f_y$ (MPa)	Measured $f_u$ (MPa)	Parameter $\alpha$	CVN upper shelf (J)
A572-Grade 50 (345) from flange	420	490	2.6	254
A572-Grade 50 (345) from plate	390	590	1.12	146
A514-Grade 110 (760)	800	850	1.5	144
HPS70W (480)	590	690	2.9	278
JIS-SN490B (345)	340	470	2.9	211
JIS-SM490YBTMC-5L (345)	410	510	4.7	332
JIS-SN490B (345)	330	510	4.2	327

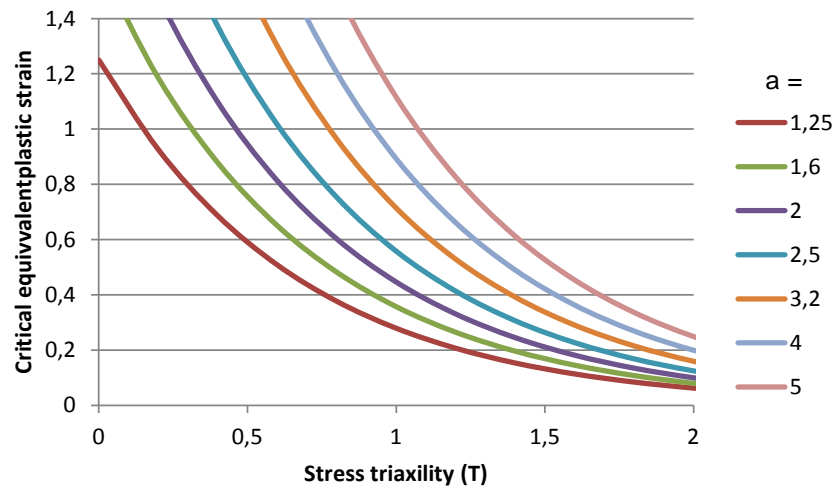


Figure 6. Critical plastic strains in SMCS fracture model.

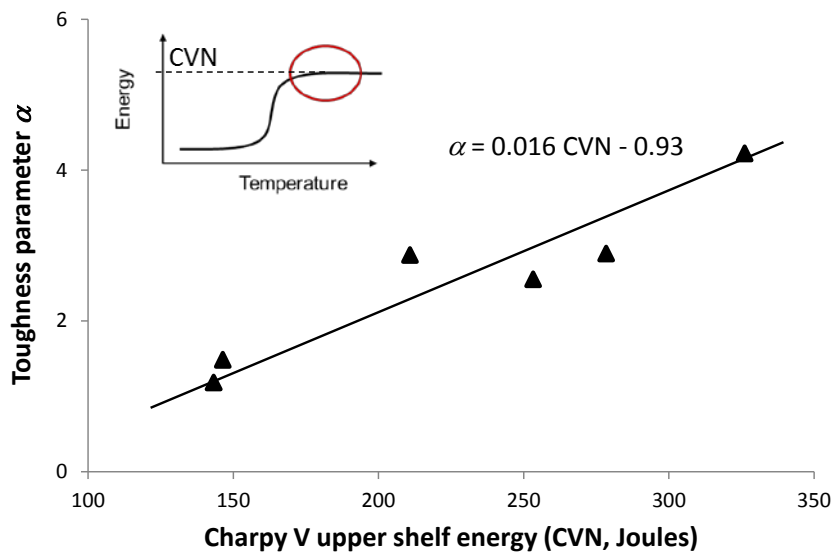


Figure 7. Relationship between toughness parameter and impact energy values [13].

The SMCS has been shown to make accurate fracture predictions for many practical conditions, such as the necked ligament between bolt holes, the necked cross section of an unnotched cylindrical bar, structural moment connection, or circumferential notch tensile (CNT)

specimen. In these cases, fracture typically initiates internally, where the stress triaxiality is relatively high ( $T > 0.75$ ) and then propagates outwards towards the surface of the material. However, there are other situations where fracture may initiate on the surface of the material, where triaxiality is typically lower ( $T = 0.33 - 0.75$ ), and then propagates inward. Fracture initiation on the surface has been observed for example in large scale tests on structural braces and column base plate tests [13].

### 1.5.3 Maximal shear stress criterion

At low stress triaxialities fracture due to void formation may develop as a combination of shear and void growth modes (Figure 8). A typical shear failure case is a notched tube under torque.

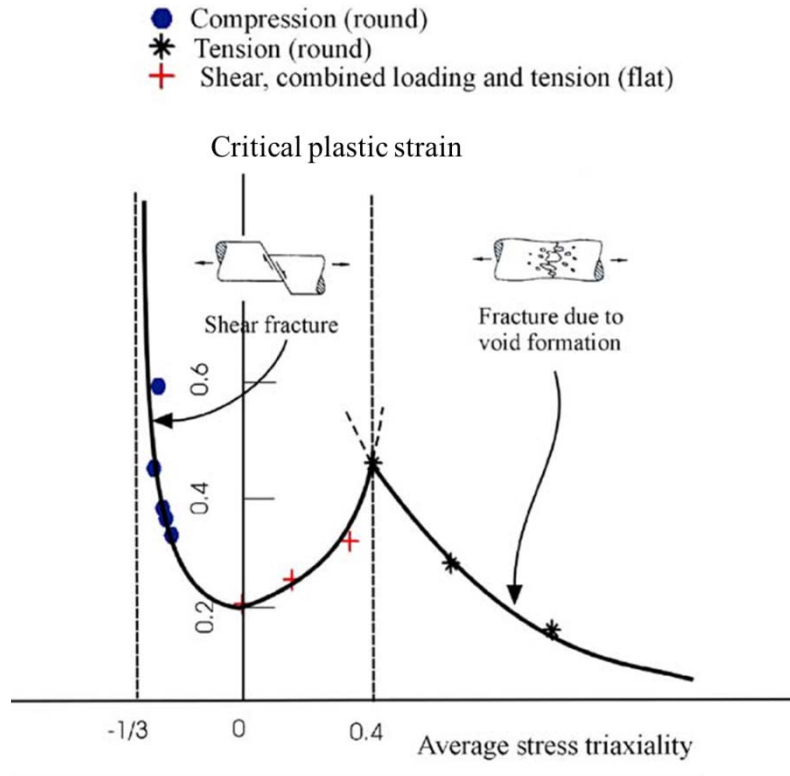


Figure 8. At low stress triaxialities shear fracture mode is dominating [14].

In shear fracture model proposed by Hooputra et al. [15], critical equivalent plastic strain at fracture is function of shear stress parameter  $\Theta$ , which is defined by

$$\Theta = \frac{1 - k_s T}{\phi} = \frac{\sigma_m - k_s \sigma_h}{\tau_{max}} \quad (5)$$

where  $T$  is stress triaxiality,  $\phi = \tau_{max}/\sigma_m = (\sigma_1 - \sigma_3)/(2\sigma_m)$  is ratio of maximum shear stress to von Mises stress and  $k_s$  is a material parameter. Critical equivalent plastic strain for shear fracture is determined by

$$\varepsilon_{cr, shear} = \frac{\varepsilon_{eq}^+ \sinh[f \cdot (\Theta - \Theta^-)] - \varepsilon_{eq}^- \sinh[f \cdot (\Theta^+ - \Theta)]}{\sinh[f \cdot (\Theta^+ - \Theta^-)]} \quad (6)$$

where  $\Theta^+ = 2 - 4k_s$  and  $\Theta^- = 2 + 4k_s$  are shear stress parameters for equibiaxial tension/compression,  $\varepsilon_{eq}^+$  and  $\varepsilon_{eq}^-$  are equivalent plastic strains in equibiaxial tension/compression at shear fracture and  $f$  is a material parameter. For determining the shear fracture parameters, the tensile tests with grooved specimen (rectangular cross section, groove depth = half sheet thickness) under  $45^\circ$  to loading direction ( $\Theta = 1.469$ ), specially

shaped shear specimens with a groove parallel to the loading direction (pure shear with  $\Theta = 1.732$ ) and biaxial tension tests ( $\Theta = 1.6$ ) have been used.

#### 1.5.4 Modified Mohr-Coulomb (MMC) fracture model

In modified Mohr-Coulomb (MMC) [16] fracture model the original M-C method is transformed and extended to three-dimensional coordinate system, where in addition to the usual equivalent plastic strain and stress triaxiality, there is a third parameter called normalized Lode angle parameter  $\theta$ . Lode angle  $\theta_L$  ranges between  $-30^\circ$  and  $30^\circ$  and depends on the size of principal stresses  $\sigma_1 \geq \sigma_2 \geq \sigma_3$  [17] and can be defined from equation

$$\tan(\theta_L) = \frac{\mu}{\sqrt{3}}, \quad \mu = \frac{2\sigma_3 - \sigma_1 - \sigma_2}{\sigma_1 - \sigma_2} \quad (7)$$

In MMC criterion Mohr–Coulomb the fracture occurs when the combination of normal stress  $\sigma_n$  and shear stress  $\tau$  reach a critical value, according to

$$\tau + c_1 \cdot \sigma_n \geq c_2 \quad (8)$$

where material constant  $c_1$  is dimensionless and  $c_2 \geq 0$  is maximal shear resistance is in MPa. The constant  $c_1$  is often referred to as a “friction” coefficient. In the limiting case of  $c_1 = 0$ , the M–C criterion reduces to the maximal shear stress criterion.

The M–C criterion is extended and modified so that the critical equivalent plastic strain at failure  $\varepsilon_p^{critical}$  can be calculated based on triaxiality and normalized Lode angle parameter  $\theta$  ( $-1 \leq \theta \leq 1$ ). If von Mises yield function is used,

$$\varepsilon_{cr} = \left\{ \frac{C}{c_2} \left[ \frac{\sqrt{1 + c_1^2}}{3} \cos\left(\frac{\theta\pi}{6}\right) + c_1 \left( T + \frac{1}{3} \sin\left(\frac{\theta\pi}{6}\right) \right) \right] \right\}^{-\frac{1}{m}} \quad (9)$$

Normalized Lode angle parameter  $\theta = 1$  for the axisymmetric tension,  $\theta = 0$  for the generalized shear (or plastic plane strain) loading condition, and  $\theta = -1$  for the axisymmetric compression or equibiaxial tension.

The model has 4 material parameters ( $C, m, c_1, c_2$ ). Parameters are  $C$  and  $m$  define material strain hardening, which can be calibrated from curve fitting of the stress–strain curve using power function (see Equation (16)). At least five type of test specimens (Figure 7), including FEM analyses, are needed for calibration of the parameters: (a) dog-bone specimen ( $T \approx 0.4$  and  $\theta \approx 1.0$ ), (b) flat specimen with cut-outs ( $T \approx 0.5$  and  $\theta \approx 0.5$ ), (c) punch test ( $T \approx 0.7$  and  $\theta = -0.9$ ), (d) butterfly specimen in tension ( $T \approx 0.6$  and  $\theta = 0$ ) and (e) butterfly specimen in simple shear ( $T \approx 0$  and  $\theta = 0$ ).



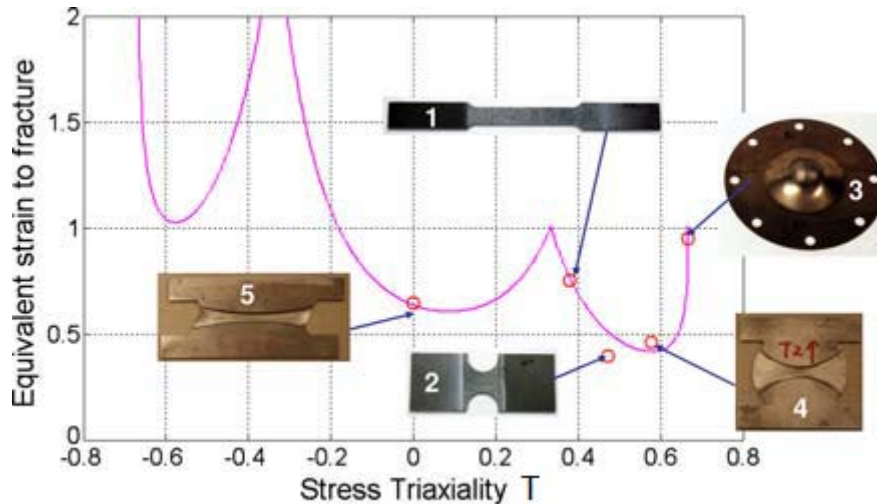


Figure 9. Calibration of MMC model for a TRIP RA-K40/70 (TRIP690) sheet, based on MMC fracture model. TRIP steel is a high-strength steel typically used in the automotive industry (nominal  $f_u = 690$  MPa,  $C = 1275.9$  MPa,  $m = 0.2655$ ,  $c_2 = 720$  MPa,  $c_1 = 0.12$ ) [16].

There exist also many other fracture models, e.g. Modified Gurson Model [18] [19]. A good review of other macroscopic ductile failure criteria is presented by Sandia National Laboratories [20]. In Sandia report there is also mentioned that analysts must be aware that a significant gap exists between the leading edge of research and the use of failure models in practical applications. Also, experts in the field believe that significantly more research is necessary before ductile failure can be reliably predicted in everyday engineering analysis. As is often the case, however, applied engineering and design require the use of models that, although they may not be entirely accurate, provide at least some realistic estimate of the load levels that are likely to induce failure in a structure. This insight can then be used to suggest appropriate testing and to recommend design margins.

## 1.6 Plastic strain–triaxiality damage data

Based on notched test results on earlier presented Table 4 and  $T = 1$  the critical plastic strain can be 30–100%, depending on the steel grade and manufacturer. Critical strain for A514-Grade 110 ( $f_y = 800$  MPa,  $f_u = 850$  MPa,  $A_{50} \geq 16\%$ ) is about 30% and for HPS 70W ( $f_y = 590$  MPa,  $f_u = 690$  MPa,  $A_{50} \geq 19\%$ ) about 70%.

In PLASTOTOUGH project, two damage curves have been derived for the profile material of the large scale tests. These two damage curves (PL) are given in Figure 10 together with several damage curves given in the literature. It can be seen in that the damage curves of one steel grade is somehow wide spread. Taking e.g. all steels S355J2 for a stress triaxiality  $T = 1.0$  the strain requirements 0.82, 0.57 and 0.44 are given. The derived critical plastic strain for steel is at least 20%, if the triaxiality is less than 1.0.

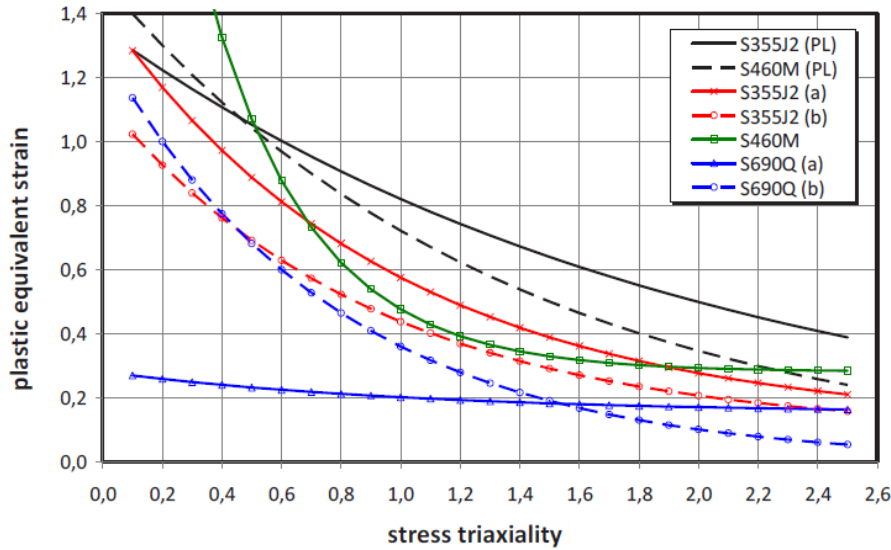


Figure 10. Damage curves from PLASTOTOUGH project [3].

Figure 11 shows damage curves for two materials, Weldox 420 ( $f_y = 415$  MPa,  $f_u = 525$  MPa,  $A_5 \geq 19\%$ ) and Weldox 960 ( $f_y = 996$  MPa,  $f_u = 1051$  MPa,  $A_5 \geq 12\%$ ) [21]. The former material is a hot rolled medium-strength steel and the latter is a quenched and annealed high-strength steel. The tests were performed on circumferentially double notched tube specimens subjected to a combination of tensile and torsional loading (Figure 12). The results show that critical plastic strain for  $T < 1$  is at least about 40% Weldox 460 and 20% for Weldox 960.

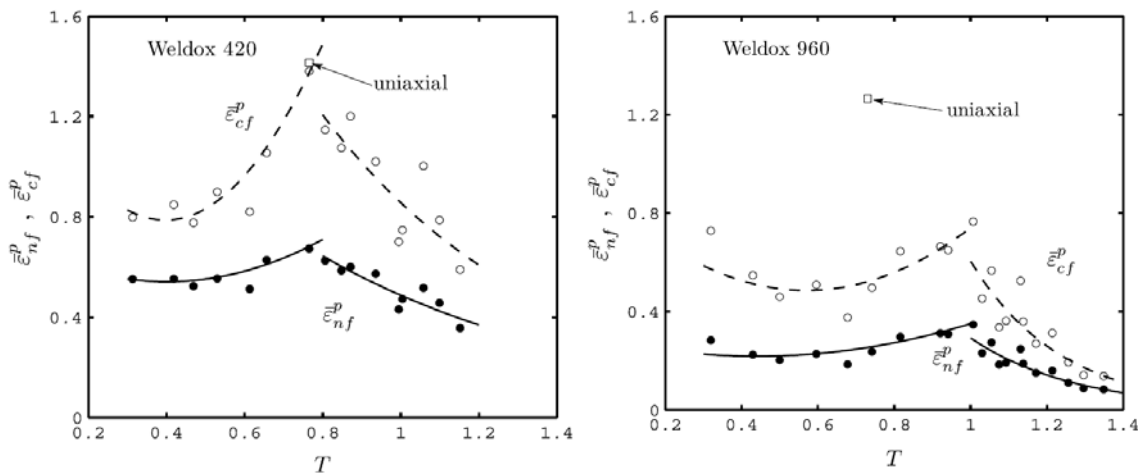


Figure 11. The effective plastic strain at failure vs. stress triaxiality  $T$  for Weldox 420 and Weldox 960.  $\bar{\epsilon}_{cf}^p$  is based on the calculated effective plastic strain at failure in the centre of the notch.  $\bar{\epsilon}_{nf}^p$  is based average effective plastic strain in the notch, evaluated from experimental load-deformation..

Figure 11 shows also that the average effective plastic strains at failure in the neck, based on the uniaxial tensile tests on smooth round bar specimens, are 2–5 times high compared to the critical plastic strains.

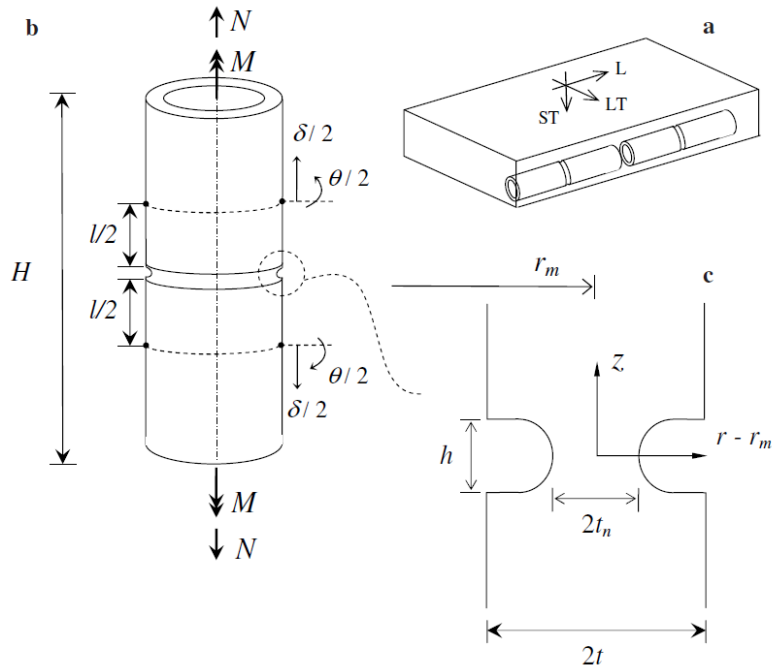


Figure 12. Tests performed on circumferentially double notched tube specimens. Specimens cut from 30 mm thick plates.

Figure 13 and Figure 14 show results for a hot forming steel type DP600 which is boron alloyed, dual phase cold forming steel (nominal  $f_y = 340\text{--}420$  MPa,  $f_u = 600$  MPa,  $A_{80} \geq 20\%$ ). The microstructure of dual phase steels is composed of soft ferrite matrix and 10–40 % of hard martensite or martensite-austenite (M-A) particles. The results show that critical plastic strain for  $T < 1$  is about 30%.

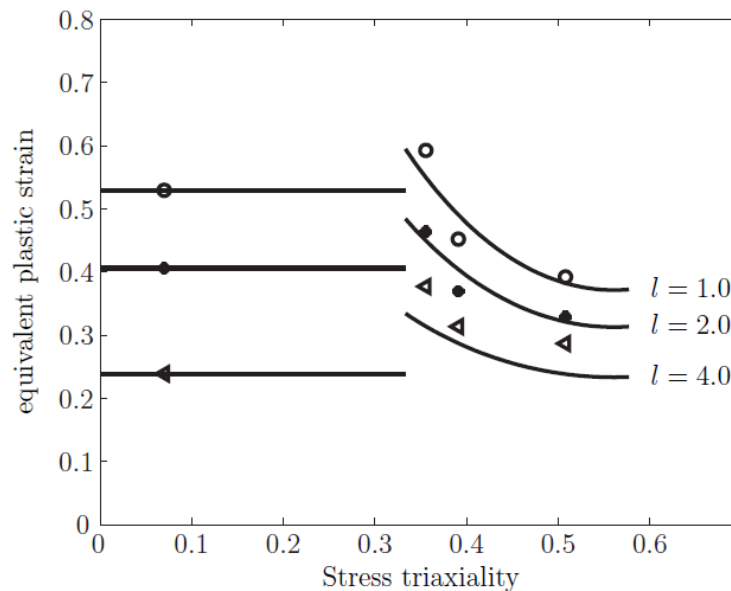


Figure 13. Tests results for DP600 steel. Solid lines indicate fracture strain limit for three different element sizes. Dots are the corresponding experimental values [22].

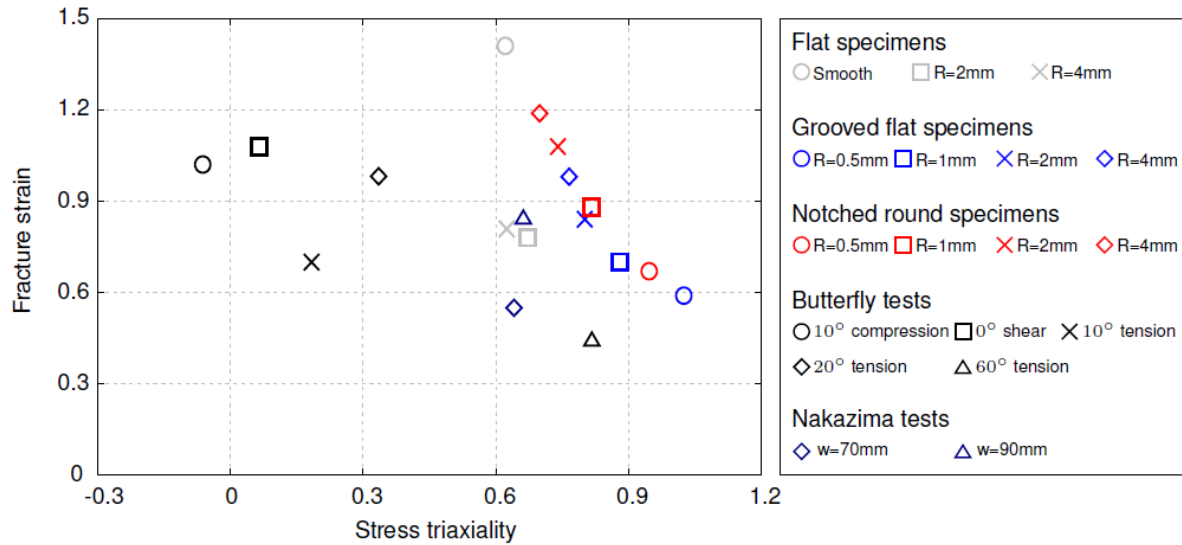


Figure 14. Fracture strain vs. stress triaxiality for DP600 steel [23].

Figure 15 shows results for notch tensile tests on a mild steel BS EN 10025 FE430A (S275, nominal values  $f_y = 275$  MPa,  $f_u \geq 410$  MPa,  $A_5 = 21\%$ ). The cylindrical specimens were cut in the rolling direction from the mild steel plate and turned with three different notch radii. The specimens were designated n05, n2 and n3 for small, medium and large radius notches ( $R$  around 0.5 mm, 2 mm and 4 mm, respectively).

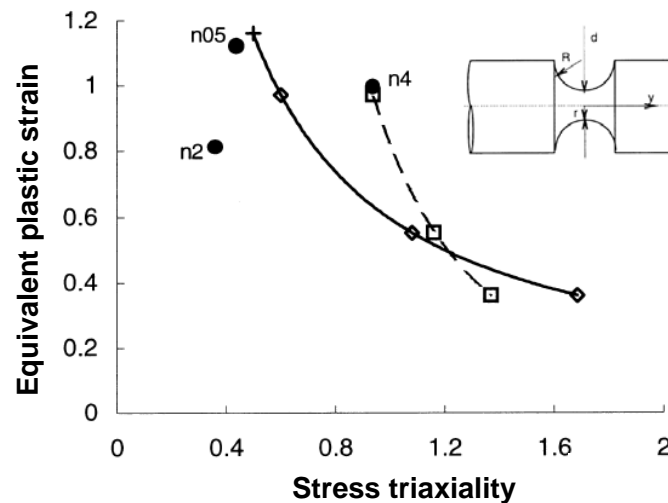


Figure 15. Failure envelope for S275 steel [24]. The figure includes a tensile test point labelled by + marker. The maximum triaxiality is based on Bridgman formulation (continuous line) and on FEM (broken line). The solid circles refer to the stress-strain state at the failure calculated by FEM.

Figure 16 and Figure 17 show results of edge fracture in simple test pieces configured with side notches and centre holes [25]. Three notched specimen shapes were selected for testing: (a) conventional, (b) centre hole, and (c) side notch. Each specimen variation was produced from seven different high strength grades: JAC 590R (C-Mn,  $f_y = 501$  MPa,  $f_u = 618$  MPa,  $A_{50} = 22\%$ ), JAC 780T (TRIP,  $f_y = 502$  MPa,  $f_u = 876$  MPa,  $A_{50} = 21\%$ ), JSC 980Y low carbon ( $f_y = 687$  MPa,  $f_u = 1043$  MPa,  $A_{50} = 13\%$ ), JSC 980Y (dual phase) mid carbon ( $f_y = 689$  MPa,  $f_u = 1072$  MPa,  $A_{50} = 14\%$ ), JAC 980Y low carbon ( $f_y = 676$  MPa,  $f_u = 1025$  MPa,  $A_{50} = 14\%$ ), JAC 980Y mid carbon ( $f_y = 646$  MPa,  $f_u = 1035$  MPa,  $A_{50} = 15\%$ ), and hot stamp 1500 boron steel ( $f_y = 983$  MPa,  $f_u = 1497$  MPa,  $A_{50} = 6.6\%$ ). All these steels had  $f_u/f_y > 1.5$  except of JAC 590R with  $f_u/f_y > 1.23$ . The results indicate that local fracture strain reveals more differentiation between the materials as compared to total elongation.

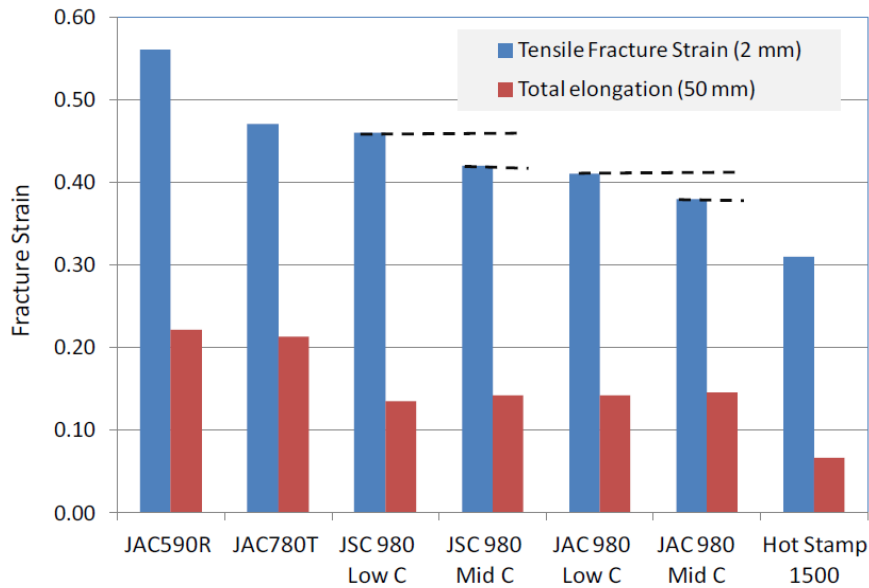


Figure 16. Total elongations and local strains at fracture of conventional “dog bone” specimens.

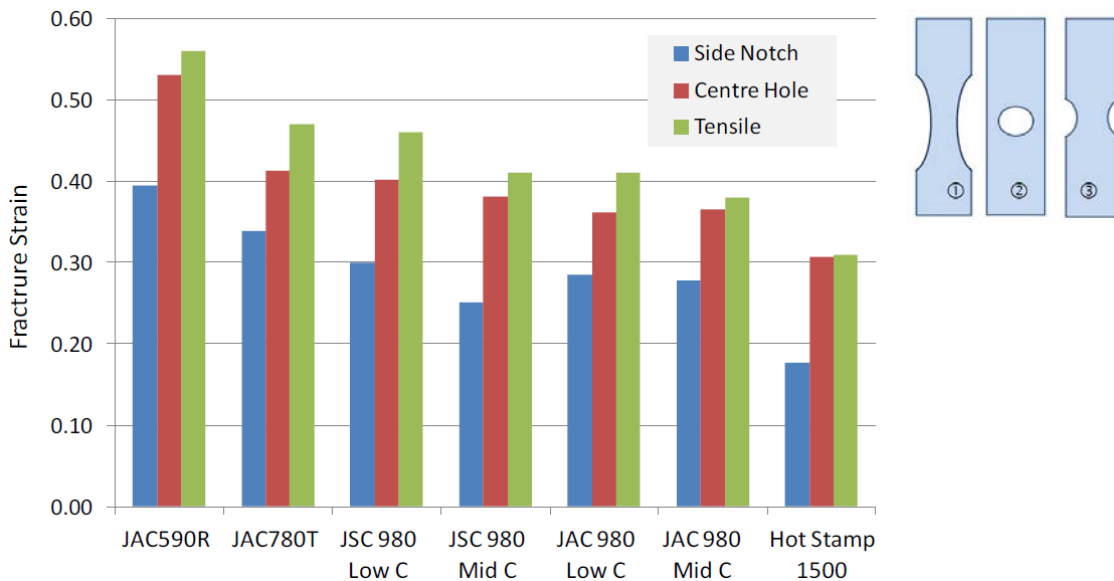


Figure 17. Fracture strains for conventional and notched test specimens. Centre hole ( $W = 50 \text{ mm}$ ,  $D = 20 \text{ mm}$ ) and Side Notch ( $W = 50 \text{ mm}$ ,  $D = 20 \text{ mm}$ ).

## 2. Stress-strain characterization

The definition of inelastic behaviour of materials in FEM software is usually based on the true stress and true plastic strain relation which is convenient for the finite element solver. On the other hand, loads and displacements produced by material testing correspond to the engineering stress-strain relation which is only slightly different as long as the deformation is uniform throughout the tested cross-section. Such difference is often neglected in modelling mild steel grades because the limit of uniform deformation is rarely reached. Utilization of high strength steels is thus introducing a new challenge. Diffuse necking (non-uniform deformation) in high strength steels is usually initiated at low tensile strains, and therefore the localized instability can occur more frequently than in mild grades. This means that constitutive models should be always based on true stress and strain values.

The commonly used true stress-strain models were developed for the very high deformations simulation (e.g. car manufacturing, cold forming, brake pressing) of standard materials where the assumption of rigid-plastic material was accurate enough. The effect of elastic deformation in high strength steels is, however, more pronounced because of the high stress levels at relatively low total strains. The material elasticity cannot be simply neglected.

## 2.1 Background

Engineering stress  $\sigma$  is the stress calculated from the load  $P$  acting on the initial cross-sectional area  $A_0$ . True stress  $\sigma_t$  is the stress calculated from the load  $P$  acting on the instantaneous cross-sectional area  $A$ .

$$\sigma = \frac{P}{A_0} \text{ and } \sigma_t = \frac{P}{A} \quad (10)$$

Engineering strain is the gauge elongation  $L-L_0$  over the initial length  $L_0$ . True strain  $\varepsilon_t$  is the rate of length increase over the instantaneous gauge length. Both can be expressed using the initial gauge length  $L_0$  as:

$$\varepsilon = \frac{L-L_0}{L_0} \text{ and } d\varepsilon_t = \frac{dL}{L}, \text{ therefore } \varepsilon_t = \ln\left(\frac{L}{L_0}\right) \quad (11)$$

If the true stress and strain values describe only material plasticity, we can assume that the volume of the material under pure plastic deformation remains constant.

$$A_0 L_0 = A_{pl} L_{pl} \quad (12)$$

Then we get from the Eqs. (11) and (12) the relation between the geometry and the true and engineering plastic strains.

$$\frac{L_{pl}}{L_0} = \frac{A_0}{A_{pl}} = e^{\varepsilon_t} = \varepsilon_{pl} + 1 \quad (13)$$

The calculation of true stress (of the rigid-plastic material) and plastic strain from their engineering counterparts is according to the Eqs. (14) and (15).

$$\sigma_{t,pl} = \sigma(\varepsilon_{pl} + 1) \text{ and including the elasticity } \sigma_t = \sigma(\varepsilon_{el} + 1)^{2\nu} (\varepsilon_{pl} + 1) \quad (14)$$

$$\varepsilon_{t,pl} = \ln(\varepsilon_{pl} + 1) \quad (15)$$

### Hollomon's model

The simplest constitutive equation for the rigid-plastic true stress and strain relation is due to Hollomon [27].

$$\sigma_{t,pl} = C \varepsilon_{t,pl}^m \quad (16)$$

Strain hardening exponent  $m$  is usually between zero and 0.5. The lower limit  $m = 0$  represents a non-hardening rigid-plastic material. The higher the value of  $m$ , the more pronounced is the strain-hardening characteristic of the material. It can be shown that the exponent  $m$  of the Eq.(16) is equal to the true plastic strain  $\varepsilon_{t,pl,u}$  at the maximum load  $P$  at the onset of necking. This is directly related to the ultimate (uniform) strain  $\varepsilon_u$  as defined by the Eurocodes [1].

$$m = \varepsilon_{t,pl,u} = \ln(\varepsilon_{pl,u} + 1) = \ln\left(\varepsilon_u - \frac{\sigma_u}{E} + 1\right) \quad (17)$$

The similar relation of constant  $C$  to the ultimate stress and strain can be derived from Eqs. (14), (15), (16) and (17).

$$C = \frac{\sigma_u e^{\varepsilon_{t,pl,u}}}{\varepsilon_{t,pl,u}^m} = \sigma_u \left(\frac{e}{m}\right)^m \quad (18)$$

### Ramberg-Osgood's model

The original equation proposed by Ramberg and Osgood in 1943 [28] is based on the knowledge of the yield point and it takes into account plastic and elastic deformation. The constant  $K$  in Eq.(19) is defined from the yield stress and strain  $\sigma_y$  and  $\varepsilon_y$  respectively.

$$\varepsilon = \frac{\sigma}{E} + K \left(\frac{\sigma}{E}\right)^n \quad \text{where } K = \varepsilon_y \left(\frac{E}{\sigma_y}\right)^n \quad (19)$$

If we assume that the second term of Eq.(19) is used to express the true stress to true plastic strain relation, we get the Eq.(20) similar to the previous model in Eq.(16).

$$\sigma_{t,pl} = \frac{E}{\sqrt[n]{K}} \varepsilon_{t,pl}^{1/n} \quad \text{where } K = \ln(\varepsilon_y + 1) \left[ \frac{E}{\sigma_y (\varepsilon_y + 1)} \right]^n \quad (20)$$

The resulting curves can be identical if the conditions of Eq. (21) are satisfied. However, the Ramberg-Osgood model is based on the yield point instead of the ultimate (uniform) stress and strain.

$$m = \frac{1}{n} \quad \text{and} \quad C = \frac{E}{\sqrt[n]{K}} \quad (21)$$

### Material elasticity

The total length, cross-sectional area and engineering strain can be calculated taking into account the effect of elastic deformation with the Poisson's ratio  $\nu$  for the cross-sectional contraction. It should be noted that the true stress value  $P/A$  requires re-calculation if the elastic deformation of area is also accounted for.

$$\varepsilon = \varepsilon_{el} + \varepsilon_{pl} = \frac{\sigma}{E} + \varepsilon_{pl} \quad (22)$$

$$L = L_{pl} + \Delta L_{el} = L_0(\varepsilon + 1) \quad \text{and} \quad A = A_{pl}(1 - \nu\varepsilon_{el})^2 = \frac{A_0}{\varepsilon_{pl} + 1} \left(1 - \nu \frac{\sigma}{E}\right)^2 \quad (23)$$

$$A = A_{pl}(1 - \nu\varepsilon_{el})^2 = \frac{A_0}{\varepsilon_{pl} + 1} \left(1 - \nu \frac{\sigma}{E}\right)^2 \quad (24)$$

### Strains beyond the ultimate load

When the load reaches its maximum value, diffuse necking starts and the stresses and strains are not uniformly distributed anymore. The stress state is no longer uniaxial and therefore the



strains calculated by Eq. (11) will have different values for different gauge length  $L_0$ . Even though many theoretical models exist for predicting true stress and strain relationship beyond the necking point [29] we chose the direct iteration of calculated finite element results because it was more convenient due to the numerical nature of this study [30].

## 2.2 True stress-strain curves for Abaqus models

This section describes the iterative approach for the true stress-strain characterization of measured tensile test data (see Table 5). It is based on the study published by ManSoo et al. [30]. The algorithm was implemented in the Abaqus finite element software [31] and it was used to calculate improved true stress and strain relationship beyond the ultimate load. The criterion was that the average difference  $r$  between calculated loads and the measured ones should be smaller than the limit value  $r_{lim}$  (see Figure 18).

Table 5. Measured values of tested coupons.

S275 to S700		$t$ (mm)	$b$ (mm)	$f_y$ (MPa)	$f_u$ (MPa)	$\varepsilon_u (A_{gt})$	$\varepsilon_f (A_5)$	$E$ (MPa)	orientation
1	CHS275-1	7.97	19.8	300	418	0.179	0.359	172061	Rolling
2	CHS355-1	9.98	19.8	393	550	0.134	0.281	162137	Rolling
3	CHS700-1	10	20	708	792	0.095 <sup>1)</sup>	0.206	210000 <sup>2)</sup>	Rolling
S960		$t$	$b$	$f_y$	$f_u$	$\varepsilon_u (A_{gt})$	$\varepsilon_f (A_{80})$	$E$	orientation
4	CHS960-1	8.07	20.10	1060	1157	0.034	0.109	205142	Rolling
5	CHS960-2	8.08	19.98	1056	1167	0.039	0.115	206121	Rolling
6	CHS960-3	8.07	20.01	1061	1167	0.033	0.105	207249	Rolling
7	CHS960-4	8.07	20.11	1059	1157	0.038	0.112	207881	Rolling
8	CHS960-5	8.07	20.03	1061	1156	0.034	0.107	206614	Rolling
9	CHS960-6	8.10	19.96	1055	1158	0.032	0.100	204822	Rolling
10	CHS960-7	8.08	20.04	1062	1158	0.032	0.101	205123	Rolling
11	CHS960-8	8.09	20.13	1062	1162	0.034	0.111	204592	Rolling
12	CHS960-9	8.06	20.23	1062	1169	0.025	0.082	209650	Transverse
13	CHS960-10	8.05	20.15	1067	1174	0.022	0.095	207736	Transverse
14	CHS960-11	8.07	20.22	1061	1170	0.025	0.089	211583	Transverse
15	CHS960-12	8.06	20.16	1063	1167	0.024	0.085	208074	Transverse
16	CHS960-13	8.06	20.23	1061	1172	0.026	0.087	207249	Transverse
17	CHS960-14	8.08	20.15	1079	1194	0.030	0.100	209316	Transverse
18	CHS960-15	8.06	20.18	1058	1171	0.025	0.088	211805	Transverse
19	CHS960-16	8.06	20.20	1067	1174	0.024	0.080	210898	Transverse
Average S960		8.07	20.12	1062	1167	0.030	0.098	207741	

<sup>1)</sup> Value obtained additionally from the stress-strain curve

<sup>2)</sup> Modulus of elasticity was not measured, 210 GPa was used instead as recommended by EN 1993

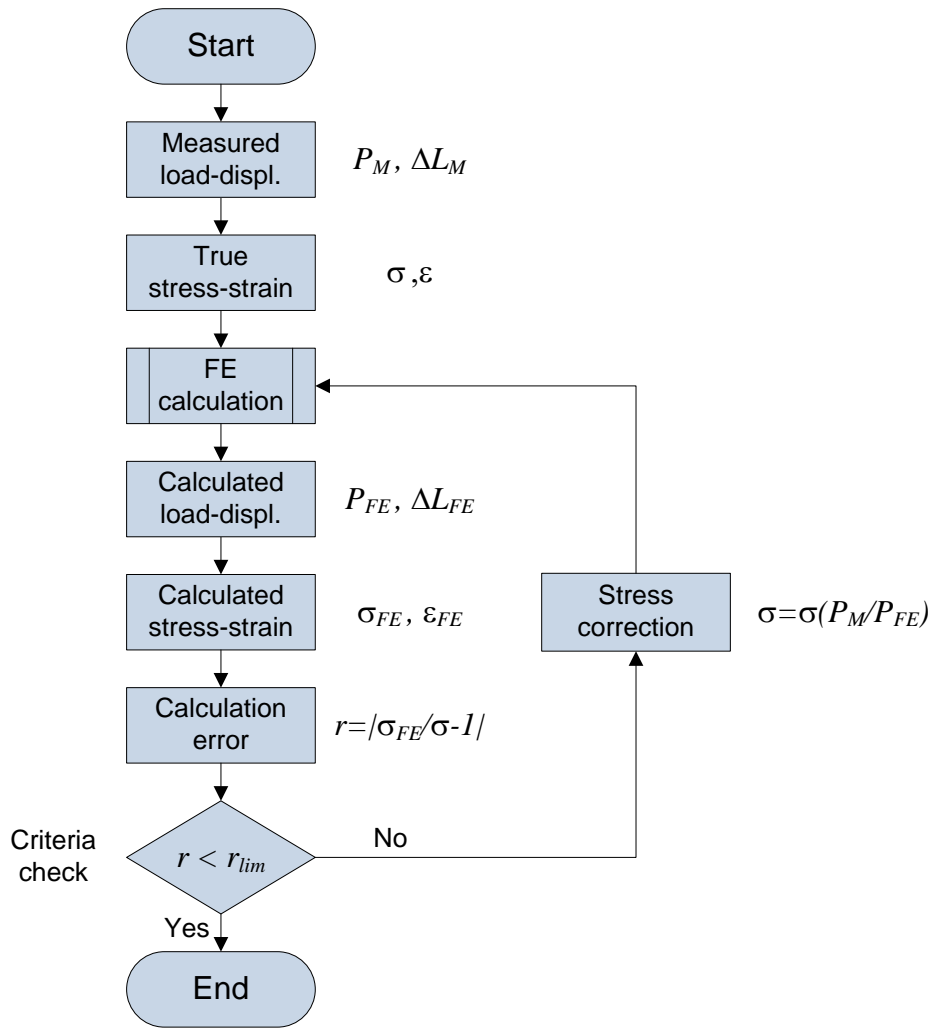


Figure 18. Iterative procedure used for stress-strain characterization of measured data.

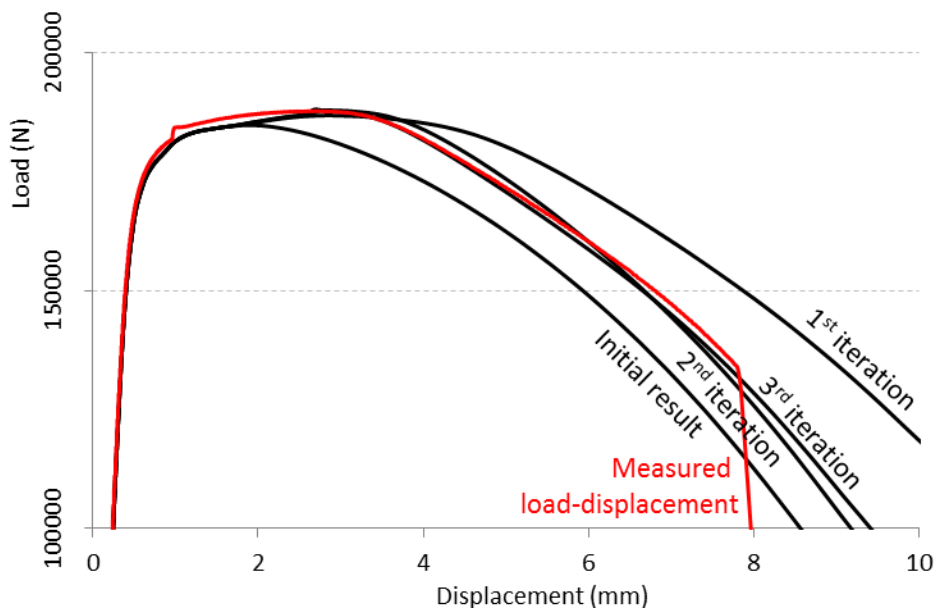


Figure 19. Example of numerical stress-strain characterization (material CHS960-1).

In each step the average true plastic axial strain in the middle section of the coupon was calculated. Then the true stress of the material model corresponding to this strain was corrected. The correction was based on the ratio of relevant measured and calculated loads. The initial assumption for the true stress-strain relation was Hollomon's model [27] with parameters  $C$  and  $m$  calculated from the test data in Table 5.

The biggest drawback of such method is the calculation of true plastic axial strain from the finite element results. It doesn't exactly represent the material true plastic strain in the model. Moreover, their difference grows with larger deformation and it also creates a small discontinuity in the predicted true stress-strain curve near the ultimate load point. The studied coupon tests, however, converged quickly despite this effect (see Figure 19) and the load-displacement prediction was very accurate, mainly due to the large number of calculation points.

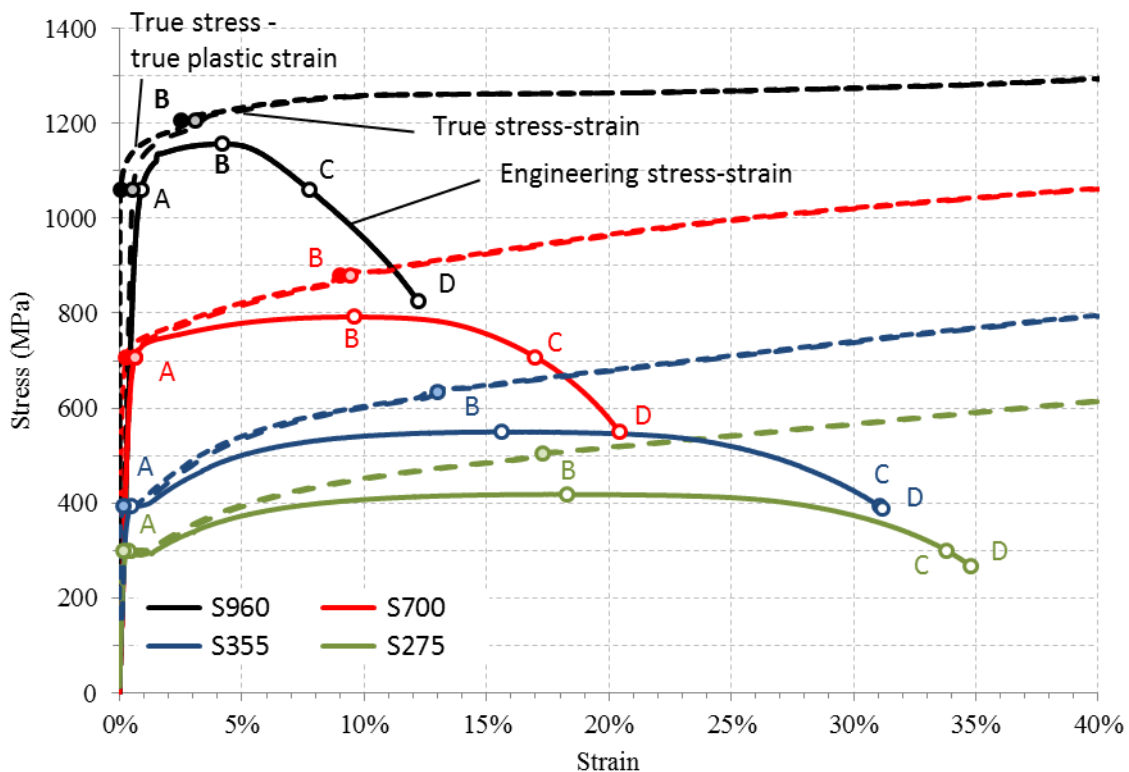


Figure 20. Calculated stress-strain relations tested steels.

The average true stress-strain curve for S960 was generated from the 16 coupon tests and their numerical iteration results. Then we have calculated true stress-strain relationship for one coupon test from S700, one from S355 and one from S275. The engineering and true stress-strain curves are presented in Figure 20. Points A to D (in Figure 20) show the location of yield limit (A), ultimate load (B), location of yield load in the descending part of the diagram (C) and the ductile failure (D). Point C is used for the evaluation of ductile limits according to the method 4 from Table 8. The figure shows clearly that the effect of material elasticity is more pronounced in high strength steels such as S700 and S960.

Finite element calculations provided two parameters that are usually basis of ductile failure predictive models; the maximum equivalent plastic strain  $\varepsilon_{eq}$  and the stress triaxiality  $T$ . Both maximums are always in the middle cross-section. However, their location within this cross-section does not have to be the same. They are both located in the middle point of this cross-section in the case of coupon test, but in CHT specimens their position differs.

The results presented in Table 6 present calculated maximum equivalent plastic strains at failure ( $\epsilon_{eq,f}$ ), at the limit elongation  $\epsilon_R$  ( $\epsilon_{eq,R}$ ), and at the corresponding limit of 10% or 15% elongation ( $\epsilon_{eq,10(15)}$ ) depending on the steel grade.

Table 6. Maximum equivalent plastic strain and stress triaxiality in coupon tests calculated by FEM.

<b>S275 to S700</b>		$\epsilon_{eq,f}$	$T_f$	$\epsilon_R$	$\epsilon_{eq,R}$	$T_R$	$\epsilon_{eq,10(15)}$	$T_{10(15)}$
1	CHS275-1	1.879	0.818	0.338	1.459	0.728	0.167	0.355
2	CHS355-1	1.382	0.813	0.278	1.329	0.785	0.184	0.356
3	CHS700-1	1.144	0.861	0.170	0.603	0.571	0.108	0.383
<b>S960</b>		$\epsilon_{eq,f}$	$T_f$	$\epsilon_R$	$\epsilon_{eq,R}$	$T_R$	$\epsilon_{eq,10}$	$T_{10}$
4	CHS960-1	1.143	0.931	0.061	0.288	0.558	0.734	0.763
5	CHS960-2	1.019	0.860	0.051	0.286	0.572	0.565	0.666
6	CHS960-3	1.111	0.946	0.056	0.302	0.578	0.772	0.794
7	CHS960-4	1.062	0.875	0.052	0.284	0.569	0.624	0.690
8	CHS960-5	1.005	0.876	0.056	0.308	0.582	0.653	0.696
9	CHS960-6	0.957	0.899	0.059	0.307	0.581	0.746	0.810
10	CHS960-7	1.018	0.900	0.048	0.295	0.550	0.770	0.784
11	CHS960-8	1.043	0.866	0.053	0.287	0.571	0.627	0.689
12	CHS960-9	0.785	0.828	0.073	0.334	0.577	0.940	0.894
13	CHS960-10	1.105	0.954	0.060	0.297	0.567	0.975	0.899
14	CHS960-11	0.908	0.879	0.069	0.317	0.564	0.915	0.882
15	CHS960-12	0.842	0.825	0.066	0.312	0.551	0.927	0.859
16	CHS960-13	0.862	0.860	0.061	0.290	0.574	0.911	0.881
17	CHS960-14	1.085	0.954	0.059	0.286	0.557	0.852	0.855
18	CHS960-15	1.004	0.898	0.070	0.333	0.570	1.029	0.909
19	CHS960-16	0.758	0.817	0.054	0.290	0.573	0.954	0.900
<i>Average S960</i>		<i>0.982</i>	<i>0.886</i>	<i>0.059</i>	<i>0.301</i>	<i>0.568</i>	<i>0.812</i>	<i>0.811</i>

It can be observed that coupon specimens of S960 tolerated about 10 times higher equivalent true plastic strains than the engineering strain at the failure elongation  $A_{80}$ .

## 2.3 Verification of true stress-strain material models

The material models from S960, S700, S355 and S275 were used to predict the load-displacement of CHT (centre-hole tension) tests. The numerical results were compared to the real experiments from S960 and S700. Test specimens from S960 were fabricated from the same batch as the coupons used in the previous study. However, the material for S700 tests was different in coupons and in CHT specimens. Steel grades S355 and S275 were not tested experimentally.

Five specimens with the hole (diameters from 8 to 40 mm, see Figure 21) and one without the hole were calculated for each steel grade. Then the numerical results were compared to the real experimental data. The results are As can be seen from Figure 22 the predicted load-displacement is very close to the experimental results in the case of steel S960. The numerical results on Figure 23 show small deviation from the tested values that can be caused by different material source used in coupon testing than the material used in CHT experiments.

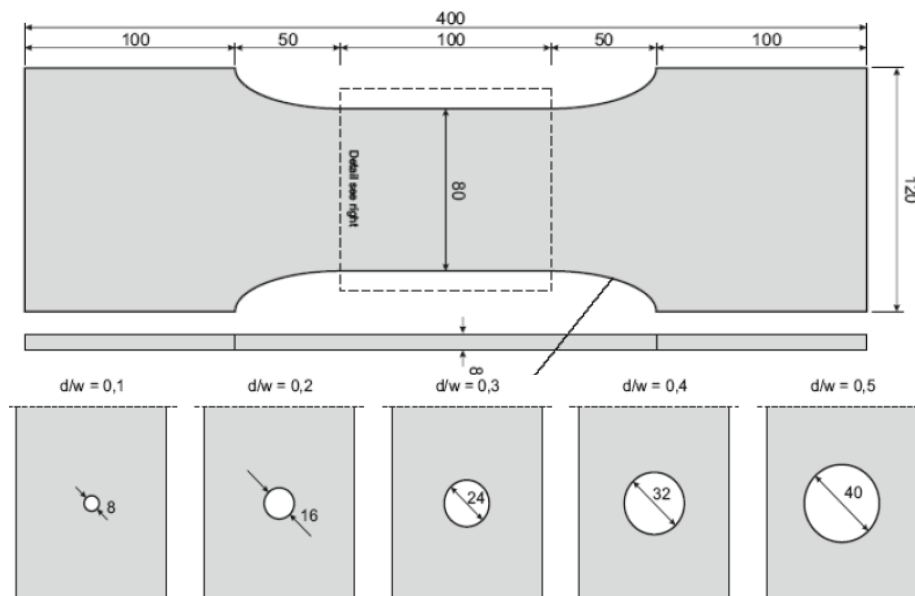


Figure 21. Shape of the CHT test specimen CHT-8 to CHT-40.

All numerical models were calculated with three symmetry planes (see Figure 24). Later observation of experimentally tested pieces, however, revealed that the failure of specimen with small hole or without hole was rather asymmetrical due to the high aspect ratio of rectangular cross-sectional parts. Therefore we also tested those specimens with only two symmetry planes (see Figure 25) and asymmetrical imperfections. The difference between FEM models could be observed only in reference CHT-0 tests without hole.

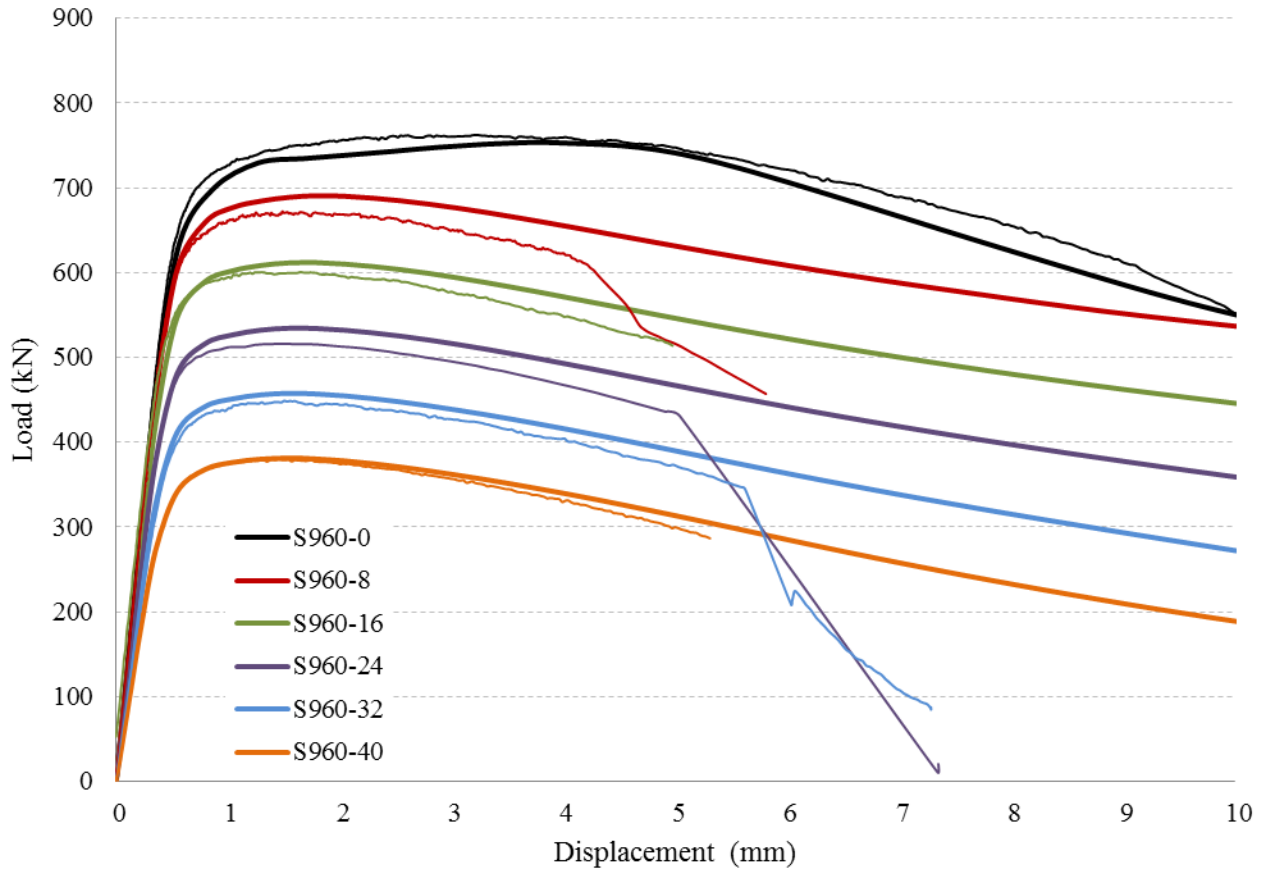


Figure 22. Comparison of numerical and experimental (thin line) results of CHT grade S960.

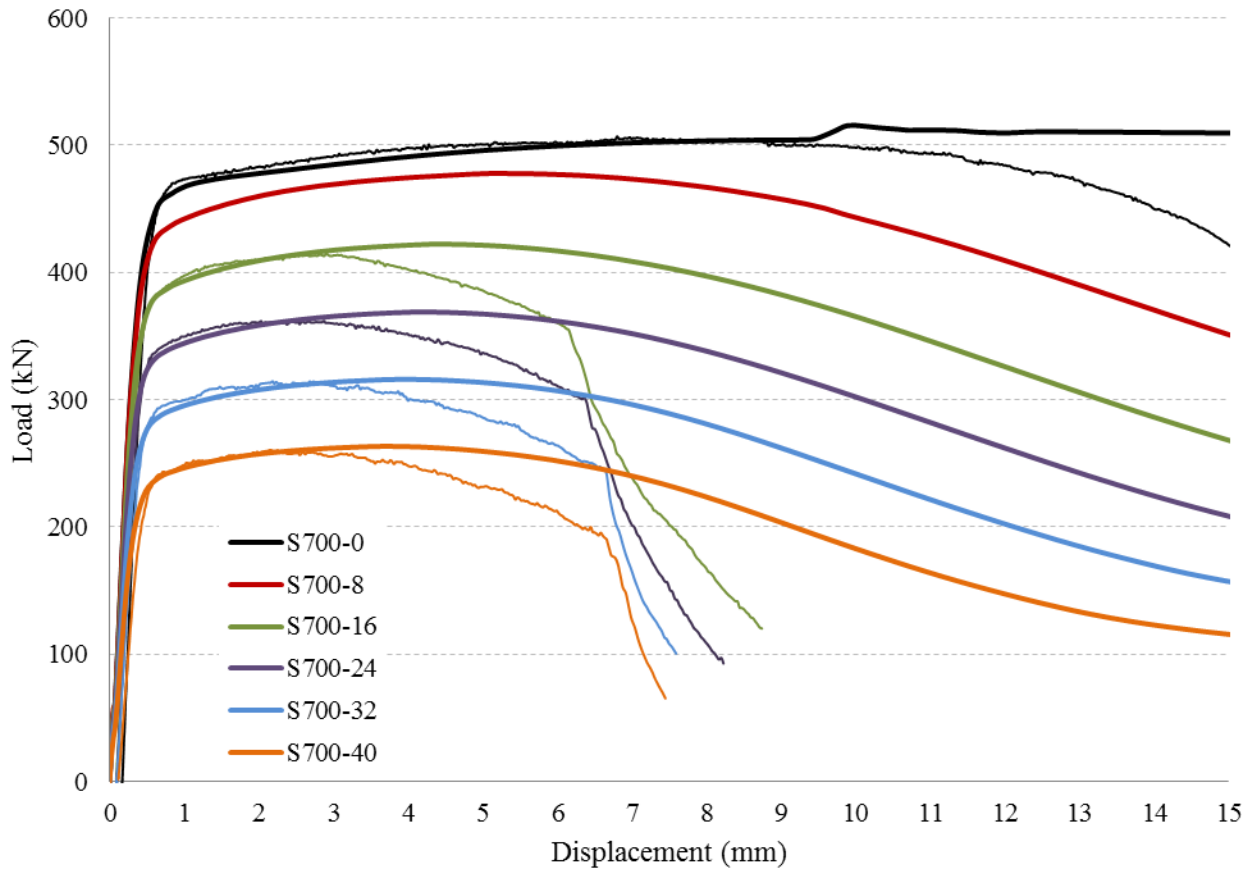


Figure 23. Comparison of numerical and experimental (thin line) results of CHT grade S960.



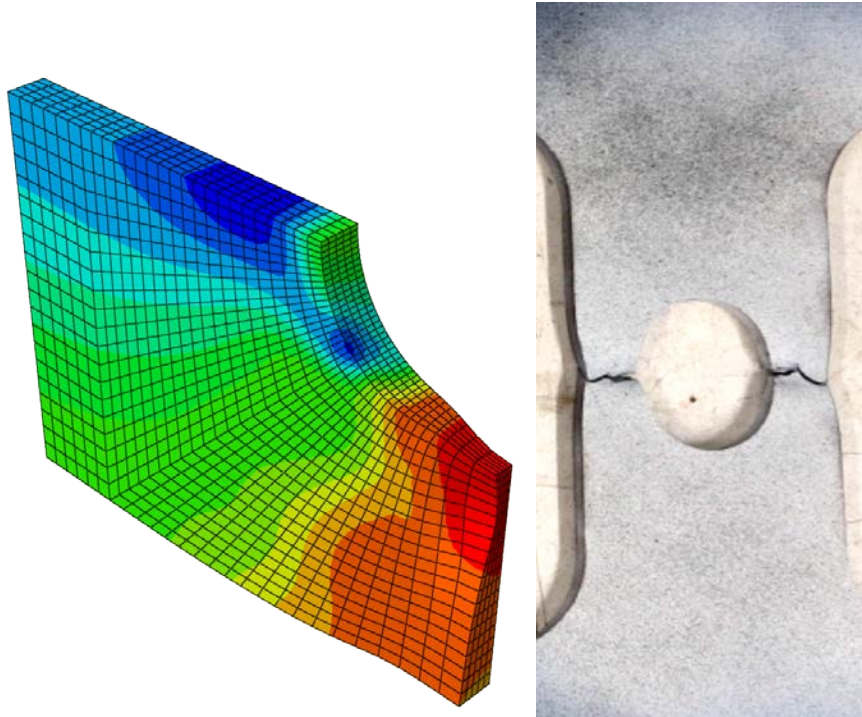


Figure 24. Finite element model of CHT specimen and the real specimen [32] with symmetrical failure (stress distribution, S960 with hole diameter 40 mm).

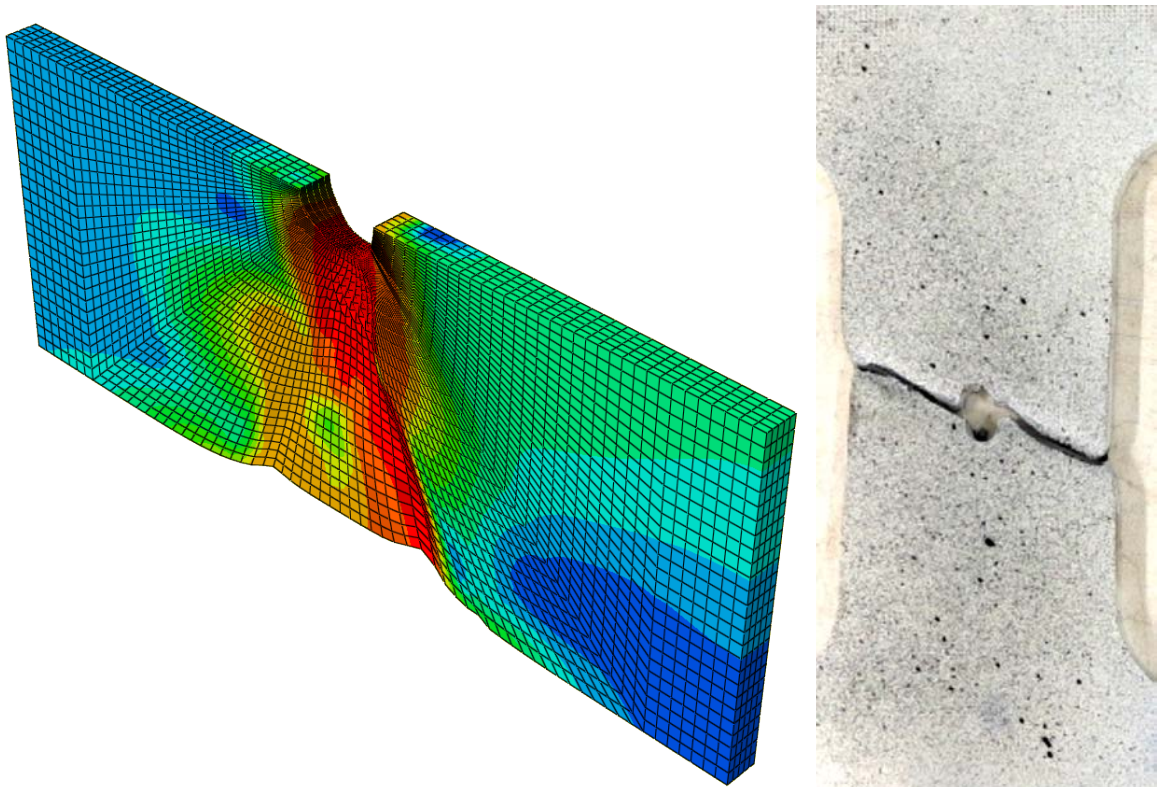


Figure 25. Finite element model of CHT specimen and the real specimen [32] with asymmetrical failure (stress distribution, S960 with hole diameter 8 mm).



The prediction of CHT specimens' failure could be compared to the real results of 11 experiments (5 from S700 and 6 from S960). The measured elongation at failure  $\varepsilon_{f,CHT}$  and the corresponding levels of equivalent plastic strain  $\varepsilon_{eq,f,CHT}$  and triaxiality  $T_{f,CHT}$  from the FEM models are presented in Table 7.

Table 7. Maximum equivalent plastic strain and stress triaxiality in CHT tests at failure calculated by FEM.

Test no.	$\varepsilon_{f,CHT}$	$\varepsilon_{eq,f,CHT}^{1)}$	$\varepsilon_{eq,f,CHT}^{2)}$	$T_{f,CHT}^{1)}$	$T_{f,CHT}^{2)}$	$\frac{\varepsilon_{eq,f,CHT}}{\varepsilon_{eq,f}^{3)}$	$\frac{\varepsilon_{eq,f,CHT}}{\varepsilon_{eq,R}^{3)}$	
1	S700-0	0.198	0.147		0.338		0.128 <sup>4)</sup>	0.234
2	S700-16	0.077	0.977	0.580	0.422	0.652	0.854	1.620
3	S700-24	0.080	0.922	0.652	0.395	0.647	0.806	1.337
4	S700-32	0.082	0.886	0.670	0.412	0.649	0.774	1.469
5	S700-40	0.083	0.850	0.687	0.428	0.651	0.743	1.410
6	S960-0	0.110	0.435		0.531		0.443 <sup>4)</sup>	1.445
7	S960-8	0.040	0.871	0.442	0.579	0.666	0.887 <sup>4)</sup>	2.894
8	S960-16	0.050	0.985	0.646	0.551	0.717	1.003	3.272
9	S960-24	0.050	0.992	0.632	0.521	0.751	1.011	3.296
10	S960-32	0.060	1.048	0.806	0.504	0.786	1.068	3.482
11	S960-40	0.050	0.917	0.714	0.467	0.765	0.934	3.047

<sup>1)</sup> Values at the location of the maximum  $\varepsilon_{eq,f,CHT}$

<sup>2)</sup> Values at the location of the maximum  $T_{f,CHT}$ ,

<sup>3)</sup> The average value of 16 coupon test results was used for S960  $\varepsilon_{eq,f} = 0.098$  and  $\varepsilon_{eq,R} = 0.059$

<sup>4)</sup> Test were failing in finally shear, and therefore exhibited lower strains in the central cross-section

As can be seen from the table, two different values of  $\varepsilon_{eq,f,CHT}$  and  $T_{f,CHT}$  are reported for specimens with hole. In those tests, the position of maximum equivalent plastic strain was different than the position of maximum triaxiality (see red areas in Figure 26).

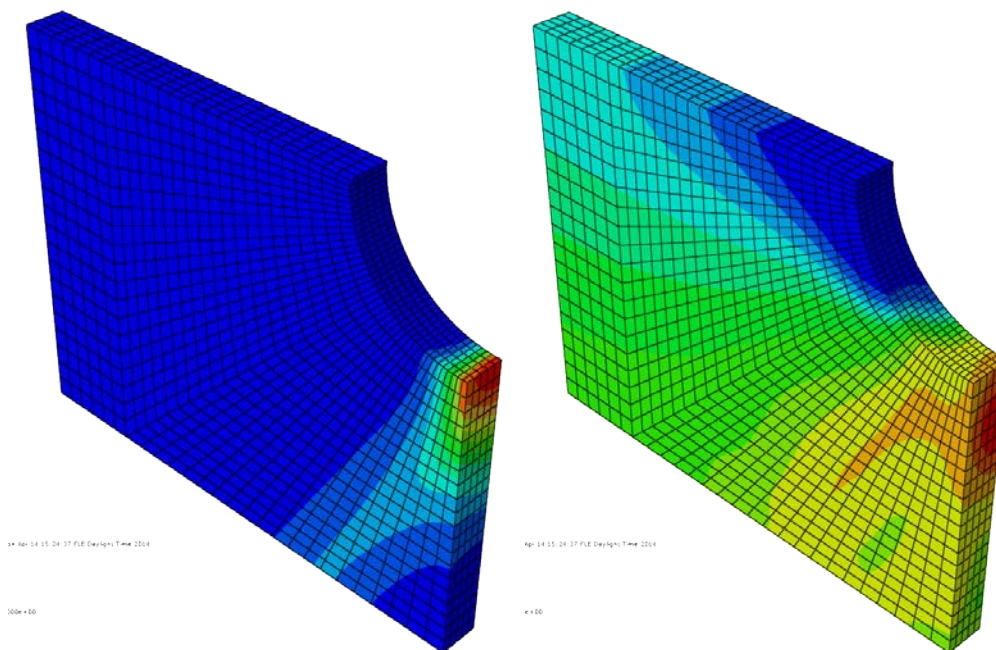


Figure 26. Location of maximum equivalent strain (left) and triaxiality (right) in CHT specimen.

### 3. Strain limits for FEM modelling

The goal of this section is to propose and evaluate the limit criteria for the design of critical details with stress concentration by finite element methods. It is convenient to use strains (for instance in the form of equivalent plastic strain) as a measure. Such calculations are facing several challenges. The most difficult is probably to predict the level of strain at ductile failure because this depends on many factors, but especially on stress triaxiality. Then the mesh size and choice of element types used in FEM are affecting the results as well.

#### 3.1 Simple limits for equivalent plastic strain

The ductile failure criterion is usually based on critical plastic strain. However, critical strain at failure is not a fixed material parameter; it depends also on the three dimensional stress and strain state. Therefore it is difficult to set a simple ductility failure criterion, which describes well the ductile fracture initiation of the material. Ductility depends also on the deformation history of the material. It has been noticed that the ductile failure is related to strain hardening and Charpy V impact energy at upper shelf energy. The results can also be affected by differences in testing and modelling. Some simple or more complex criteria for FEM calculation, shown in Table 8, can however be considered.

Criteria from 1 to 7 from Table 8 will be explored in more detail in this report. They are presented in Figure 27 for our model of steel grade S700. It should be noted that the criteria 3, 4, 6 and 7 may require the FEM calculation of coupon test to be able to convert engineering strain (or elongation) into the true strain.

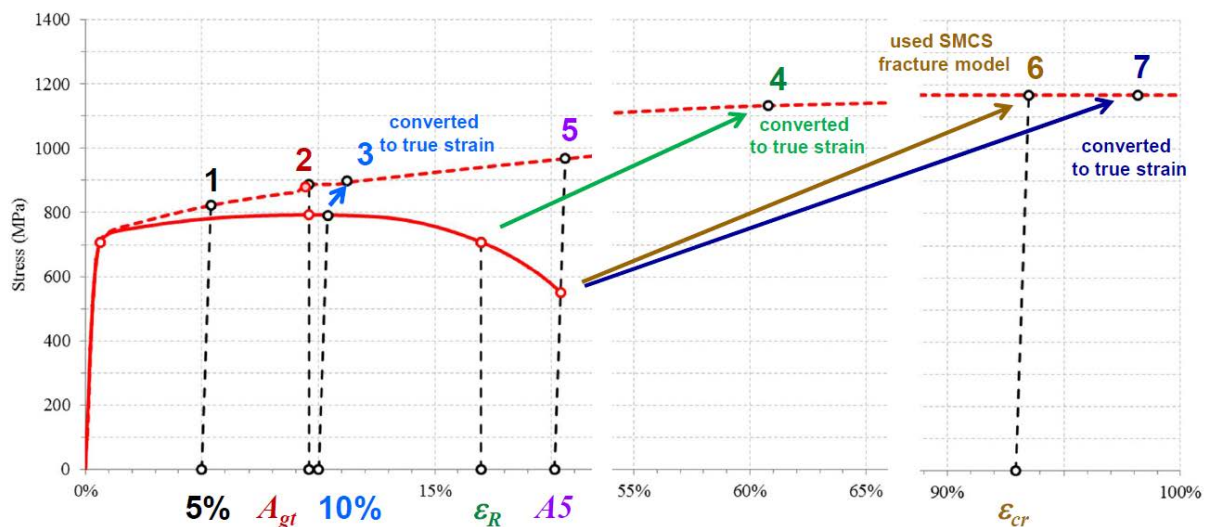


Figure 27. Example application of criteria 1 to 7 from Table 8 (solid line: engineering stress-strain, dashed line: true stress-strain relationship).

The data shown in Table 9 and Table 10 indicate that limiting plastic strains to  $A5$  elongation (method 5 in Table 8) and stress triaxiality to  $T < 1$  could be a suitable simplified failure criterion for engineering use. The fracture elongation grows proportionally with the critical plastic strain predicted by this criterion. The tables (Table 9 and Table 10) are based on the data presented in the previous chapters. However, the comparison is not very consistent, mainly because the real  $A5$  fracture elongation is not given in the references. The reason why critical (true peak) strain is always higher than the fracture (engineering average) strain in tensile testing is that the deformations in test specimens near the failure are always localized. Also in the conventional tensile testing the local plastic strains at failure after necking are proportional to  $A5$  fracture elongation.

Table 8. Proposed criteria for equivalent true plastic strains in FEM calculations.

**(1) Limiting true plastic strains to 5%, as given in design codes** - means that in practise plastic strains are mostly lower than uniform elongations determined from material testing (Figure 3). Therefore the limit may be too conservative for crack and residual stress free materials under static loading and large deformations, and especially for mild steels. On the other hand, ultra-high strength steel grades may already reach maximum load before 5%.

**(2) Limiting true plastic strains to values corresponding to  $A_{gt}$  elongation** - means that only uniform deformation is accepted. The order of magnitude is from 5% to 20%, depending on the material (Figure 3). The limit may be too conservative for ductile materials and details with high stress concentration.

**(3) Limiting true plastic strains to the level at minimum failure elongation prescribed by the Eurocode** - The elongation at failure has to be at least 15% (or 10% for high strength steels). Then the critical plastic strain  $\epsilon_{cr} = \epsilon_{eq,10(15)}$  can be obtained from the FEM simulation of real coupon test. The drawback of this method is that the real failure strains are lower in details with holes and sharp notches than in coupons. On the other hand it might be too conservative for mild steels where the real failure happens far beyond 15%.

**(4) Limiting true strains to the values obtained in material testing at the level of yield load in descending part of load-displacement diagram (after necking)** – This method assumes that the real failure happens at lower load level than the yield load, and therefore the predicted limits  $\epsilon_{cr} = \epsilon_{eq,R}$  will be conservative. The level of conservativeness is, however, varying greatly with the steel grades and it cannot be guaranteed in some cases.

**(5) Limiting true plastic strains to the numerical value of  $A_5$  elongation** - means that engineering plastic elongation at failure of tension test is never reached (peak true strains beyond the maximum load are higher than the average engineering strains), but the limit is still flexible to accommodate different steel grades. The order of magnitude is from 7% to 40%, depending on the material (Figure 3, Table 2). Based on the comparison of available test data it has always been safe (see Table 9). However, some cases may exist with very high triaxiality and high strength steel where this criterion would not be safe. The advantage is that the limit value is based on standard testing.

**(6) Using simple fracture model (e.g. SMCS) to predict critical plastic strains at triaxiality  $T=1.0$**  - High triaxiality such as 1.0 produces conservative limits for ductile failure of most of the typical structural details. The order of magnitude of critical strains is from 20% to 80%, depending on the material. The method may be unsafe for shear failure. Very rough estimation of fracture model's parameters can be obtained from standard coupon tests or Charpy V upper shelf test. However, material and CNT tests (possibly with supplementary shear tests) including complementary FEM analyses will provide much more precise prediction. Fracture model approach and its application to components with a high portion of shear stress will be investigated in RFCS-Match project (2013-2016) [26]. There the suitability of minimum upper shelf impact value as a toughness parameter will be tested.

**(7) Limiting true strains to the values obtained in material testing at the level of failure (A5).** This criterion has same kind approach as in the criteria 3 and 4.

**(8) Using critical plastic strain determined by complex fracture model based on experiments and limiting the range of triaxiality to  $T<1.0$**  - Such models for ductile fracture are usually used for simulations of sheet forming or car deformations in accidents. Selecting the lowest critical strain in the whole range or shear and ductile failure modes makes this approach safe for most of the applications. The question is which model is chosen and how the test results made for calibration of the model can be generalized. A great number of different tests and complementary FEM analyses have to be done.

Table 9. Rough comparison of critical strain to fracture elongation of coupons.

	$f_y$ (MPa)	$f_u$ (MPa)	Fracture elongation	$\epsilon_{cr}$ (method 5)	$\frac{\epsilon_{cr}}{\text{Fracture el.}}$
TRIP RA-K40/70	410 – 510	690 – 790	$A_{80} = 23\%$	> 40%	1.7
A514-Grade 110	> 800	> 850	$A_{50} > 16\%$	> 30%	1.9
HPS 70W	> 590	> 690	$A_{50} > 19\%$	> 70%	3.7
S275 (FE430A)	> 275	> 410	$A_{50} > 21\%$	> 60%	2.9
S355J2	> 355	> 510	$A_{50} > 20\%$	> 50 – 80%	2.5 – 4
S460 M	> 460	> 530	$A_5 > 17\%$	> 50 – 70%	2.9 – 4
S690QL	> 690	> 770	$A_5 > 14\%$	> 20%	1.4
Weldox 460	415	525	$A_5 > 19\%$	> 40%	2.1
Weldox 960	996	1051	$A_5 > 12\%$	> 20%	1.7
DP600	340 – 420	600	$A_{80} > 20\%$	30%	1.5

Table 10. Rough comparison of critical strain to fracture elongation in conventional notched test specimens (Figure 17).

	$f_y$ (MPa)	$f_u$ (MPa)	Fracture elongation	$\epsilon_{cr}$ (method 5)	$\frac{\epsilon_{cr}}{\text{Fracture el.}}$
JAC 590R	501	618	$A_{50} = 22\%$	39%	1.8
JAC 780T	502	876	$A_{50} = 21\%$	34%	1.6
JSC 980Y LC	687	1043	$A_{50} = 13\%$	30%	2.3
JSC 980Y MC	689	1072	$A_{50} = 14\%$	25%	1.7
JAC 980Y LC	676	1025	$A_{50} = 14\%$	28%	2.0
JAC 980Y MC	646	1035	$A_{50} = 15\%$	28%	1.9
Hot Stamp 1500	983	1497	$A_{50} = 6.6\%$	18%	2.7

The criterion 5 for  $A_5$  is potentially better criterion than criterion 4, where the fracture elongation is taken from the point corresponding to the yield load in the descending part of stress-strain curve. Fracture elongation  $A_5$  is always determined in standard material testing and the limit values for design are given in EN 1993-1-1 and EN 1993-1-12 standards. It gives also better values for high strength steels because in that case the engineering stress at fracture is much higher than the yield stress (Figure 3).

### 3.2 Evaluation of proposed strain limits

The results of criteria calculation are shown in Table 11, Figure 28, Figure 29, Figure 30 and Figure 31. The figures show calculated load-displacement relationship using optimized material models with indicated points of studied criteria 1 to 7 from Table 8. The relation between maximum equivalent plastic strain in the middle cross-section and the maximum observed equivalent strain at the outer edge of calculated specimen is also demonstrated. It is discussed in detail in Annex A: Strain concentration in CHT specimens.

Table 11. Equivalent strain criteria used in CHT tests evaluation.

Grade	Limit equivalent plastic strain $\epsilon_{cr}$ for criteria 1 to 7						
	1	2 ( $A_g$ )	3 ( $\epsilon_{eq,10(15)}$ )	4 ( $\epsilon_{eq,R}$ )	5 ( $A_5$ )	6	7 ( $\epsilon_{eq,f}$ )
S275	5.0%	17.9%	16.7% <sup>1)</sup>	146%	35.9%	143%	188%
S355		13.4%	18.4% <sup>1)</sup>	133%	28.1%	107%	138%
S700		9.8%	10.8% <sup>2)</sup>	60.3%	20.6%	92.9%	114%
S960		3.0%	81.2% <sup>2)</sup>	30.1%	9.8% <sup>3)</sup>	83.4%	98.2%

<sup>1)</sup> 15% elongation according to EN 1993-1-1 [1]

<sup>2)</sup> 10% elongation according to EN 1993-1-12 [2]

<sup>3)</sup> A5 value was not available; we used  $A_{80}$  instead

- The results show that the *criterion 1* (5% strain) is conservative in all cases.

The *criterion 2* ( $A_g$ , see Table 5) was also very conservative but mostly resulted in higher strains than the first method. It should be noted that with increasing material strength, the  $A_g$  decreases even below 5% (as in S960).  $\epsilon_{eq,10(15)}$  is reported in Table 6.

- The problem of using 10% or 15% engineering strain converted to true strain in *criterion 3* is that this value may be lower than  $A_{gt}$  elongation (as in S275 to S700) providing conservative prediction or higher than  $A_{gt}$  (S960). Then the predicted limits are much higher. The good prediction of S960 tests is a pure coincidence.

It is safe to assume that that high strength steels fail at the level of plastic strains corresponding to the point C of Figure 20 as in the *criterion 4*. However, the strains in lower grade steels are too large and very close to the real failure of coupons (see Figure 20). It is almost certain that some details with holes and sharp notches would not be able to reach such strains. Unfortunately, the lower grade steels were not tested in CHT configuration. All values of  $\epsilon_{eq,R}$  are reported in Table 6.

As can be seen from the comparison to real experiments in Figure 28 and Figure 29, the *criterion 5* keeps consistent level of safety throughout all the grades and still provides better results than methods 1 and 2. The required values of fracture elongation are in Table 6.

The SMCS model was selected for the evaluation of *criterion 6*. It corresponded well to the real failures observed in experiments. The critical strain at  $T = 1$  was obtained from the values of simulated coupon test  $\epsilon_{eq,f}$  and  $T_f$  (see Table 6).

$$\epsilon_{cr} = \alpha \cdot e^{-1.5} = (\epsilon_{eq,f} / e^{-1.5T_f}) \cdot e^{-1.5} = \epsilon_{eq,f} e^{1.5T_f - 1.5} \quad (25)$$

- The highest prediction was achieved by the *criterion 7*; mostly beyond the real failure. Therefore it is not useful.



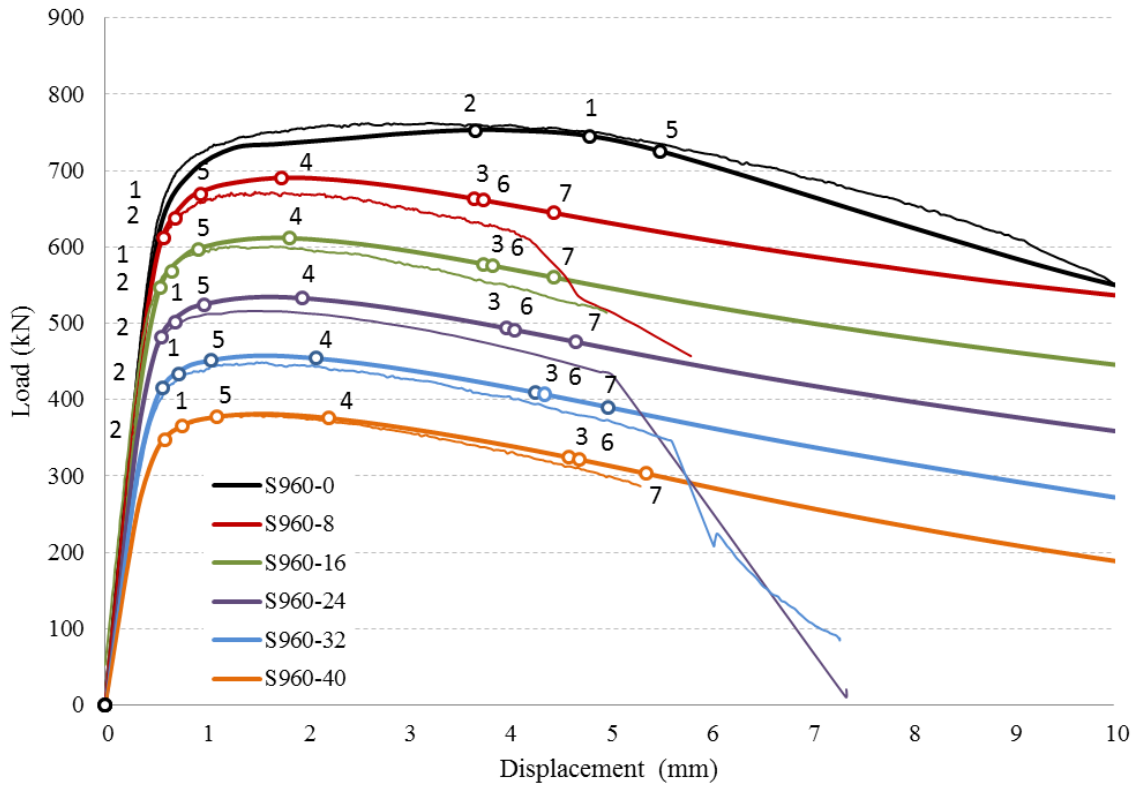


Figure 28. Comparison of numerical and experimental (thin line) results of CHT tests from grade S960; ductility criteria 1-7 are indicated by round markers.

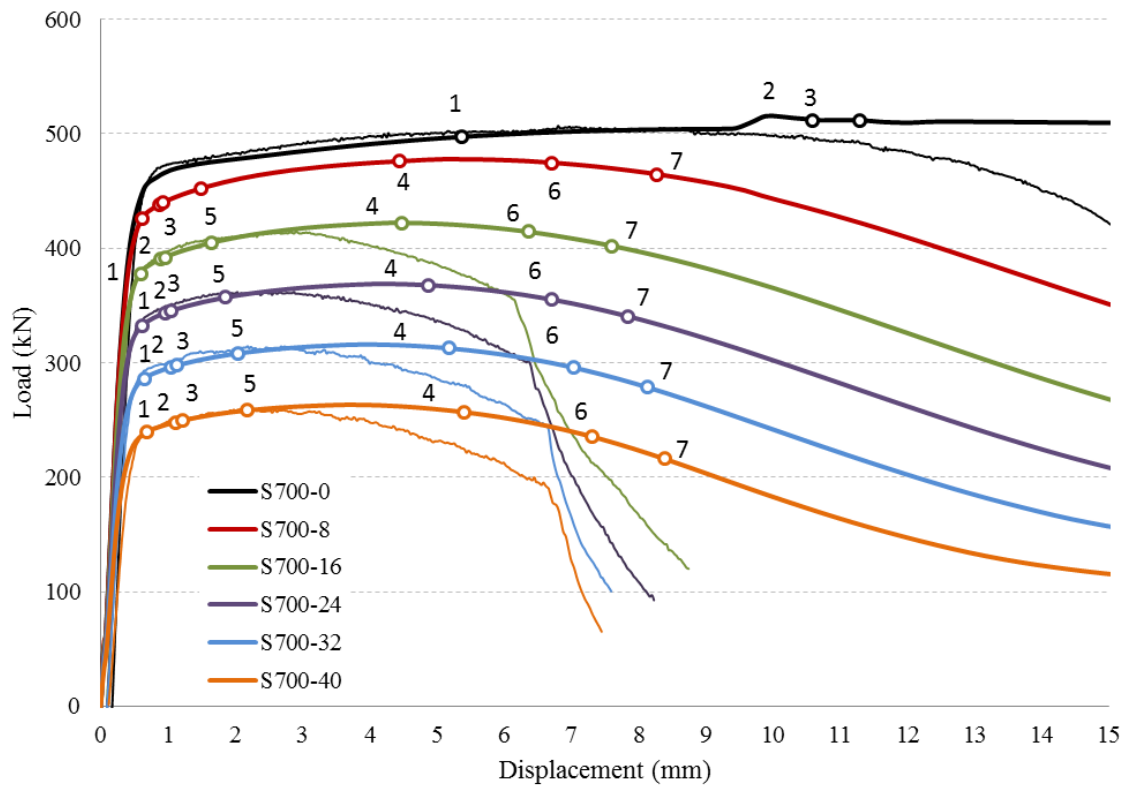


Figure 29. Comparison of numerical and experimental (thin line) results of CHT tests from grade S700; ductility criteria 1-7 are indicated by round markers.

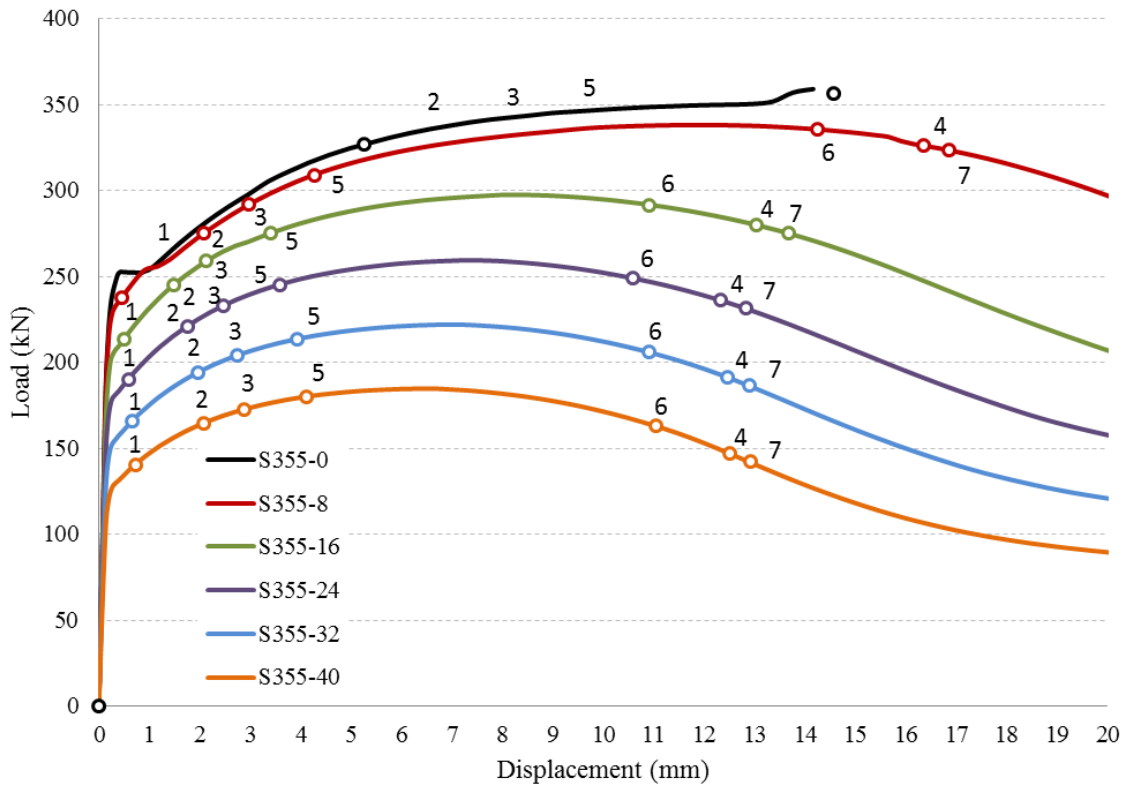


Figure 30. Numerical results of CHT tests from grade S355; ductility criteria 1-7 are indicated by round markers.

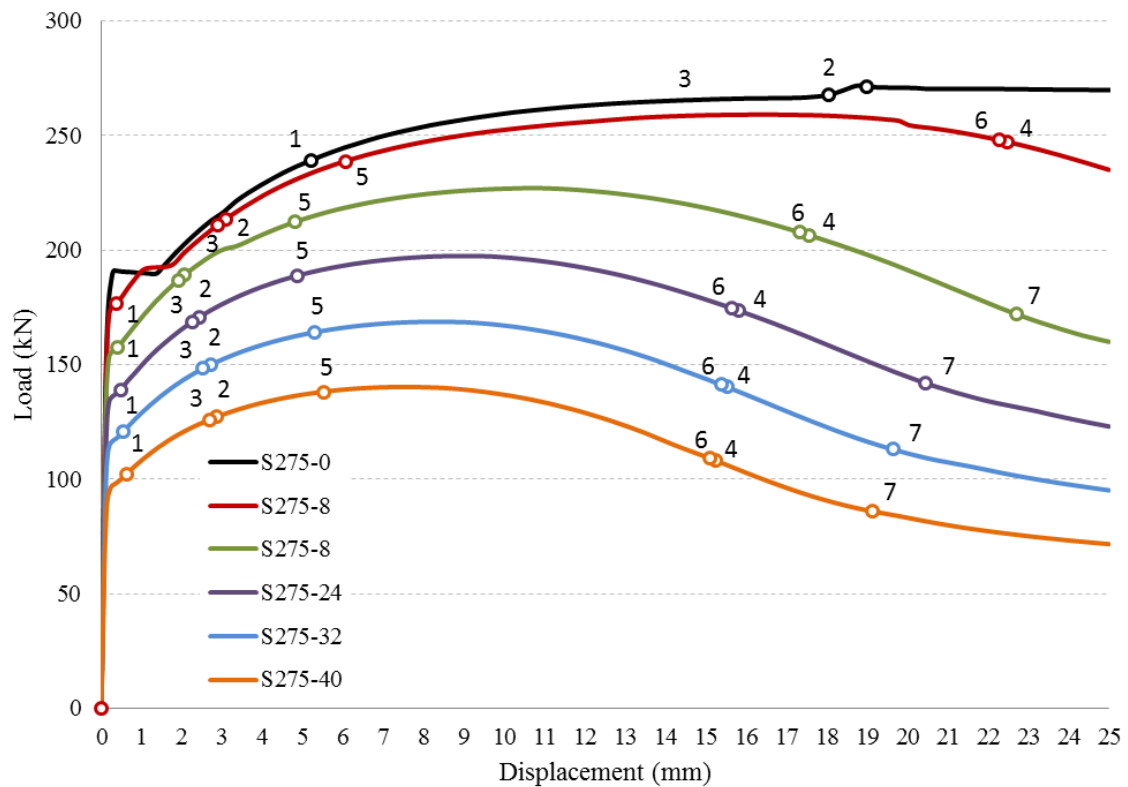


Figure 31. Numerical results of CHT tests from grade S275; ductility criteria 1-7 are indicated by round markers.



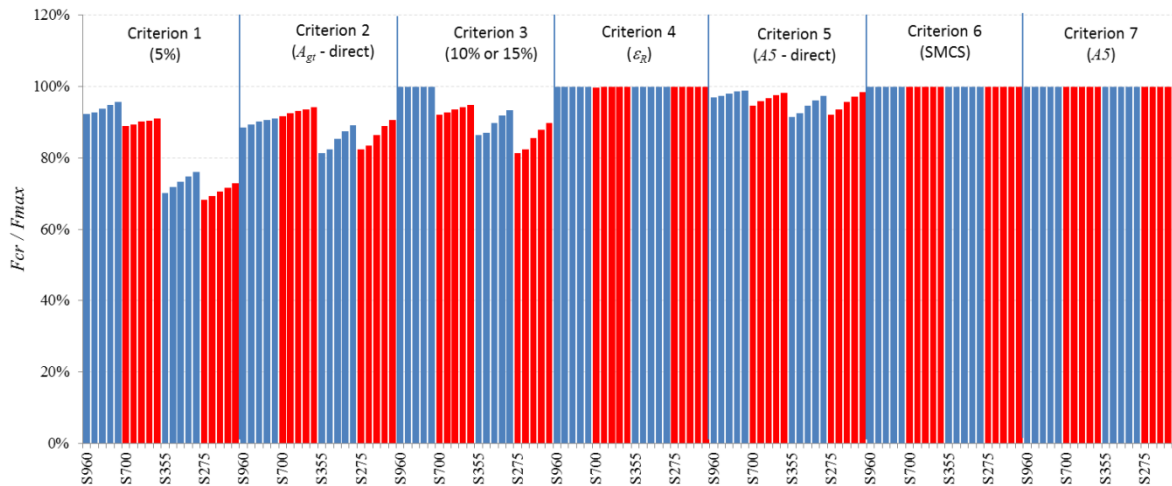


Figure 32. Comparison of maximum critical load reached in criteria 1 to 7.

### 3.3 The effect of mesh size

The effect of mesh size was studied on the specimen without hole (S700-0) and with the smallest hole (S700-8). The distance between nodes was reduced 3 times in the denser models (see Figure 33) which resulted in about 10 times larger models and calculation times (see Table 12).

Table 12. Comparison of model parameters with standard and denser mesh.

	Standard mesh		Dense mesh	
Hole diameter (mm)	0	8	0	8
Maximum distance between nodes (mm) <sup>1)</sup>	1.5		0.5	
Number of nodes x 10 <sup>3</sup>	12.8	9.72	123	88.5
Number of elements x 10 <sup>3</sup>	10.3	7.67	101	72.4
Output size (MB)	305	201	820	861
Calculation time (min) <sup>2)</sup>	18	19	234	288

<sup>1)</sup> In-plane nodes (spacing in the through-thickness direction was not changed)

<sup>2)</sup> Intel® Core™ i5-3320M CPU @ 2.60 GHz and 4.00 GB RAM, Abaqus 6.13-3

As can be seen from Figure 34, the mesh size is affecting load-displacement relation and maximum principal stresses beyond the ultimate load, but the maximum equivalent plastic strains differ from the beginning (see Figure 34). However, denser mesh always means higher stresses and strains in the stress concentration area, and therefore it is safe to assume that our predicted strain limits with the standard mesh (larger elements) can be used for every FEM calculation that has at least the same mesh density. The limits will be even more conservative if the designer creates very fine mesh.

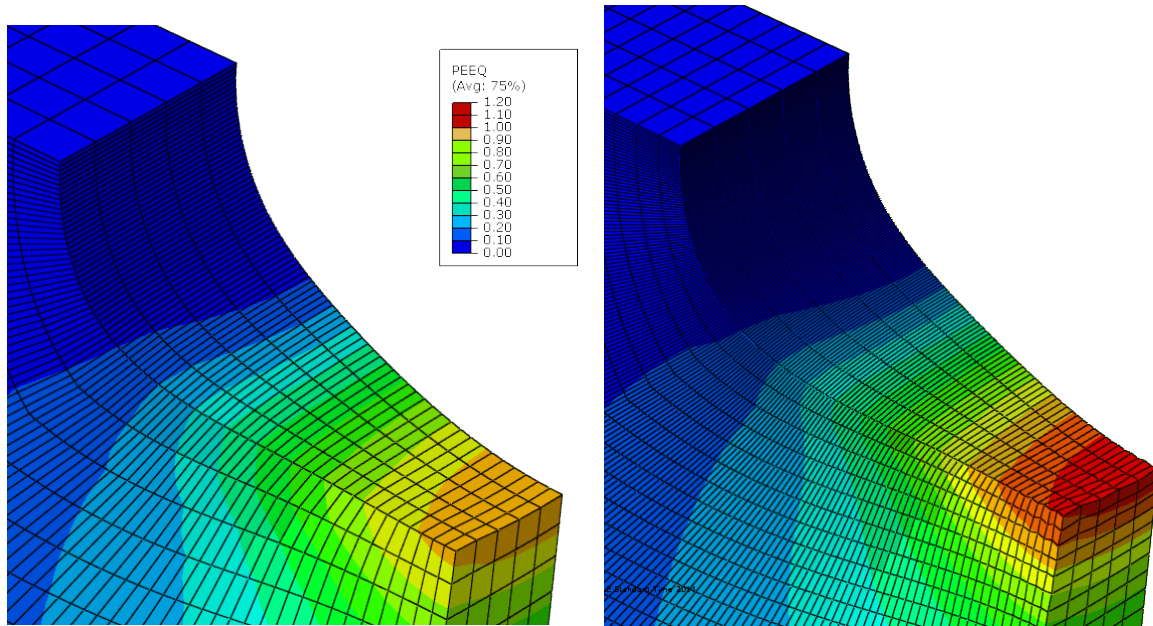


Figure 33. Comparison of equivalent strain distribution at 6 mm displacement in the standard mesh (left) and dense mesh (right).

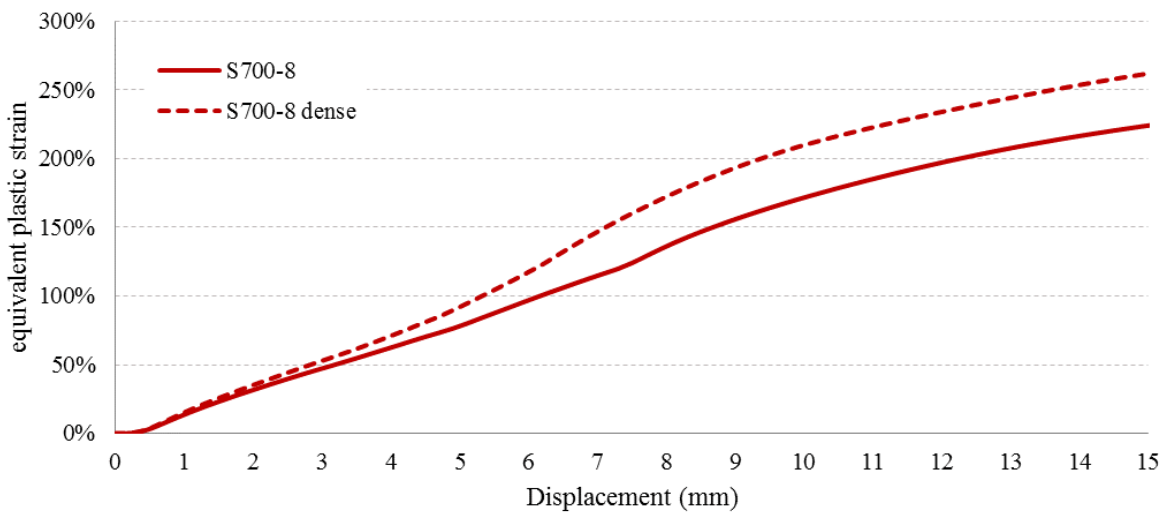
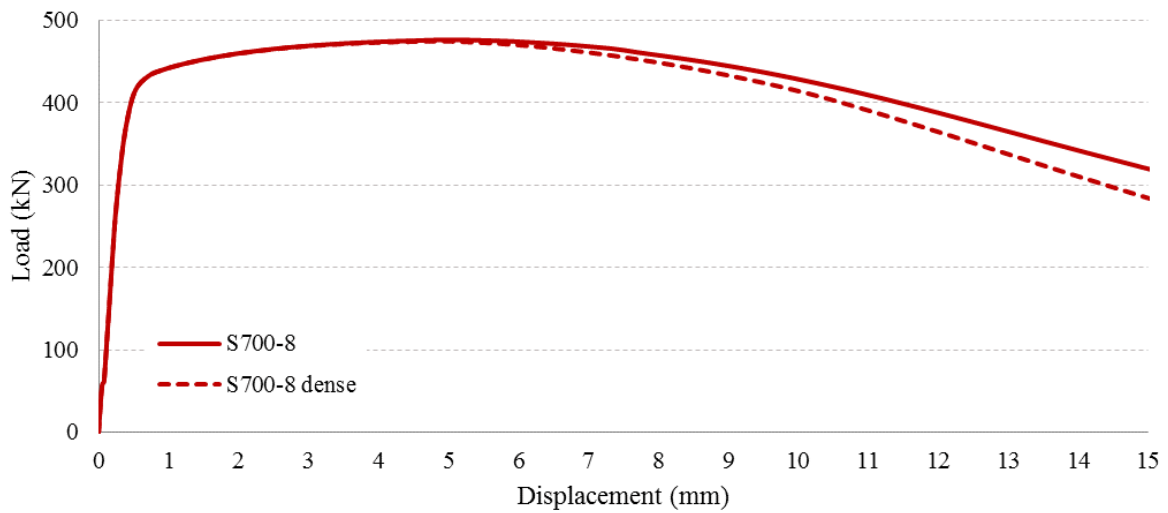


Figure 34. The effect of mesh size.

## 4. Preliminary numerical study

The following chapter describes the study on validity of existing ductility limits from Eurocode 3 and proposed new criteria. The primary focus is on high strength steels, but the results are presented for the full range of hypothetical stress-strain curves. The following design limits were used for the criteria evaluation:

- The external load must reach at least yield load in the net section  $f_y A_{net}$
- The external load must reach at least ultimate load in the net section  $f_u A_{net}$
- The deformation capacity has to be at least 3% (3 mm on 100 mm gauge length)

Our work is then divided in two parts:

- To propose the minimum required values of ductility limits written in the current form of Eurocode 3. For this purpose, we have selected a range of  $f_u/f_y$  and  $\epsilon_u$ , and investigated what is the minimum required  $A5$  elongation at coupon failure to reach the design limits.
- To propose a new alternative ductility criteria and evaluate whether the design limits are reached with these assumptions. For this purpose, the elongation at the yield load after necking  $\epsilon_R$  was used as the minimum requirement for material ductility.

In order to study the strains beyond the ultimate load, hypothetical tri-linear (engineering) stress-strain models are proposed with the variable ductile behaviour. The first preliminary parametric study covers 27 materials with different strain hardening (in true stress-strain relationship) beyond the ultimate load. The materials were selected to always reach the same limit strain  $\epsilon_R$  in the selected group, and therefore the uniform strain  $\epsilon_u$  differed within the group (see for example three materials from group X3 in Figure 35). The complete summary of material models are presented in Annex B: Simplified material models.

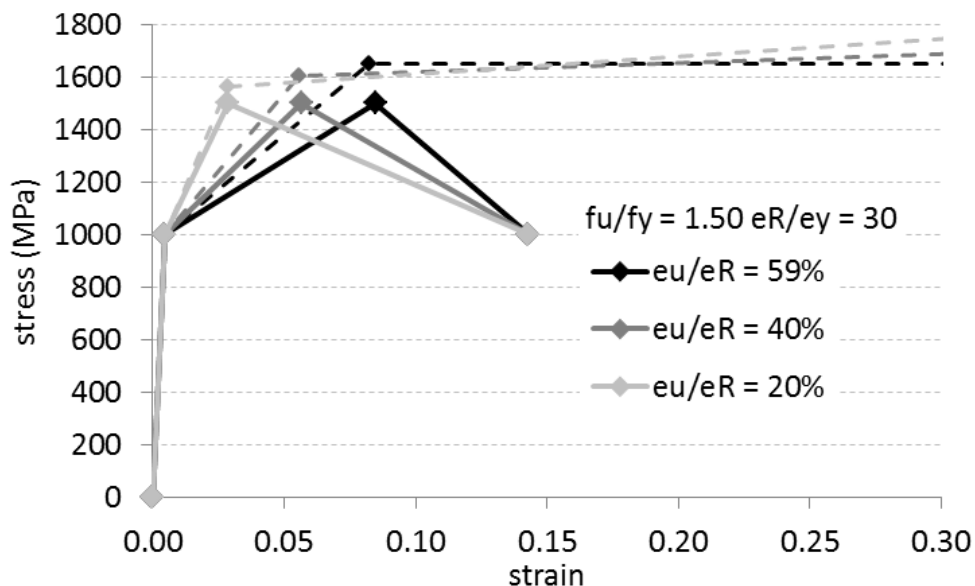


Figure 35. Example of material models of group X3 with  $f_u/f_y$  ratio 1.5 and  $\epsilon_R/\epsilon_y$  ratio 30; solid line - engineering values, dashed line - true values.

Our limiting assumption was that the steel is not softening (in true stress-strain relationship) because softening of metals happens only in connection with large microcracks or dynamic recrystallization at higher temperatures.

## 4.1 Material model parameters

### (a) Modulus of elasticity $E$

The value of Young's modulus was assumed to be constant 210 GPa as recommended by the Eurocode 3 [1].

### (b) Yield strength $f_y$

Single value 1000 MPa was used as the material yield strength.

### (c) Ultimate strength $f_u$

We have selected 1050 MPa, 1100 MPa and 1500 MPa for the material ultimate strengths. This corresponds to the ductility limits in EN 1993-1-1 and EN 1993-1-12 where the ratio  $f_u/f_y$  should be higher or equal to 1.1 or 1.05 respectively. The last option represents  $f_u/f_y$  ratio typical for mild steel grades and is used for the reference.

### (d) Limit strain $\varepsilon_R$

The limit strain  $\varepsilon_R$  is defined as the total engineering strain higher than the ultimate (uniform) strain, where the engineering stress reaches the value of the material yield strength in the descending part of the stress-strain diagram (criterion 4 of Table 8). The selected values are 4.76%, 14.3% and 28.6% which correspond to the  $\varepsilon_R/\varepsilon_y$  ratios of 10, 30 and 60 respectively. The lowest level of the limit strain can be limited by the assumption that the true stress does not decrease with higher strains (material is not softening). This happens when high  $f_u/f_y$  values are selected. Therefore we had to choose the alternative  $\varepsilon_R/\varepsilon_y$  ratios 20, 30 and 60 for the reference materials with  $f_u/f_y = 1.5$ .

### (e) Ultimate (uniform) strain $\varepsilon_u$

The value  $\varepsilon_u$  (or  $A_{gt}$  in testing standards) lies between the yield strain  $\varepsilon_y$  and the limit strain  $\varepsilon_R$ . While the lower limit can theoretically be very close to the yield strain, the ultimate (uniform) strain upper limit is strictly given by the assumption of non-softening material in terms of true stress-strain. This limit can be calculated if we assume the worst scenario when true stress does not grow after it reaches the value corresponding to the ultimate load. Finite element calculations predict this limit to be between 37% and 95% of  $\varepsilon_R$  in the selected material models. The whole procedure is described in the Annex C: The upper limit of ultimate strain. Then two more values of  $\varepsilon_u$  were selected; the lower value 20% of  $\varepsilon_R$  and the average between the upper limit and lower value that ranges between 29% and 58% of  $\varepsilon_R$ .

The summary of simplified material model parameters is in Table 13 and their stress-strain diagrams in the Annex B: Simplified material models. Materials are sorted into three groups according to their ultimate strength (group A:  $f_u/f_y = 1.05$ , group B:  $f_u/f_y = 1.1$  and the reference group X:  $f_u/f_y = 1.5$ ). The second character in material designation represents the limit strain value (1:  $\varepsilon_R/\varepsilon_y = 10$ , 2:  $\varepsilon_R/\varepsilon_y = 20$ , 3:  $\varepsilon_R/\varepsilon_y = 30$  and 6:  $\varepsilon_R/\varepsilon_y = 60$ ). Finally, three different positions of the ultimate strain are marked with letters a, b and c.

Table 13. Simplified material model parameters.

Model		$f_u/f_y$	$\epsilon_R/\epsilon_y$	$\epsilon_R$	$\epsilon_u/\epsilon_R$	$\epsilon_u$
1	A1a	1.05	10	0.048	0.67	0.032
2	A1b				0.43	0.021
3	A1c				0.20	0.010
4	A3a		30	0.143	0.90	0.128
5	A3b				0.55	0.078
6	A3c				0.20	0.029
7	A6a		60	0.286	0.95	0.272
8	A6b				0.58	0.165
9	A6c				0.20	0.057
10	B1a	1.10	10	0.048	0.48	0.023
11	B1b				0.34	0.016
12	B1c				0.20	0.010
13	B3a		30	0.143	0.83	0.119
14	B3b				0.52	0.074
15	B3c				0.20	0.029
16	B6a		60	0.286	0.92	0.264
17	B6b				0.56	0.161
18	B6c				0.20	0.057
19	X2a	1.50	20	0.095	0.37	0.036
20	X2b				0.29	0.027
21	X2c				0.20	0.019
22	X3a		30	0.143	0.59	0.085
23	X3b				0.40	0.057
24	X3c				0.20	0.029
25	X6a		60	0.286	0.81	0.232
26	X6b				0.51	0.145
27	X6c				0.20	0.057

## 4.2 True stress-strain curves

True stress-strain curves for the Abaqus model were obtained using similar approach as for the real measured data. In this case the desired load-displacement could be easily calculated from the given points of engineering stress-strain curve (see Figure 37). However, since only single data point exists beyond the ultimate (uniform) strain, the former iteration method was inconvenient because it produces relatively large bias in terms of predicted true strains. Therefore more robust method was selected that compares loads directly and the correction factor  $c$  is divided by two in each step. As can be seen from the Figure 36, the stress correction is related to the distance from the ultimate (uniform) strain (factor  $m$  of the Hollomon's model [27]). This method is slower but more reliable for the simplified material models. For instance the material A1b on Figure 37 fulfilled the criteria after 7 iterations.

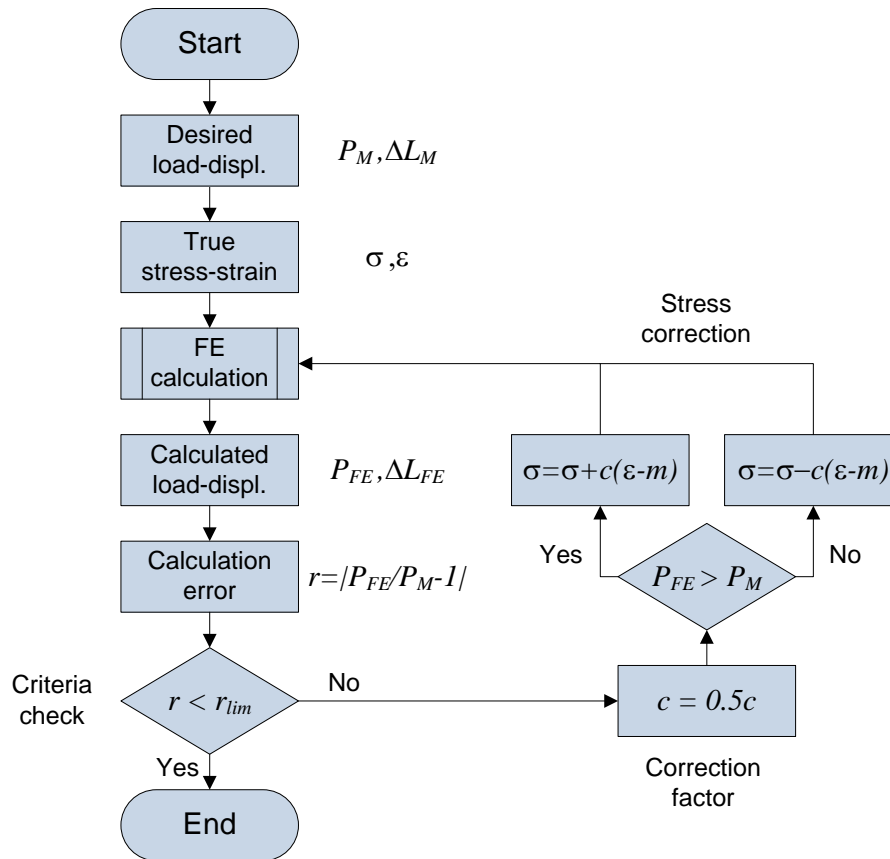


Figure 36. Iterative procedure used for simplified material models.

The resulting true stress-strain model is also tri-linear, where the slope of the last segment is called  $\gamma$  and is expressed in MPa per % of true strain in Table 14. There is no upper limit of true plastic strains in the final material models. The slope  $\gamma$  varies between 0 and 16.5 MPa/% in A1a and X6c materials respectively.

$$\gamma = \frac{\sigma_{t,100} - \sigma_{t,u}}{1 - \varepsilon_{t,pl,u}} \quad (26)$$

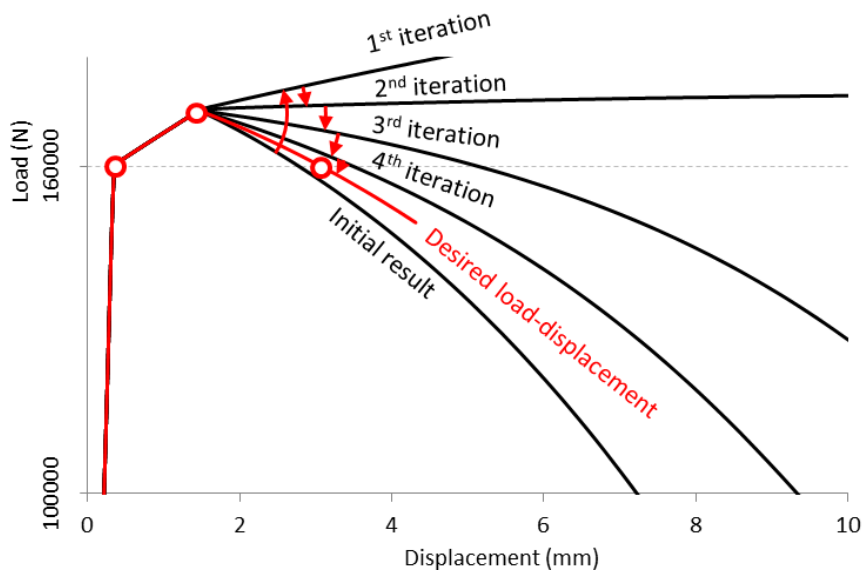


Figure 37. Example of numerical stress-strain characterization (model A1b).

Table 14. Simplified true stress-strain models' parameters.

Model	$\varepsilon_{t,pl,u}$	$\sigma_{t,u}$ (MPa)	$\sigma_{t,100}$ (MPa)	$\gamma$ (MPa/%)	
1	A1a	0.0264	1096	1096	0.00
2	A1b	0.0155	1084	1386	3.07
3	A1c	0.0044	1072	1586	5.16
4	A3a	0.1159	1198	1315	1.32
5	A3b	0.0706	1145	1907	8.20
6	A3c	0.0232	1092	2091	10.2
7	A6a	0.2367	1352	1810	6.00
8	A6b	0.1481	1238	2293	12.4
9	A6c	0.0508	1123	2314	12.6
10	B1a	0.0173	1138	1138	0.00
11	B1b	0.0108	1131	1245	1.15
12	B1c	0.0042	1123	1374	2.52
13	B3a	0.1079	1246	1246	0.00
14	B3b	0.0663	1195	1830	6.80
15	B3c	0.0230	1145	2038	9.14
16	B6a	0.2301	1408	1556	1.92
17	B6b	0.1443	1292	2311	11.9
18	B6c	0.0505	1177	2349	12.3
19	X2a	0.0279	1573	1573	0.00
20	X2b	0.0198	1560	1560	0.00
21	X2c	0.0117	1548	1682	1.36
22	X3a	0.0746	1648	1648	0.00
23	X3b	0.0482	1605	1930	3.41
24	X3c	0.0211	1562	2221	6.73
25	X6a	0.2029	1874	1874	0.00
26	X6b	0.1288	1740	2753	11.6
27	X6c	0.0487	1606	3171	16.5

The final true stress-strain curves are presented in Annex B: Simplified material models and their parameters in Table 14. The table shows calculated true stress and true plastic strain at the ultimate load  $\sigma_{t,u}$  and  $\varepsilon_{t,pl,u}$  respectively. It should be noted that the first point of the material plasticity definition in finite element solvers is true yield stress which is always 1003 MPa in our study.

### 4.3 Maximum plastic strain and stress triaxiality

The limit deformation corresponding to the limit engineering strain  $\varepsilon_R$  is considered to be the failure of simulated specimen. Because this area is beyond the ultimate load, the strain in the critical cross-section is not uniformly distributed. Then the maximum equivalent plastic strain  $\varepsilon_{eq}$  and the stress triaxiality  $T$  are always in the middle of coupon cross-section. Those two parameters are usually basis of ductile failure predictive models. They are presented in Figure 38, Figure 39 and Table 15. The results are calculated at the limit strain  $\varepsilon_R$  ( $\varepsilon_{eq,R}$  and  $T_R$ ) and minimum elongation at failure allowed by EN 1993-1-12, 10% ( $\varepsilon_{eq,10}$  and  $T_{10}$ ).



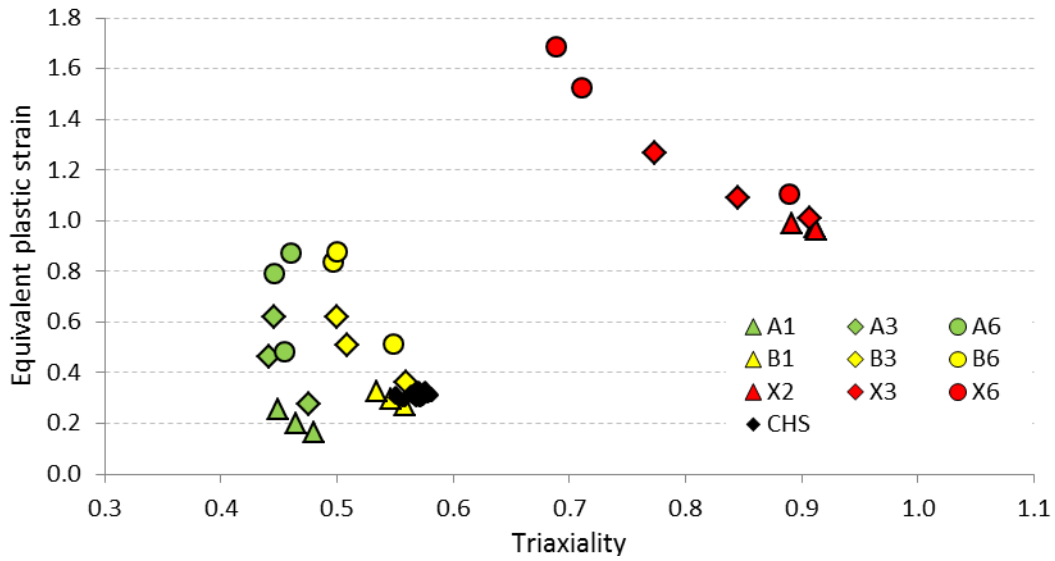


Figure 38. Maximum equivalent plastic strain and stress triaxiality at the limit strain  $\varepsilon_R$ .

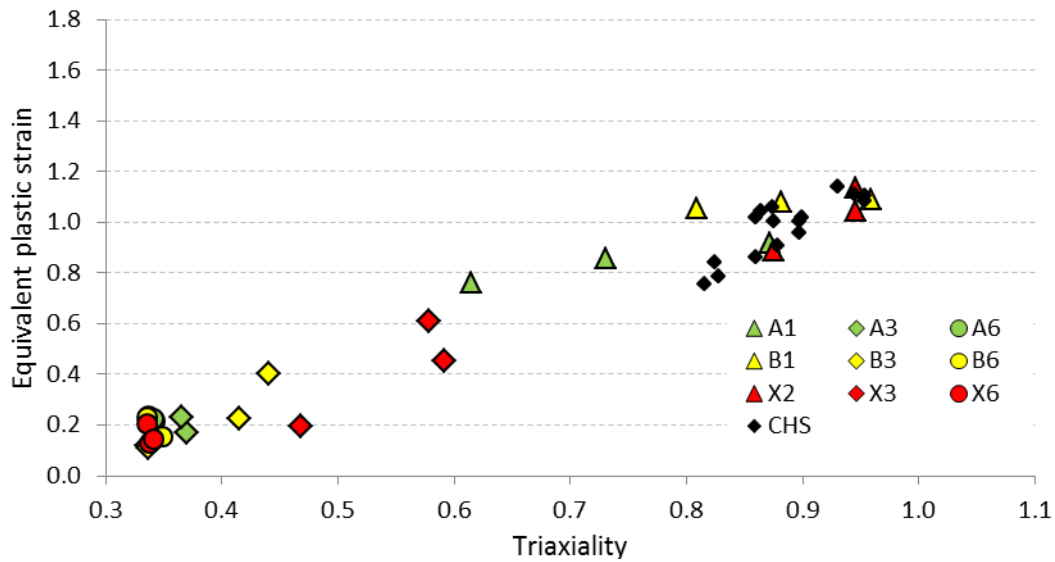


Figure 39. Maximum equivalent plastic strain and stress triaxiality at the limit elongation 10%.

The simplified models results in Figure 38 and Figure 39 are compared to the 16 values of real experiments with S960 steel (see Table 6).

Table 15. Maximum equivalent plastic strain and stress triaxiality.

Model		$\varepsilon_R$	$\varepsilon_{eq,R}$	$T_R$	$\varepsilon_{eq,10}$	$T_{10}$
1	A1a	0.048	0.171	0.481	0.916	0.872
2	A1b		0.206	0.465	0.858	0.730
3	A1c		0.266	0.450	0.760	0.615
4	A3a	0.143	0.282	0.476	0.117	0.336
5	A3b		0.473	0.441	0.172	0.370
6	A3c		0.638	0.446	0.230	0.365
7	A6a	0.286	0.492	0.455	0.237	0.337
8	A6b		0.809	0.446	0.215	0.342
9	A6c		0.951	0.461	0.227	0.341
10	B1a	0.048	0.279	0.558	1.090	0.959
11	B1b		0.303	0.546	1.081	0.882
12	B1c		0.334	0.534	1.052	0.809
13	B3a	0.143	0.370	0.559	0.109	0.337
14	B3b		0.518	0.509	0.225	0.415
15	B3c		0.629	0.500	0.400	0.440
16	B6a	0.286	0.521	0.548	0.231	0.336
17	B6b		0.847	0.496	0.156	0.346
18	B6c		0.889	0.500	0.156	0.349
19	X2a	0.095	0.976	0.912	0.887	0.875
20	X2b		0.970	0.913	1.043	0.946
21	X2c		0.995	0.891	1.137	0.946
22	X3a	0.143	1.013	0.906	0.195	0.469
23	X3b		1.097	0.846	0.451	0.591
24	X3c		1.270	0.774	0.608	0.579
25	X6a	0.286	1.109	0.890	0.205	0.336
26	X6b		1.529	0.710	0.131	0.338
27	X6c		1.820	0.689	0.145	0.342

It can be clearly observed that higher  $f_u/f_y$  ratio results also in higher stress triaxiality and equivalent plastic strain at the limit deformation  $\varepsilon_R$ . increasing the limit strain  $\varepsilon_R$  increases also the equivalent plastic strain in the most critical cross-section, however, the triaxiality tends to be lower. Finally the position of the ultimate (uniform) strain  $\varepsilon_u$  between  $\varepsilon_y$  and  $\varepsilon_R$  is also important and the most critical are the highest values. The lowest equivalent plastic strain at the limit point was therefore achieved in material A1a (17.1%) at the limit point.

#### 4.4 Evaluation of Eurocode ductility criteria

The goal of this study is to predict the minimum allowable elongation at failure  $A5$  (of coupons) for the materials with certain  $f_u/f_y$  and  $\varepsilon_u/\varepsilon_y$  to be able to reach maximum design load. The method we used here is based on the knowledge of equivalent plastic strains of both, coupon and detail with stress concentration. Then the design limit of the detail (e.g. the ultimate load as in Figure 40) can be translated to the corresponding plastic strain and then converted back to the elongation of material coupons. The assumption is that the strain at the failure is equal in both cases. It is conservative because the triaxiality at failure in CHT is always higher than the triaxiality at failure in coupons.

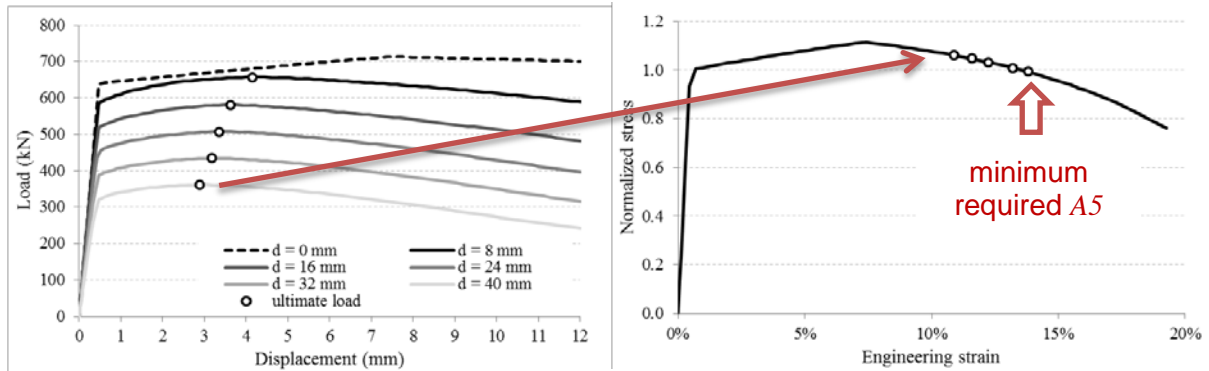


Figure 40. Example results of CHT simulations (left), from where the design limits (ultimate load in this case) is transposed to the corresponding material stress-strain curve (right).

We have calculated 135 CHT models and 27 reference models without hole using the set of simplified materials developed in the previous section. For those models we were able to propose minimum required elongation at failure to reach four design limits: (1) yield load of the net section  $f_y A_{net}$ , (2) ultimate load of the net section  $f_u A_{net}$ , and (3) 3 mm displacement. The ultimate net section load value  $f_u A_{net}$  was slightly exceeded in all of the simulations (see Table 24 in Annex D: CHT simulations of simplified material models), and therefore the limit  $f_u A_{net}$  is safe.

Table 16. A5 limits for simplified models with variable strain hardening.

Material group	$f_u/f_y$	$\epsilon_u/\epsilon_y$	A5 to reach $f_y A_{net}$	A5 to reach $f_u A_{net}$	A5 to reach 3% elongation <sup>1)</sup>	
1	A1	1.05	6.4	4.9%	5.6%	8.6%
2	A3		24.7	12.4%	14.7%	16.5%
3	A6		37.7	23.3%	26.6%	28.1%
4	B1	1.10	3.5	4.1%	4.9%	7.7%
5	B3		17.5	12.1%	16.2%	15.3%
6	B6		37.8	24.0%	29.5%	27.6%
7	X2	1.50	6.0	4.4%	6.4%	7.0%
8	X3		13.4	8.4%	13.8%	10.4%
9	X6		35.4	21.0%	95.3%	23.6%

<sup>1)</sup> 3 mm displacement on the gauge length 100 mm

The highest A5 recommendation was always produced by the smallest hole and highest  $\epsilon_u/\epsilon_R$  ratio. Therefore only materials indexed “a” are presented in the combination with the smallest hole diameter (e.g. A1a-8, B3a-8, and so on) in Table 16. Materials indexed “a” are those, where ideally plastic behaviour of true stress-strain model was assumed after necking. This means that we need only three material parameters from coupon testing to determine the ductility limit A5 of given steel grade:  $f_y$  (or  $R_{p02}$ ),  $f_u$  (or  $R_m$ ) and  $\epsilon_u$  (or  $A_{gt}$ ). As the most important parameter that governs required A5 elongation to reach the limits was recognized  $\epsilon_u/\epsilon_y$  ratio that is given in Table 16 for each of the material groups. It should be noted that all the presented results are valid only for  $f_y = 1000$  MPa and CHT specimens with hole diameter at least 8 mm.

## 4.5 Alternative ductility criteria

As an alternative to the current Eurocode ductility limits, the simple requirement was proposed that the material in coupon test has to reach at least the elongation  $\varepsilon_R$  corresponding to the yield load level after necking (point C in Figure 20). All of our tested materials fulfilled this condition, however, mild steels failed very close after  $\varepsilon_R$ . As well as in the previous section, we were testing if 5 types of CHT specimens made from 27 hypothetical materials are able to reach  $f_y A_{net}$ ,  $0.98 f_u A_{net}$ ,  $f_u A_{net}$  and 3% elongation before failure.

The simplified assumption that the strains at the failure are equal ( $\varepsilon_{eq,f,CHT} = \varepsilon_{eq,f}$ ) is unconservative, and therefore we had to predict the critical strain  $\varepsilon_{cr}$  of CHT specimens using one of the failure models. With the knowledge of strain-triaxiality relationship during the loading of CHT specimens, we have calculated the point of interception with SMCS model based on coupon data (see example results from A1a material in Figure 41). As can be seen from Table 17 and Figure 41, the critical strain was always lowest with 8 mm hole, and therefore the results presented in Table 18 and Table 19 correspond to the smallest tested diameter.

Table 17. Equivalent plastic strain  $\varepsilon_{eq,R}$  and predicted  $\varepsilon_{eq,R,CHT}$  by SMCS.

Model		Coupon $\varepsilon_{eq,R}$	CHT 8 mm $\varepsilon_{cr}$	CHT 16 mm $\varepsilon_{cr}$	CHT 24 mm $\varepsilon_{cr}$	CHT 32 mm $\varepsilon_{cr}$	CHT 40 mm $\varepsilon_{cr}$
1	A1a	17.1%	13.2%	14.6%	15.2%	15.6%	15.8%
2	A1b	20.6%	15.8%	17.4%	18.0%	18.6%	18.9%
3	A1c	26.6%	20.4%	22.5%	23.4%	24.0%	24.3%
4	A3a	28.2%	23.8%	25.7%	26.5%	26.8%	27.1%
5	A3b	47.3%	39.8%	41.6%	43.0%	43.9%	44.3%
6	A3c	63.8%	56.5%	58.4%	59.7%	60.6%	61.0%
7	A6a	49.2%	43.9%	45.7%	46.8%	47.3%	47.4%
8	A6b	80.9%	74.5%	76.3%	77.9%	78.6%	78.5%
9	A6c	95.1%	91.5%	92.1%	92.9%	93.0%	92.4%
10	B1a	27.9%	23.5%	25.3%	25.9%	26.5%	26.7%
11	B1b	30.3%	25.3%	27.4%	28.1%	28.6%	28.9%
12	B1c	33.4%	28.1%	30.3%	31.1%	31.7%	31.9%
13	B3a	37.0%	34.1%	35.0%	35.9%	36.4%	36.5%
14	B3b	51.8%	47.3%	48.7%	49.9%	50.5%	50.7%
15	B3c	62.9%	59.2%	60.7%	61.7%	62.3%	62.5%
16	B6a	52.1%	51.1%	52.2%	52.7%	52.8%	52.6%
17	B6b	84.7%	84.8%	84.6%	85.4%	85.5%	85.0%
18	B6c	88.9%	88.0%	88.9%	89.7%	89.8%	89.4%
19	X2a	97.6%	n/a <sup>1)</sup>	122.1%	111.8%	108.3%	108.2%
20	X2b	97.0%	n/a <sup>1)</sup>	125.4%	113.1%	109.0%	108.4%
21	X2c	99.5%	166.4%	129.3%	119.9%	115.7%	114.5%
22	X3a	101.3%	134.8%	114.9%	109.6%	108.3%	110.1%
23	X3b	109.7%	145.5%	129.6%	123.5%	121.9%	122.7%
24	X3c	127.0%	152.6%	144.5%	141.1%	139.8%	142.3%
25	X6a	110.9%	n/a <sup>1)</sup>	123.0%	120.8%	120.9%	124.4%
26	X6b	152.9%	n/a <sup>1)</sup>	n/a <sup>1)</sup>	n/a <sup>1)</sup>	n/a <sup>1)</sup>	n/a <sup>1)</sup>
27	X6c	182.0%	n/a <sup>1)</sup>	n/a <sup>1)</sup>	n/a <sup>1)</sup>	n/a <sup>1)</sup>	n/a <sup>1)</sup>

<sup>1)</sup>  $\varepsilon_{eq,R,CHT}$  was not reached within the simulation limits

It can be seen from Table 18 that all of the materials were able to reach 98% of ultimate load  $f_u A_{net}$ . Moreover most of them exceeded also the ultimate load itself, and therefore the design equation for the resistance of net section in Eurocode may be used in combination with this alternative ductility criterion. It has to be of course confirmed with the reliability analysis. The study is limited to the lowest  $f_u/f_y$  ratio 1.05 and it is possible that the materials with lower  $f_u/f_y$  ratio (e.g. S960 with  $f_u/f_y = 1.02$ ) may fail to satisfy these limits.

Additionally, the elongation of at least 3% (3 mm in 100 mm gauge length) was tested against the proposed criterion. The results in form of calculated elongation at the level of  $\epsilon_{cr}$  are presented in Table 19. Also here the materials with high  $f_u/f_y$  ratio show better performance and, in fact, most of the material models similar to high strength steels didn't reach the desired elongation.

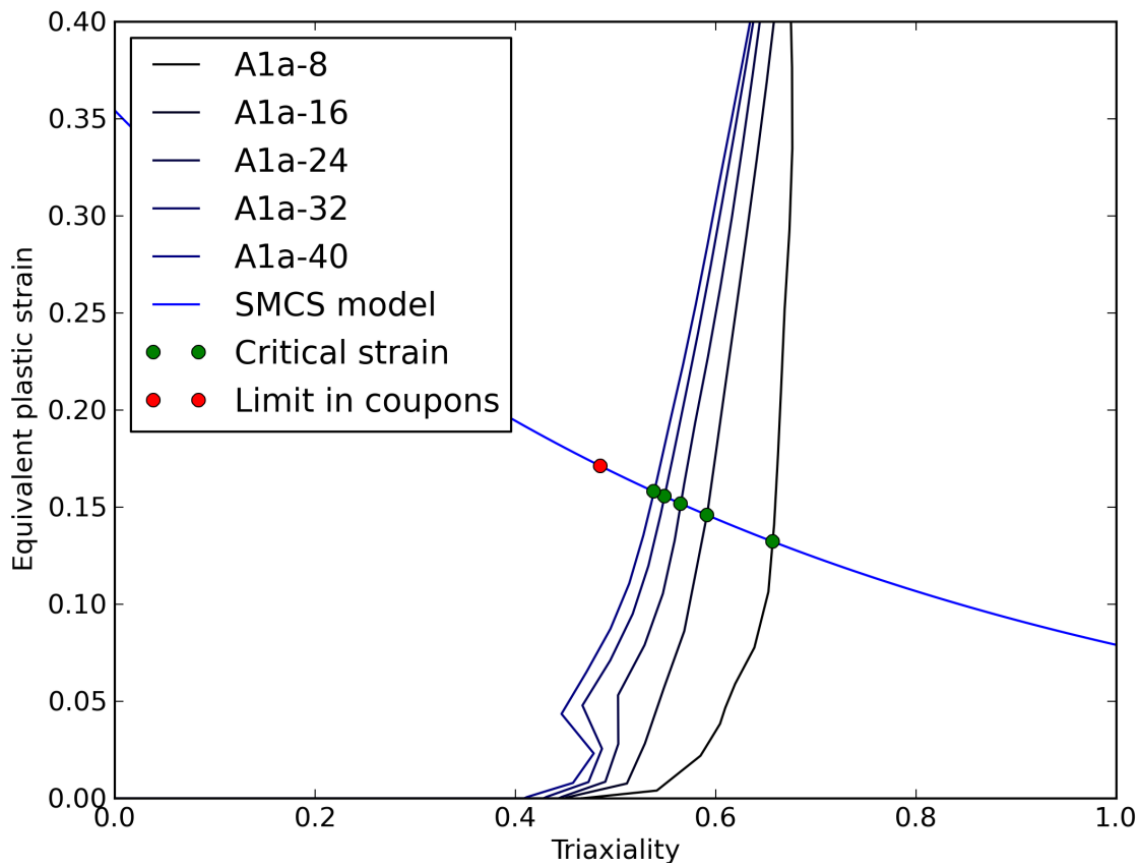


Figure 41. Calculation of critical strain  $\epsilon_{cr}$  based on SMCS model from coupon test data.

Table 18. Maximum load at  $\varepsilon_{cr}$  for all studied materials.

Material group		$f_u/f_y$	$\varepsilon_u/\varepsilon_R$	$\varepsilon_R = 10\varepsilon_y$	$\varepsilon_R = 30\varepsilon_y$	$\varepsilon_R = 30\varepsilon_y$
1	A1	1.06	0.63	$\geq 0.98 f_u A_{net}$	$\geq f_u A_{net}$	$\geq f_u A_{net}$
2	A3		0.43	$\geq 0.98 f_u A_{net}$	$\geq f_u A_{net}$	$\geq f_u A_{net}$
3	A6		0.18	$\geq f_u A_{net}$	$\geq f_u A_{net}$	$\geq f_u A_{net}$
4	B1	1.11	0.86	$\geq f_u A_{net}$	$\geq f_u A_{net}$	$\geq f_u A_{net}$
5	B3		0.51	$\geq f_u A_{net}$	$\geq f_u A_{net}$	$\geq f_u A_{net}$
6	B6		0.22	$\geq 0.98 f_u A_{net}$	$\geq f_u A_{net}$	$\geq f_u A_{net}$
7	X2	1.52	0.88	$\geq f_u A_{net}$	$\geq f_u A_{net}$	$\geq f_u A_{net}$
8	X3		0.60	$\geq f_u A_{net}$	$\geq f_u A_{net}$	$\geq f_u A_{net}$
9	X6		0.58	$\geq f_u A_{net}$	$\geq f_u A_{net}$	$\geq f_u A_{net}$

 Table 19. Elongation at  $\varepsilon_{cr}$  for all studied materials.

Material group		$f_u/f_y$	$\varepsilon_u/\varepsilon_R$	$\varepsilon_R = 10\varepsilon_y$	$\varepsilon_R = 30\varepsilon_y$	$\varepsilon_R = 30\varepsilon_y$
1	A1	1.06	0.63	0.74%	0.80%	0.88%
2	A3		0.43	0.98%	1.42%	1.85%
3	A6		0.18	1.48%	2.51%	3.19%
4	B1	1.11	0.86	1.09%	1.10%	1.11%
5	B3		0.51	1.40%	1.80%	2.11%
6	B6		0.22	1.91%	3.15%	3.64%
7	X2	1.52	0.88	4.82%	4.47%	4.26%
8	X3		0.60	6.62%	6.14%	5.17%
9	X6		0.58	$\geq 7.5\%$	$\geq 7.5\%$	$\geq 7.5\%$

## 5. Final parametric study

---

The smaller preliminary numerical study on 27 material models combined with five configurations of centre hole tension (CHT) specimens was followed by larger study on 196 material models combined with the most critical configuration of CHT specimen and side notch tension (SNT) specimen. This created a database of 750 numerical test results of coupons, CHT and SNT details with 223 different material models.

The results of the preliminary numerical study confirmed our assumption that the most conservative results were obtained from the materials without strain hardening beyond the ultimate load (A1c, A3c, A6c, B1c ...) but the effect of strain hardening slope was not very significant. Therefore the final parametric study considers all the materials without strain hardening after  $\varepsilon_u$  and it is focused on larger variation of basic material parameters ( $f_u/f_y$  and  $\varepsilon_u$ ) and the effect of material strength  $f_y$ . No iterations were needed to obtain true stress-strain hardening rate in this study.

### 5.1 Material model parameters

#### (a) Modulus of elasticity $E$

The value of Young's modulus was assumed to be constant 210 GPa as recommended by the Eurocode 3 [1].

#### (b) Yield strength $f_y$

In this study the effect of variable material strength was covered by selecting the engineering stress at yield 250 MPa, 500 MPa, 750 MPa or 1000 MPa.

#### (c) Ultimate strength $f_u$

The ultimate strength varies from the yield strength level (ideally elastic-plastic material) to  $1.5 f_y$  in the second parametrical study. The selected  $f_u/f_y$  ratios are 1.0, 1.02 (limit for S960 according to EN 10025-6), 1.05 (limit for S460 to S700 according to EN 1993-1-12), 1.10 (limit for S275 to S355 according to EN 1993-1-1) and then 1.2, 1.3 and 1.5 to cover typical range of mild steel grades.

#### (d) Ultimate (uniform) strain $\varepsilon_u$

The value  $\varepsilon_u$  (or  $A_{gt}$  in testing standards) was proposed to be 2%, 5%, 10%, 20%, 30%, 40% and 50%. However, the low  $f_u/f_y$  ratios didn't allow higher uniform strains to be developed during simulation of coupon tests before the onset of diffuse necking and the resulting upper limits of uniform strains were sometimes lower (49% for  $f_u/f_y = 1.5$ , 48% for  $f_u/f_y = 1.3$ , 47% for  $f_u/f_y = 1.2$ , 42% for  $f_u/f_y = 1.1$ , 31% for  $f_u/f_y = 1.05$ , 25% for  $f_u/f_y = 1.02$  and 20% for  $f_u/f_y = 1.0$ ) as demonstrated on Figure 42.



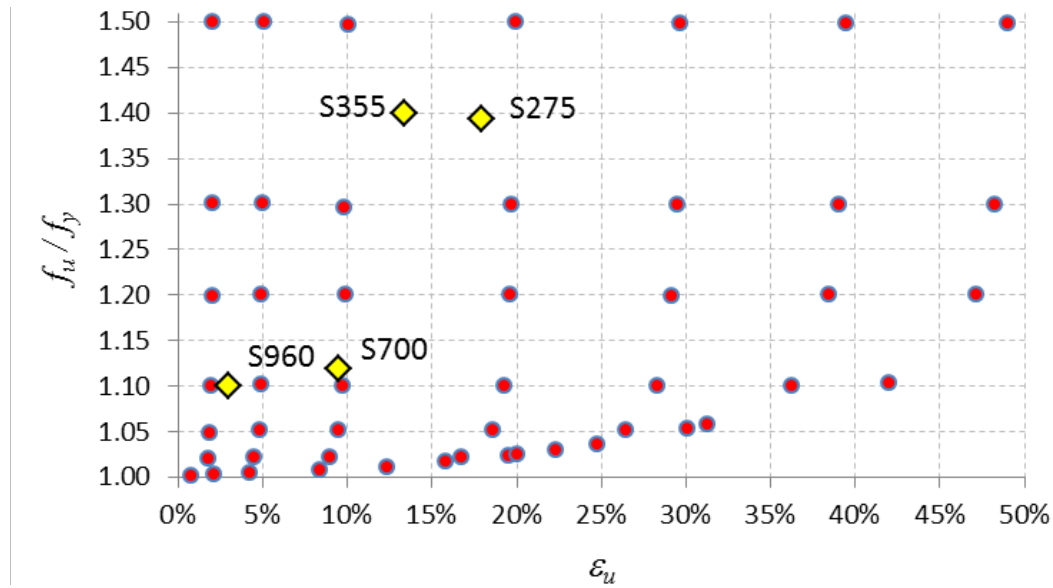


Figure 42. Example of simplified material model parameters (red dots) and experimental results (yellow diamonds) from the material group S1.

## 5.2 Evaluation of Eurocode ductility criteria

The selection of uniform strain values in the preliminary numerical study was not very practical for this kind of evaluation and many materials and geometries showed to provide always conservative results. Therefore 196 new material models (Table 20 and Table 21) were selected with no strain hardening after necking (ideally plastic true stress-strain curve) and only the smallest diameter of hole in CHT tests (8 mm). In addition to those 196 coupon and 196 CHT calculations, we have calculated 196 similar details with side notch in tension (SNT). This is practically the same numerical model with the longitudinal symmetry plane on the opposite side than the CHT specimen.

The evaluation method was the same as in previous study and the virtual tests covered both, coupons and details with stress concentration (CHT or SNT). Our observation was that CHT is always more critical than SNT and the highest required elongation at failure  $A5$  is always produced by the smallest hole or notch in the specimens. Therefore only the results from CHT tests with 8 mm hole will be presented herewith. Moreover, the results of the final numerical study revealed that the highest  $A5$  requirement is always reached in specimens with the highest strength (1000 MPa in our case). Therefore only results of material group S4 are shown in Table 22 and Table 23.

Table 20. Simplified material models of final parametric study (Part 1).

Model		$f_{y}$ (MPa)	$f_u/f_y$	$\epsilon_u$	Model		$f_{y}$ (MPa)	$f_u/f_y$	$\epsilon_u$
1	S1A1	250	1.00	1%	50	S2A1	500	1.00	1%
2	S1A2			2%	51	S2A2			2%
3	S1A3			4%	52	S2A3			4%
4	S1A4			8%	53	S2A4			9%
5	S1A5			12%	54	S2A5			13%
6	S1A6			16%	55	S2A6			13%
7	S1A7			20%	56	S2A7			20%
8	S1B1		1.02	2%	57	S2B1		1.02	2%
9	S1B2			5%	58	S2B2			5%
10	S1B3			9%	59	S2B3			9%
11	S1B4			17%	60	S2B4			17%
12	S1B5			20%	61	S2B5			20%
13	S1B6			22%	62	S2B6			22%
14	S1B7			25%	63	S2B7			25%
15	S1C1		1.05	2%	64	S2C1		1.05	2%
16	S1C2			5%	65	S2C2			5%
17	S1C3			10%	66	S2C3			10%
18	S1C4			19%	67	S2C4			19%
19	S1C5			26%	68	S2C5			27%
20	S1C6			30%	69	S2C6			31%
21	S1C7			31%	70	S2C7			32%
22	S1D1		1.10	2%	71	S2D1		1.10	2%
23	S1D2			5%	72	S2D2			5%
24	S1D3			10%	73	S2D3			10%
25	S1D4			19%	74	S2D4			19%
26	S1D5			28%	75	S2D5			29%
27	S1D6			36%	76	S2D6			37%
28	S1D7			42%	77	S2D7			42%
29	S1E1		1.20	2%	78	S2E1		1.20	2%
30	S1E2			5%	79	S2E2			5%
31	S1E3			10%	80	S2E3			10%
32	S1E4			20%	81	S2E4			20%
33	S1E5			29%	82	S2E5			29%
34	S1E6			39%	83	S2E6			39%
35	S1E7			47%	84	S2E7			47%
36	S1A1		1.30	2%	85	S2A1		1.30	2%
37	S1A2			5%	86	S2A2			5%
38	S1F3			10%	87	S2F3			10%
39	S1F4			20%	88	S2F4			20%
40	S1F5			30%	89	S2F5			30%
41	S1F6			39%	90	S2F6			39%
42	S1F7			48%	91	S2F7			49%
43	S1G1		1.50	2%	92	S2G1		1.50	2%
44	S1G2			5%	93	S2G2			5%
45	S1G3			10%	94	S2G3			10%
46	S1G4			20%	95	S2G4			20%
47	S1G5			30%	96	S2G5			30%
48	S1G6			40%	97	S2G6			40%
49	S1G7			49%	98	S2G7			49%

Table 21. Simplified material models of final parametric study (Part 2).

Model	$f_{y}$ (MPa)	$f_u/f_y$	$\epsilon_u$	Model	$f_{y}$ (MPa)	$f_u/f_y$	$\epsilon_u$
99	S3A1	1.00	1%	148	S4A1	1.00	1%
100	S3A2		2%	149	S4A2		2%
101	S3A3		4%	150	S4A3		4%
102	S3A4		9%	151	S4A4		8%
103	S3A5		12%	152	S4A5		12%
104	S3A6		16%	153	S4A6		16%
105	S3A7		20%	154	S4A7		19%
106	S3B1	1.02	2%	155	S4B1	1.02	2%
107	S3B2		5%	156	S4B2		2%
108	S3B3		9%	157	S4B3		9%
109	S3B4		17%	158	S4B4		17%
110	S3B5		20%	159	S4B5		21%
111	S3B6		22%	160	S4B6		22%
112	S3B7		25%	161	S4B7		25%
113	S3C1	1.05	2%	162	S4C1	1.05	2%
114	S3C2		5%	163	S4C2		5%
115	S3C3		10%	164	S4C3		10%
116	S3C4		19%	165	S4C4		19%
117	S3C5		26%	166	S4C5		27%
118	S3C6		30%	167	S4C6		31%
119	S3C7		32%	168	S4C7		32%
120	S3D1	1.10	2%	169	S4D1	1.10	2%
121	S3D2		5%	170	S4D2		5%
122	S3D3		10%	171	S4D3		10%
123	S3D4		19%	172	S4D4		19%
124	S3D5		29%	173	S4D5		29%
125	S3D6		37%	174	S4D6		37%
126	S3D7		42%	175	S4D7		42%
127	S3E1	1.20	2%	176	S4E1	1.20	2%
128	S3E2		5%	177	S4E2		5%
129	S3E3		10%	178	S4E3		10%
130	S3E4		20%	179	S4E4		20%
131	S3E5		30%	180	S4E5		30%
132	S3E6		39%	181	S4E6		39%
133	S3E7		48%	182	S4E7		48%
134	S3A1	1.30	2%	183	S4A1	1.30	2%
135	S3A2		5%	184	S4A2		5%
136	S3F3		10%	185	S4F3		10%
137	S3F4		20%	186	S4F4		20%
138	S3F5		30%	187	S4F5		30%
139	S3F6		39%	188	S4F6		40%
140	S3F7		49%	189	S4F7		49%
141	S3G1	1.50	2%	190	S4G1	1.50	2%
142	S3G2		5%	191	S4G2		5%
143	S3G3		10%	192	S4G3		10%
144	S3G4		20%	193	S4G4		20%
145	S3G5		30%	194	S4G5		30%
146	S3G6		40%	195	S4G6		40%
147	S3G7		50%	196	S4G7		50%

Table 22. A5 limits for CHT tests of simplified models without strain hardening.

Material group		$f_{uffy}$	$\varepsilon_u$	A5 to reach $f_y A_{net}$	A5 to reach $f_u A_{net}$	A5 to reach 3% elongation <sup>1)</sup>
1	S4A1	1.00	1%	1.2%	1.2%	7.0%
2	S4A2		2%	1.4%	1.5%	8.2%
3	S4A3		4%	1.5%	1.5%	11.0%
4	S4A4		8%	1.8%	1.8%	15.7%
5	S4A5		12%	2.0%	2.3%	19.7%
6	S4A6		16%	2.2%	4.3%	23.4%
7	S4A7		20%	2.3%	8.6%	26.8%
8	S4B1	1.02	2%	2.1%	2.4%	8.0%
9	S4B2		5%	2.6%	4.9%	10.3%
10	S4B3		9%	2.4%	7.4%	14.0%
11	S4B4		17%	2.3%	8.1%	20.5%
12	S4B5		20%	2.4%	9.9%	24.6%
13	S4B6		22%	2.4%	13.6%	27.7%
14	S4B7		25%	2.5%	18.2%	30.6%
15	S4C1	1.05	2%	2.1%	3.1%	8.0%
16	S4C2		5%	2.7%	6.9%	10.5%
17	S4C3		10%	2.7%	11.8%	14.4%
18	S4C4		19%	2.6%	20.1%	22.2%
19	S4C5		26%	2.6%	27.1%	29.0%
20	S4C6		30%	2.6%	29.5%	33.1%
21	S4C7		32%	2.6%	31.7%	35.7%
22	S4D1	1.10	2%	2.1%	3.9%	8.0%
23	S4D2		5%	2.7%	8.8%	10.2%
24	S4D3		10%	2.7%	14.6%	14.3%
25	S4D4		19%	2.7%	24.0%	22.5%
26	S4D5		28%	2.7%	32.0%	30.7%
27	S4D6		36%	2.7%	38.9%	37.9%
28	S4D7		42%	2.7%	43.5%	42.6%
29	S4E1	1.20	2%	2.2%	4.3%	7.5%
30	S4E2		5%	2.5%	9.0%	8.6%
31	S4E3		10%	2.7%	15.0%	12.9%
32	S4E4		20%	2.9%	25.1%	22.1%
33	S4E5		30%	3.0%	34.7%	31.0%
34	S4E6		39%	3.0%	43.7%	39.5%
35	S4E7		48%	3.0%	52.2%	45.1%
36	S4F1	1.30	2%	2.2%	4.1%	7.1%
37	S4F2		5%	2.3%	8.9%	7.7%
38	S4F3		10%	2.6%	15.2%	12.1%
39	S4F4		20%	2.8%	25.4%	21.3%
40	S4F5		30%	2.9%	35.1%	30.5%
41	S4F6		40%	2.9%	44.5%	37.7%
42	S4F7		49%	2.9%	53.6%	39.2%
43	S4G1	1.50	2%	1.9%	4.1%	6.7%
44	S4G2		5%	2.6%	9.1%	7.0%
45	S4G3		10%	2.3%	14.9%	11.4%
46	S4G4		20%	2.6%	25.9%	20.6%
47	S4G5		30%	2.7%	35.8%	26.5%
48	S4G6		40%	2.8%	45.5%	28.8%
49	S4G7		50%	2.8%	55.0%	30.3%

<sup>1)</sup> 3 mm displacement on the gauge length 100 mm

Table 23. A5 limits for SNT tests of simplified models without strain hardening.

Material group		$f_{u/f_y}$	$\varepsilon_u$	A5 to reach $f_y A_{net}$	A5 to reach $f_u A_{net}$	A5 to reach 3% elongation <sup>1)</sup>
1	S4A1	1.00	1%	1.1%	1.1%	5.3%
2	S4A2		2%	1.2%	1.2%	6.3%
3	S4A3		4%	1.3%	1.3%	9.1%
4	S4A4		8%	1.4%	1.4%	13.9%
5	S4A5		12%	1.6%	1.7%	18.0%
6	S4A6		16%	1.7%	2.0%	21.3%
7	S4A7		20%	1.9%	2.2%	23.6%
8	S4B1	1.02	2%	2.1%	2.1%	6.2%
9	S4B2		5%	2.2%	2.5%	8.4%
10	S4B3		9%	2.0%	2.3%	12.1%
11	S4B4		17%	1.9%	2.2%	18.7%
12	S4B5		20%	1.9%	2.3%	22.9%
13	S4B6		22%	1.9%	2.4%	25.4%
14	S4B7		25%	2.0%	2.8%	27.0%
15	S4C1	1.05	2%	2.1%	2.2%	6.2%
16	S4C2		5%	3.2%	3.9%	8.4%
17	S4C3		10%	2.2%	4.0%	12.4%
18	S4C4		19%	2.1%	3.9%	20.4%
19	S4C5		26%	2.1%	3.9%	27.3%
20	S4C6		30%	2.1%	4.1%	30.2%
21	S4C7		32%	2.1%	4.4%	30.7%
22	S4D1	1.10	2%	2.2%	2.9%	6.2%
23	S4D2		5%	3.1%	6.2%	8.1%
24	S4D3		10%	3.2%	11.5%	12.4%
25	S4D4		19%	2.3%	20.8%	20.8%
26	S4D5		28%	2.2%	29.4%	29.1%
27	S4D6		36%	2.2%	35.7%	32.0%
28	S4D7		42%	2.2%	36.5%	32.0%
29	S4E1	1.20	2%	2.2%	3.5%	5.9%
30	S4E2		5%	2.9%	7.6%	7.7%
31	S4E3		10%	3.1%	13.7%	11.9%
32	S4E4		20%	3.2%	24.4%	20.8%
33	S4E5		30%	3.2%	33.8%	29.2%
34	S4E6		39%	3.2%	42.4%	29.9%
35	S4E7		48%	3.2%	50.4%	30.2%
36	S4F1	1.30	2%	2.2%	3.6%	5.8%
37	S4F2		5%	2.7%	7.9%	7.3%
38	S4F3		10%	3.0%	14.1%	11.6%
39	S4F4		20%	3.1%	25.1%	20.6%
40	S4F5		30%	3.2%	35.0%	26.5%
41	S4F6		40%	3.2%	44.2%	27.5%
42	S4F7		49%	3.2%	52.8%	28.1%
43	S4G1	1.50	2%	1.8%	3.7%	5.6%
44	S4G2		5%	2.4%	8.0%	6.9%
45	S4G3		10%	2.8%	14.2%	11.2%
46	S4G4		20%	3.0%	25.5%	20.2%
47	S4G5		30%	3.1%	36.1%	22.4%
48	S4G6		40%	3.1%	45.7%	23.6%
49	S4G7		50%	2.3%	54.8%	24.3%

<sup>1)</sup> 3 mm displacement on the gauge length 100 mm

The graphs in Figure 43 and Figure 44 are the maximum values obtained from CHT and SNT virtual tests. They show that the calculated  $A_5$  requirement was always reached in tested steels (measured values were higher).

For instance high-strength steel S700 with uniform elongation  $\epsilon_u$  9.5% and  $f_u/f_y$  ratio 1.12 (see Table 5) would require  $A_5$  at least 14.5% to reach  $f_u A_{net}$  (Figure 43) and 13.5% to reach 3 mm elongation (Figure 44). The measured value was 20.6%, and therefore the steel easily satisfies the requirements. However, 3 mm (3%) elongation of S960 was very close to the calculated limit.

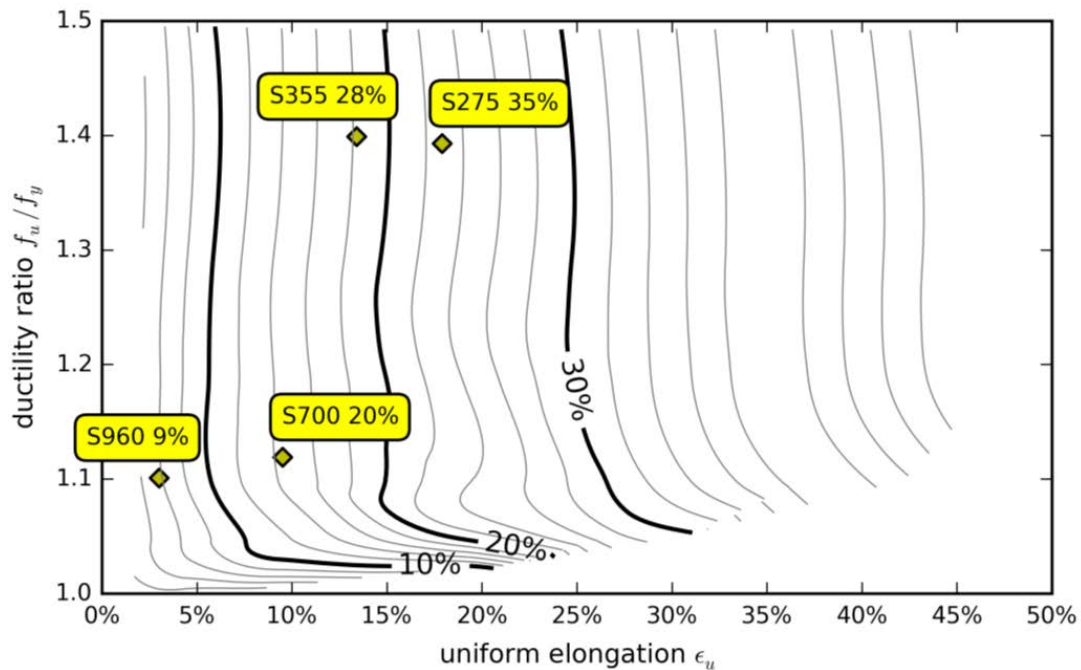


Figure 43.  $A_5$  required to reach  $f_u A_{net}$  compared to measured values.

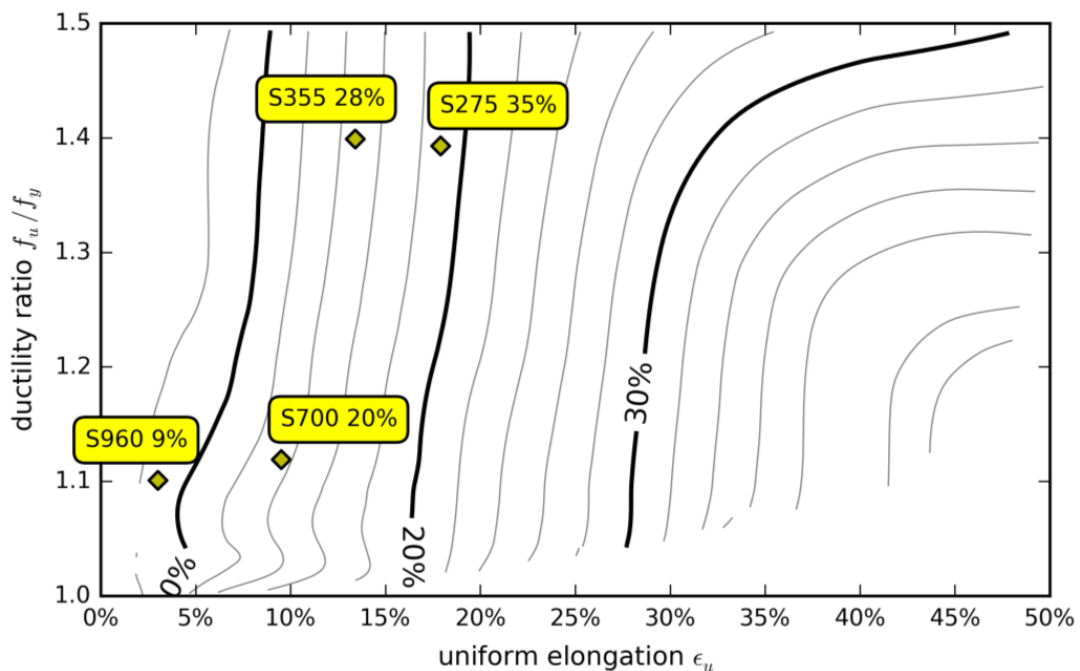


Figure 44.  $A_5$  required to reach 3% elongation compared to measured values.



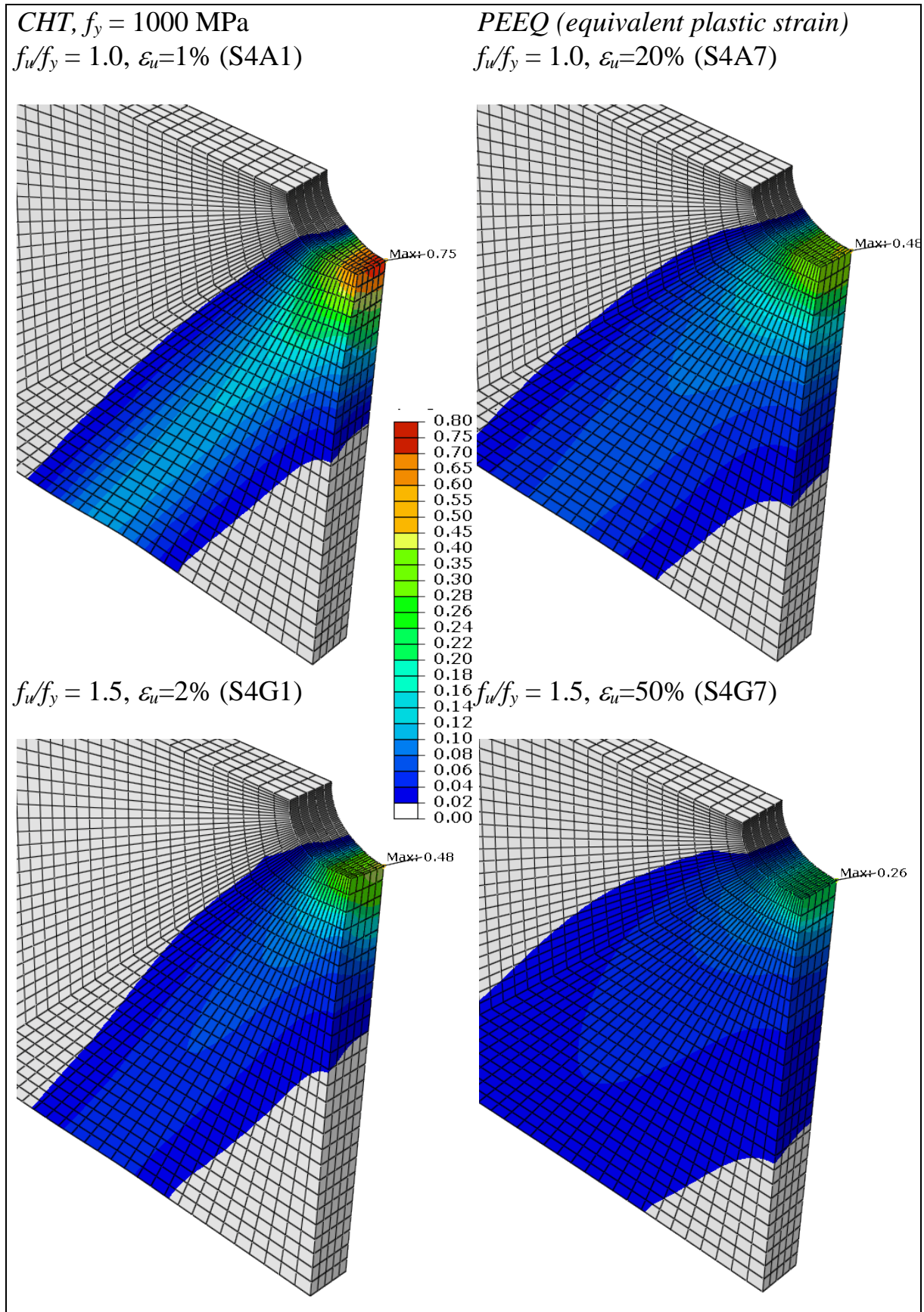


Figure 45. Equivalent plastic strain distribution in CHT specimens at 3% elongation.



The four examples in Figure 45 show the differences in equivalent plastic strains in four extreme cases of CHT tests (S4A1, S4A7, S4G1 and S4G7) at 3 mm (3%) elongation. The material with lowest  $f_u/f_y$  ratio and uniform elongation  $\varepsilon_u$  shows the most significant strain concentration near the hole (75%) and visible necking. On the other hand, the last case (S4G7) with maximum strain 26% didn't reach the uniform strain 50% at all, and therefore no diffuse necking could be observed at this deformation.

It is obvious that materials with the uniform strain  $\varepsilon_u$  higher than the current Eurocode A5 limit (10% or 15%) will also have higher elongation at failure. In that sense it is not clear whether the fixed value of minimum A5 is justified in the Eurocode because it cannot guarantee that the design load will be carried without damaging the material in such cases where A5 is just slightly higher than  $\varepsilon_u$ . For instance reaching the design ultimate load in the cross-section requires always certain "necking capacity" of the material. Therefore we have proposed two approaches to address this problem.

The solution proposed in the following section prescribes minimum required necking capacity as the difference between failure elongation A5 and the uniform elongation  $\varepsilon_u$ . This method relies only on existing material parameters, and should be more easy to implement.

### 5.3 Alternative ductility criteria

Assuming that some design situation may allow development of strains beyond uniform load, and thus localized diffuse necking in tensioned parts, we propose to establish a necking capacity parameter  $A5 - \varepsilon_u$  as a limiting factor rather than fixed value of A5. This will be more consistent rule for all steel grades regardless their real uniform strain. The necking capacity is the strain difference between failure elongation A5 and uniform strain  $\varepsilon_u$  and it is described in Figure. 46.

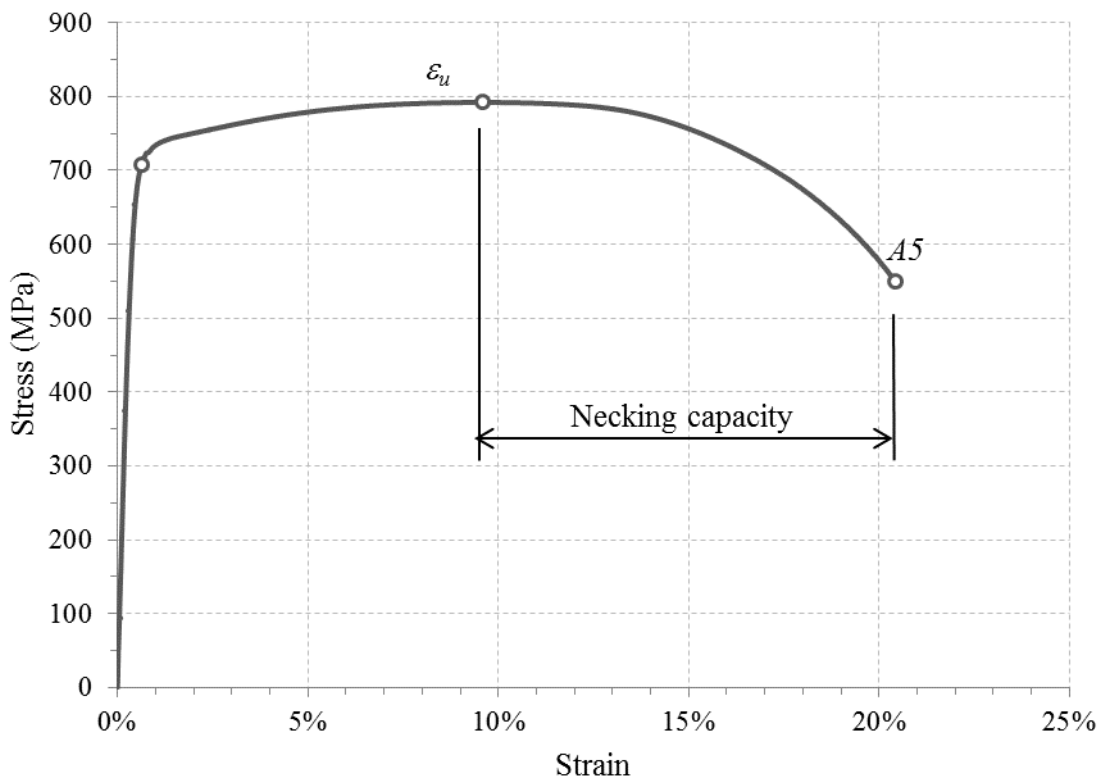


Figure. 46 Definition of necking capacity of material tests (coupons) required to reach design loads (example grade S700).

As it is demonstrated in Figure 47, certain capacity is always needed to reach the ultimate load in net section ( $f_u A_{net}$ ) and it has to be higher than 6%. On the other hand, some materials with

high uniform strain  $\epsilon_u$  or  $f_u/f_y$  ratio don't need necking capacity at 3% elongation at all (see Figure 48).

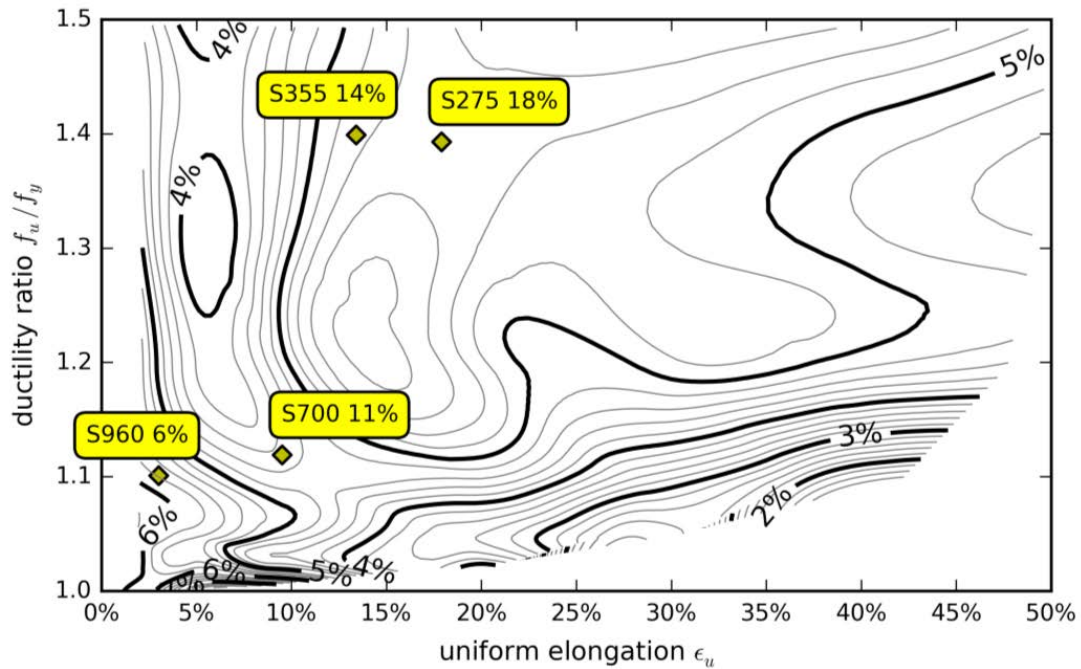


Figure 47.  $A5-\epsilon_u$  required to reach  $f_u A_{net}$  compared to measured values.

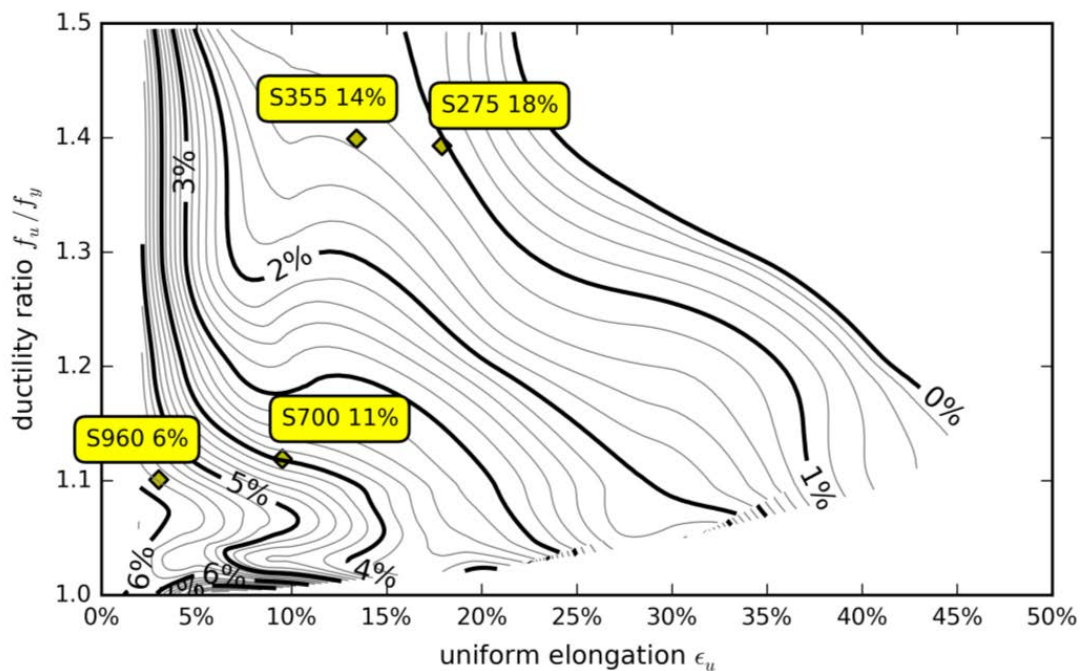


Figure 48.  $A5-\epsilon_u$  required to reach 3% elongation compared to measured values.

## 6. Summary and conclusions

---

The virtual testing toolbox developed in VILMA project and presented in this report was used to provide insight into the basic questions whether the Eurocode's material requirements are correct or not, could they be eased or not, and how much they could be eased. It was not possible to give general answer because of the limited experimental results; only such answer related to the particular cases of CHT (Centre Hole in Tension) and SNT (Side Notch in Tension) specimens. However, we present clear and working method how the solution can be extended for more details and may enable to cover all needed design situations in the future.

Prediction of ductile fracture is an important topic in evaluating performance of structural components and connections, when large local deformations must be accommodated before the design resistance is reached. Ductile fracture is usually identified as the fracture initiating event in structural steel members subjected to high plastic strains. This study uses macroscopic ductile failure criteria in ductile fracture initiation. They are describing ductile fracture of crack-free details. The ductile failure criterion is usually based on critical von Mises equivalent plastic strain. However, the critical strain is affected by stress state, loading history, strain rate and temperature. Stress state is usually described at least by stress triaxiality and often some other parameters are used too.

### 6.1 Ductility limits

Ductility is defined as a measure of a material's ability to undergo appreciable plastic deformation before fracture. Ductility in Eurocodes is based on the ratio  $f_u/f_y$ ,  $\varepsilon_u/\varepsilon_y$  and permanent elongation at fracture  $A_5$  (Table 1), which are given in material standards (Table 2) or proved by material tension tests. Possibly because of many factors affecting to the ductility, in FE modelling the plastic strains are usually limited to 5% by EN standards up to strength S460–S700.

Based on tests shown in the literature review for notched specimens, the critical plastic strain in details with high stress concentration is always higher than  $A_5$  of straight coupons (Table 9 and Table 10). For most usual structural steels in EN standards  $A_5$  ranges between 7% (S960) and 24% (S235). However, many times higher critical plastic strains can be allowed if it is predicted by more sophisticated methods usually used in simulation of sheet forming or material deformations in accidents. There the stress state needs to be described at least by triaxiality parameter  $T$  which is defined by the ratio of hydrostatic and equivalent stress. In most usual structural details  $0 < T < 1.0$  at failure (Table 3, Figure 9).

One of the simplest and possibly most used ductile failure models is SMCS (Stress Modified Critical Strain). In SMCS model the critical strain depends only on stress triaxiality and material-dependent toughness parameter (Figure 6). The accuracy of the method has been verified in many practical conditions, such as the necked ligament between bolt holes, structural moment connection, material tension specimen and circumferential notch tensile (CNT) specimen. In these cases, fracture typically initiates internally, where the stress triaxiality is relatively high ( $T > 0.75$ ) and then propagates outwards to the surface of the material. However, there are other situations where fracture may initiate on the surface of the material, where triaxiality at failure is usually lower. Fracture initiation on the surface has been observed for example in large scale tests on structural braces and column base plate tests. Then more complicated predictive models may be needed.

### 6.2 Strain limits for FEM modelling

Critical plastic strains at failure have been studied by CHT specimens (tension test specimens with holes, dimensions  $b = 80$  mm,  $t = 8$  mm,  $d = 8$  to 40 mm, Figure 21). The failure elongation was determined by testing and plastic strains were obtained from FE calculations. Two materials, S960 ( $A_{80} = 9.8\%$ ) and S700 (measured  $A_5 = 17\%$ ), were under consideration. It

should be noted that material properties of S700 were not from the same batch as CHT specimens (e.g.  $A5$  for material used in FE modelling was 21%) because the full material test data was not available from the same batch as CHT tests. According to FE calculations the plastic strains, corresponding to the elongation at fracture of CHT specimens, were in tests 87–105% for S960 and 85–98% for S700 (Table 15). However, the lowest plastic strain at failure, 44% for S960, was obtained in the case of equal size CHT specimen without the hole. The failure of this specimen was so called sheet necking, where the final failure is inclined to the tension axis across the width of the specimen. This kind of failure, where the final failure is shear failure, is typical for specimens with high cross-section aspect ratio and low hardening ability. It should be noted that in spite of lower local plastic strains, the overall elongation (gauge length 100 mm) of non-holed specimens was roughly double compared to the holed specimens (Figure 21). Low strain hardening is typical for high strength steels, and also the fracture curves in literature show that they can be more prone to fail in shear ( $T=0$  to 0.6) than usual steels.

The elongations of holed CHT specimens have also been compared to SMCS failure criteria. Usually the toughness parameter of SMCS fracture model is determined by smooth-notched CNT (Circular Notch in Tension) specimens (Figure 5). Because the test results were not available, the toughness parameter was here determined from material tension tests made for rectangular cross sections. Based on SMCS model the critical strain was reduced to correspond to  $T = 1.0$  (reduction for S700 from 114% to 93% and for S960 from 98% to 83%). The idea of this approach is that only tension specimens are needed for determining the critical plastic strain and in modelling of structures the triaxiality parameter is limited to 1.0. This approach predicts quite well the failure elongations of CHT experiments (criterion 6 in Figure 27).

Maximum load calculated by the net section resistance ( $N_u = A_{net}f_u$ ) of the holed CHT specimens has been also been compared with the forces corresponding different values of plastic strains. In addition of materials S960 ( $f_u/f_y = 1.10$ ,  $A5 = 9.8\%$ ) and S700 ( $f_u/f_y = 1.12$ ,  $A5 = 21\%$ ), also S355 ( $f_u/f_y = 1.40$ ,  $A5 = 28\%$ ) and S275 ( $f_u/f_y = 1.39$ ,  $A5 = 36\%$ ) have been studied. If the plastic strains are limited to SMCS critical strain, the net section resistance is reached in all cases (Figure 27, criterion 6). If the plastic strain is limited to  $A5$  (criterion 5), the net section resistance is slightly underestimated in all cases. The underestimation is less than 3% for S960 and S700, and less than 9% for S355 and S275. The largest underestimating occurs in the case of smallest holes.

Maximum plastic strain of CHT specimens at hole are also compared to outer corner strain at mid-specimen. The aim of this comparison is to see, if the full net section can reach the yield before the failure strains at hole. The results show that the maximum plastic strains at hole can be about 5–10 times the corner strains (Appendix A). The smallest factors concern S275 and highest ones S960. The result means that when 0.2% proof stress is reached at the corner, the maximum plastic strains at the hole are only 1–2%. Secondly, when for example the  $A5$  plastic strains are reached at the hole, the edge strains are 1 to 7 %. The smallest values concern S960 and highest ones S235.

### 6.3 Numerical studies

The applied approach was to test the validity of ductility limits for wide range of hypothetical materials to be able to reach given design limits. Therefore the prediction of material failure in FEM models was not needed. However, the proposed failure criteria for strain (as described in the previous section) may be utilized in FEM models for instance in situations where the clear design limits of Eurocode are missing or they are too conservative.

Our method is using parametric range of two existing criteria ( $f_u/f_y$ ) and ( $\varepsilon_u/\varepsilon_y$ ) as variable parameters to calculate the safe minimum value of the third criterion ( $A5$ ) to be able to achieve design limits of Eurocode. We have recognized that the results are dependent on the slope of the stress-strain curve after uniform elongation (after the diffuse necking initiation). This slope can be characterized by single parameter, for instance  $\varepsilon_R$ , the elongation when the load

decreases back to the yield level. Unfortunately any of the possible material parameters given in testing standards doesn't provide complete description of this slope (e.g.  $A5$  elongation doesn't indicate at which load level the failure happened). The most conservative situation is when the material is not hardening after reaching uniform load and true stress-strain relation is ideally plastic beyond that point. In the presented study we used the CHT (Centre Hole in Tension) tests with range of  $f_u/f_y$  from 1.05 to 1.5 and  $\varepsilon_u/\varepsilon_R$  from 0.2 to maximum possible to reach the elongation at yield load  $\varepsilon_R$  which was ranging from  $10\varepsilon_y$  to  $60\varepsilon_y$ .

We have investigated the criterion prescribing that the elongation  $\varepsilon_R$  has to be reached in coupon tests. This limit was performing very well for net section failure of materials with  $f_u/f_y \geq 1.05$ , but the. We recommend combining this criterion with limited minimum elongation at failure (from the previous study in Table 19) to ensure sufficient plastic capacity of the material.

The parametric study was then extended by a wide selection of non-hardening materials covering the range of  $f_u/f_y$  from 1.0 to 1.5,  $\varepsilon_u$  from 2% to 50% and  $f_y$  from 250 to 1000 MPa with additional SNT geometry (Side Notch in Tension).

To be able to transfer strains between coupons and CHT/SNT models, we assumed conservatively that the true strain at failure of material tests coupons is the same as the one of studied details (CHT/SNT specimens). In reality it is always higher (Figure 41). The results show that it is possible to predict the minimum required elongation at failure  $A5$  for the particular structural detail and design limit. Such method can be extended to more structural details and the requirements can be reduced by using notched tests instead of coupons or integrating more complex ductile failure models than the simple assumption of equal strains.

The final parametric study investigated the possibility to replace the current limits with different criterions. One example is so-called "necking capacity"  $A5-\varepsilon_u$ . The results of the study showed clearly that if this capacity is at least 6%, all materials can reach ultimate load in net section of CHT/SNT specimens.

It should be noted that all of the results are valid only for the range of parameters that was agreed within the project working group:

- CHT/SNT-like details with holes or notches under axial tension
- holes or notches at least 8 mm in diameter
- yield strength up to 1000 MPa
- $f_u/f_y$  up to 1.50

Therefore the results should be considered as a proposal for the method of further evaluation of the ductility criteria with wider range of material parameters, more details and loading situations (e.g. loaded holes in bolted connections, welded plates, bended beams).



## References

---

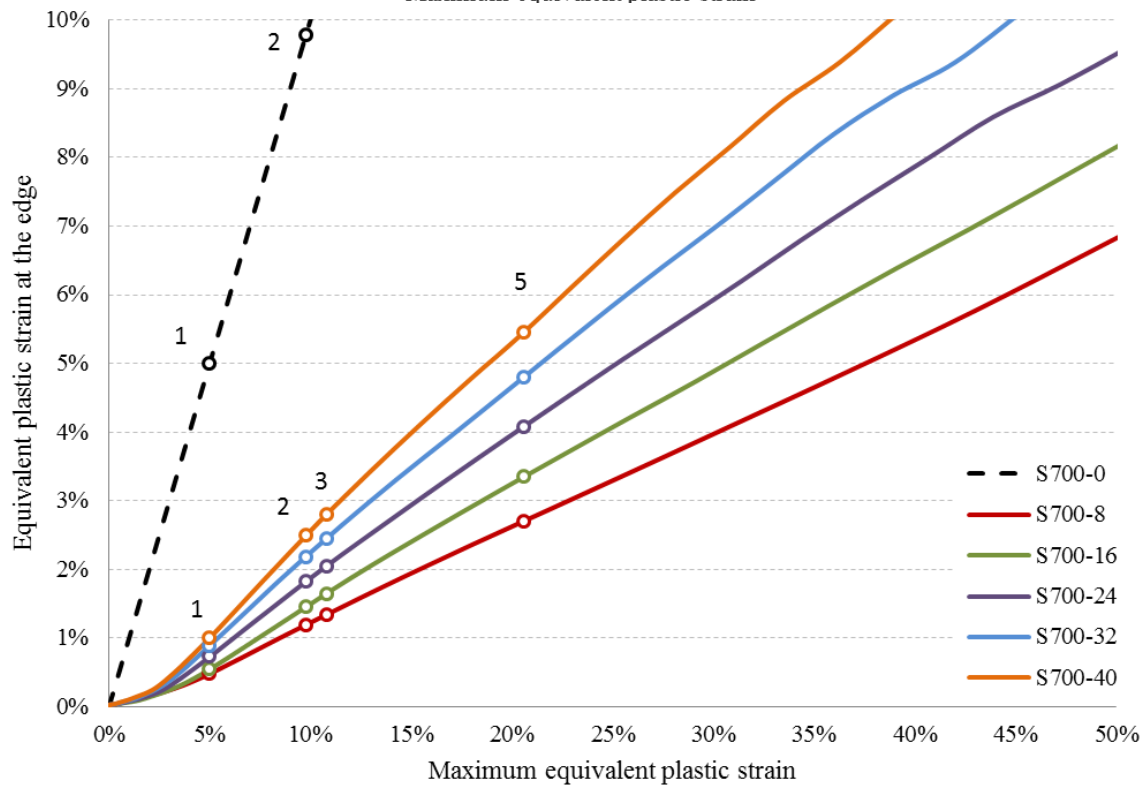
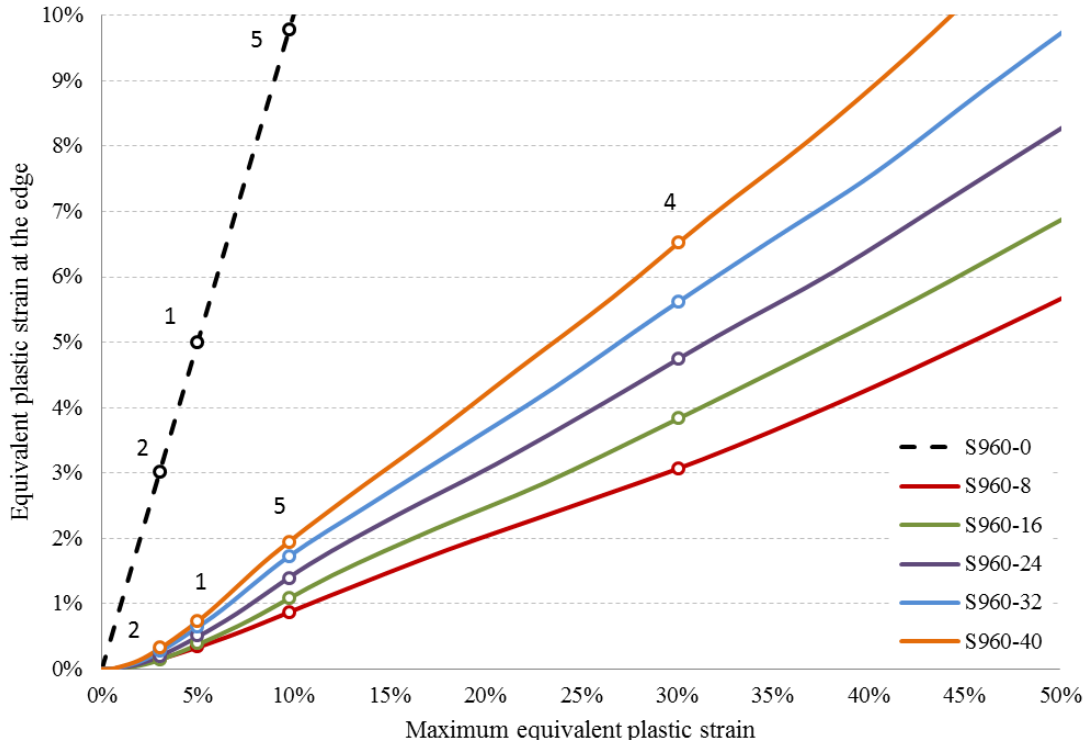
- [1] EN 1993-1-1
- [2] EN 1993-1-12
- [3] Schäfer, D., Eichler, B., Amlung L. 2010. Modern plastic design for steel structures. European Commission, Directorate-General for Research and Innovation. Research Fund for Coal and Steel. Final report EUR 24227. RFSR-CT-2005-00039 PLASTOTOUGH. <http://bookshop.europa.eu/en/modern-plastic-design-for-steel-structures-pbKINA24227/>
- [4] <http://www.encyclo.co.uk/define/ductility>
- [5] EN 10002-1: Metallic materials – Tensile testing – Part 1: Method of test at ambient temperature.
- [6] EN 1992-1-1: Eurocode 2: Design of concrete structures - Part 1-1: General rules and rules for buildings
- [7] Dhalla, A.K., Winter, G., "Suggested Steel Ductility Requirements", Journal of the Structural Division, ASCE, Vol. 100, No. ST2, February 1974, pp. 445–462.
- [8] EN 1993-1-5: Eurocode 3: Design of steel structures. Part 1-5: Plated structural elements.
- [9] EN 1993-1-6: Eurocode 3: Design of steel structures - Part 1-6: Strength and Stability of Shell Structures.
- [10] EN 13445-3:2009 Unfired pressure vessels - Part 3: Design. Annex B (normative): Design by Analysis – Direct Route.
- [11] Kanvinde A. M; and Deierlein G. G. 2006. Void Growth Model and Stress Modified Critical Strain Model to Predict Ductile Fracture in Structural Steels Journal of Structural Engineering, Vol. 132, No. 12.
- [12] Rice, J. R., and Tracey, D. M. 1969. On the ductile enlargement of voids in triaxial stress fields." J. Mech. Phys. Solids, 17(3), 201–217.
- [13] Myers, A.T., Deierlaine G.G, Kanvinde, A. 2009. Testing and probabilistic simulation of ductile fracture initiation in structural steel components and weldments. The John A. Blume Earthquake Engineering Center at Stanford University. Report No. 170. [https://blume.stanford.edu/sites/default/files/TR170\\_Myers\\_0.pdf](https://blume.stanford.edu/sites/default/files/TR170_Myers_0.pdf)
- [14] Bao, Y., Wierzbicki, T. 2004. On fracture locus in the equivalent strain and stress triaxiality space. International Journal of Mechanical Sciences 46 (2004) 81–98.
- [15] Hooputra, H., Gese H., H Dell H., Werner H. 2004. A comprehensive failure model for crashworthiness simulation of aluminium extrusions. International Journal of Crashworthiness, 9:5 (2004) 449–464.
- [16] Bai, Y., Wierzbick, T. 2010. Application of extended Mohr–Coulomb criterion to ductile fracture. International Journal of Fracture, January 2010, Volume 161, Issue 1, pp 1–20.
- [17] Levanger, H. 2012. Simulating Ductile Fracture in Steel using the Finite Element Method: Comparison of Two Models For Describing Local Instability due to Ductile Fracture. Msc. Thesis. University of Oslo. <https://www.duo.uio.no/handle/10852/10876>
- [18] Nahshon K., Hutchinson, J.W. 2008. Modification of the Gurson Model for shear failure. European Journal of Mechanics A/Solids 27 (2008) 1–17.
- [19] Dunand, M., Mohr, D. 2011. On the predictive capabilities of the shear modified Gurson and modified Mohr–Coulomb fracture models over a wide range. Journal of the Mechanics and Physics of Solids 59(2011)1374–1394.
- [20] Corona, E., Reedlunn, B. 2013. A Review of Macroscopic Ductile Failure Criteria. SAND2013-7989. <http://prod.sandia.gov/techlib/access-control.cgi/2013/137989.pdf>

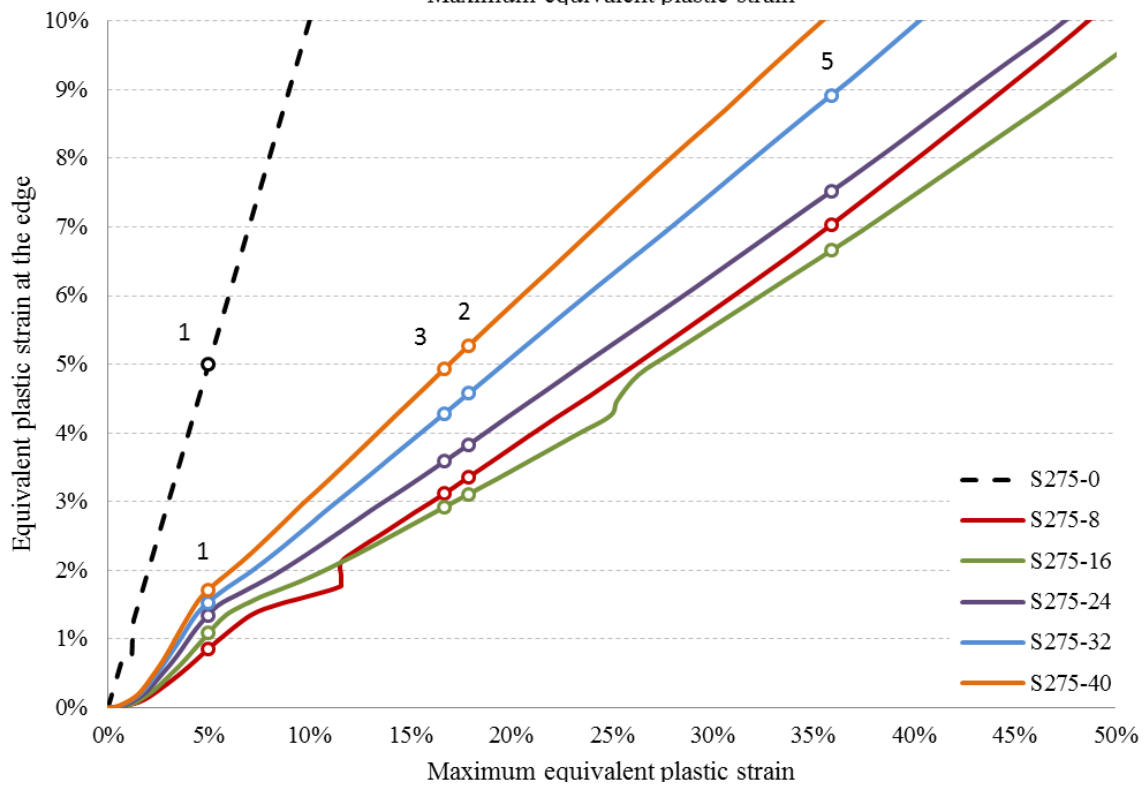
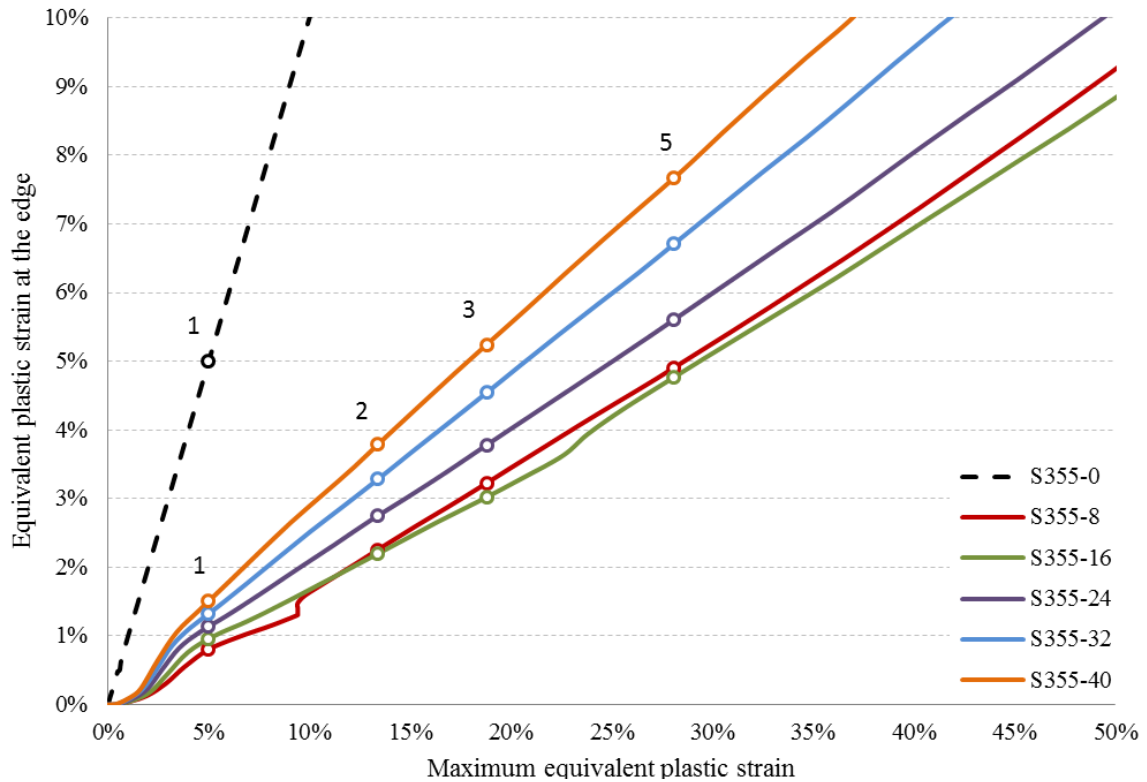


- [21] Barsoum, I., Faleskog, J. 2006. Rupture mechanisms in combined tension and shear Experiments. *International Journal of Solids and Structures* 44 (2007) 1768–1786.
- [22] Östlund, R. 2011. Modelling and Characterisation of Fracture Properties of Advanced High Strength Steels. Luleå University of Technology. Licentiate Thesis in Solid Mechanics. [https://pure.ltu.se/portal/files/33787478/Rickard\\_stlund.pdf](https://pure.ltu.se/portal/files/33787478/Rickard_stlund.pdf)
- [23] Basaran, M. 2011. Stress State Dependent Damage Modeling with a Focus on the Lode Angle Influence. RWTH Aachen University. Doctoral Thesis. <http://darwin.bth.rwth-aachen.de/opus3/volltexte/2011/3833/pdf/3833.pdf>
- [24] Alves, M., Norman Jones, N. 1999. Influence of hydrostatic stress on failure of axisymmetric notched specimens. *Journal of the Mechanics and Physics of Solids* 47 (1999) 643-667
- [25] Dykeman, J., Skye, M., Huang, G., Zhu, H. Ramisetti, N., Yan, B. J Chintamani, J. 2011. Characterization of Edge Fracture in Various Types of Advanced High Strength Steel. SAE paper 2011-01-1058. <http://papers.sae.org/2011-01-1058/>
- [26] MATCH: Material Choice for Seismic Resistant Structures, RFSR-CT-2013 00024 [ftp://ftp.cordis.europa.eu/pub/coal-steel-rtd/docs/summaries-rfcs\\_en.pdf](ftp://ftp.cordis.europa.eu/pub/coal-steel-rtd/docs/summaries-rfcs_en.pdf)
- [27] Hollomon
- [28] Ramberg-Osgood
- [29] Choung, J. M., Cho, S. R. 2008. Study on true stress correction from tensile tests. *Journal of Mechanical Science and Technology* 22 (2008) 1039–1051.
- [30] ManSoo Joun, Jea Gun Eom, Min Cheol Lee. 2008. A new method for acquiring true stress–strain curves over a large range of strains using a tensile test and finite element method. *Mechanics of Materials* 40 (2008) 586–593.
- [31] Abaqus manual
- [32] Valkonen, I. 2014. 20<sup>th</sup> European Conference on Fracture (ECF20): Ultimate limit loads in welded joints and in net sections of high strength steels with yield stress 960 MPa. *Procedia Materials Science* 3 ( 2014 ) 720–725.

## Annex A: Strain concentration in CHT specimens

The FEM results of calculated CHT tests with optimized real materials (S960, S700, S355 and S275) in Figure 28, Figure 29, Figure 30 and Figure 31 show that the relation between the concentrated equivalent plastic strain in the middle cross-section and the maximum equivalent plastic strain at the outer edge of the specimen is fairly linear.





We have approximated this up until 100% of maximum equivalent plastic strain by a simple linear equation:

$$\varepsilon_{eq} = k \cdot \varepsilon_{eq,ed} \quad (27)$$

As can be seen from the figures, the coefficient  $k$  depends on the hole diameter  $d$  and on the material strength  $f_y$ . Our linear regression in Eq. (28) shows good agreement with the calculated data. The 1.5% error is mostly attributed to smallest holes ( $d = 8$  mm) in mild steel grades (S355 and S275) that didn't exactly follow the trend. Those two materials were also excluded from the linear regression (see Figure 49).

$$K = \frac{1}{(0.0051 - 2 \cdot 10^{-6} f_y)d + (0.12 - 2 \cdot 10^{-5} f_y)} \quad (28)$$

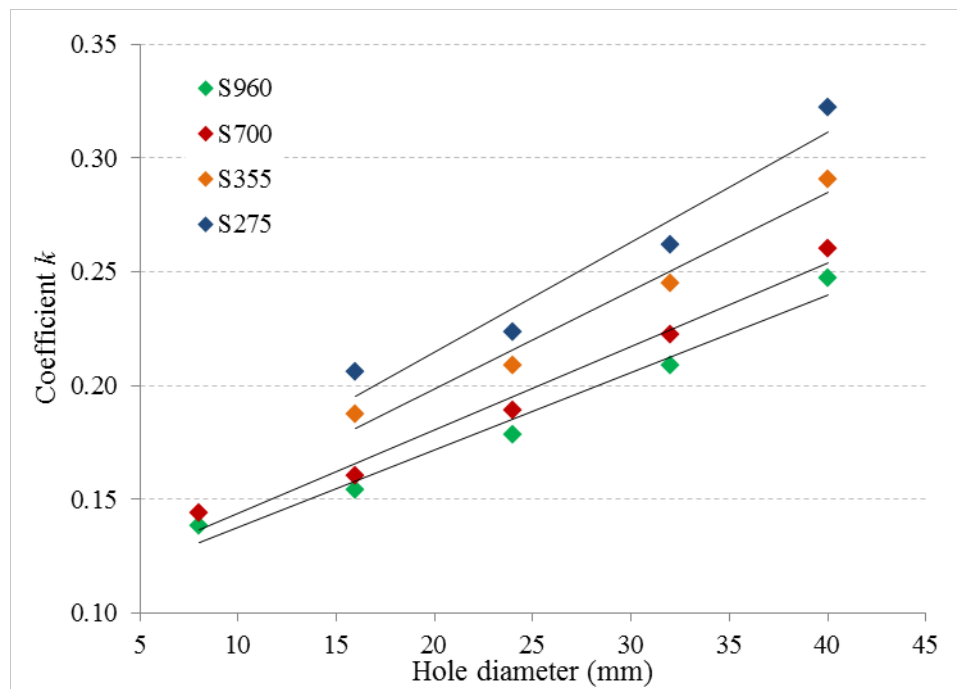


Figure 49 Strain concentration factor relation to the hole diameter

The lower the factor  $k$  is, the more concentrated stresses and strains are to be expected in the middle cross-section. This area is typically at the edge of the hole in CHT specimens. Increased strength of material also contributes to the differences between the observed equivalent plastic strains.

## Annex B: Simplified material models

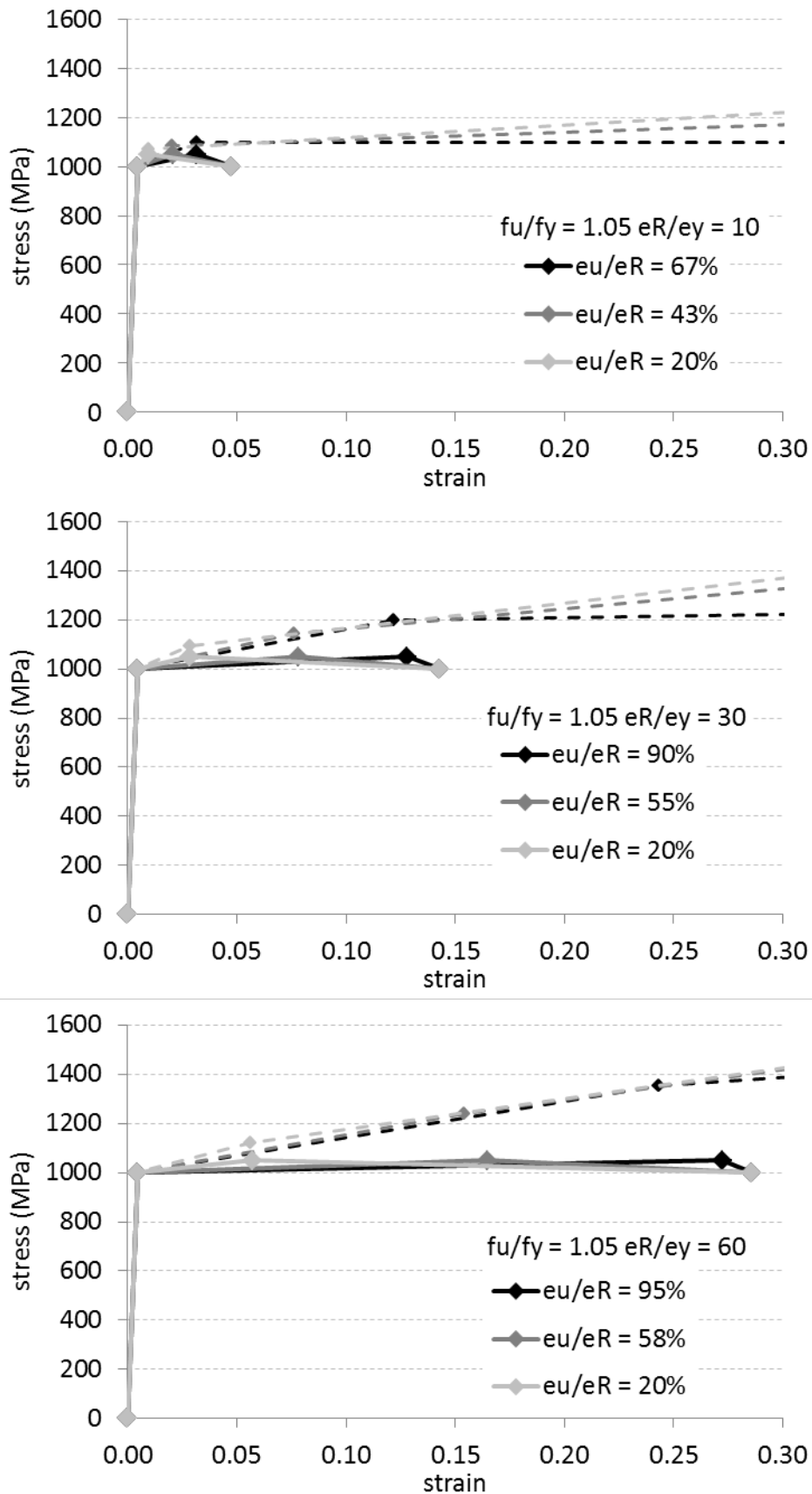


Figure 50 Stress-strain diagrams (solid – engineering values, dashed – true values) of selected simplified material models Group A

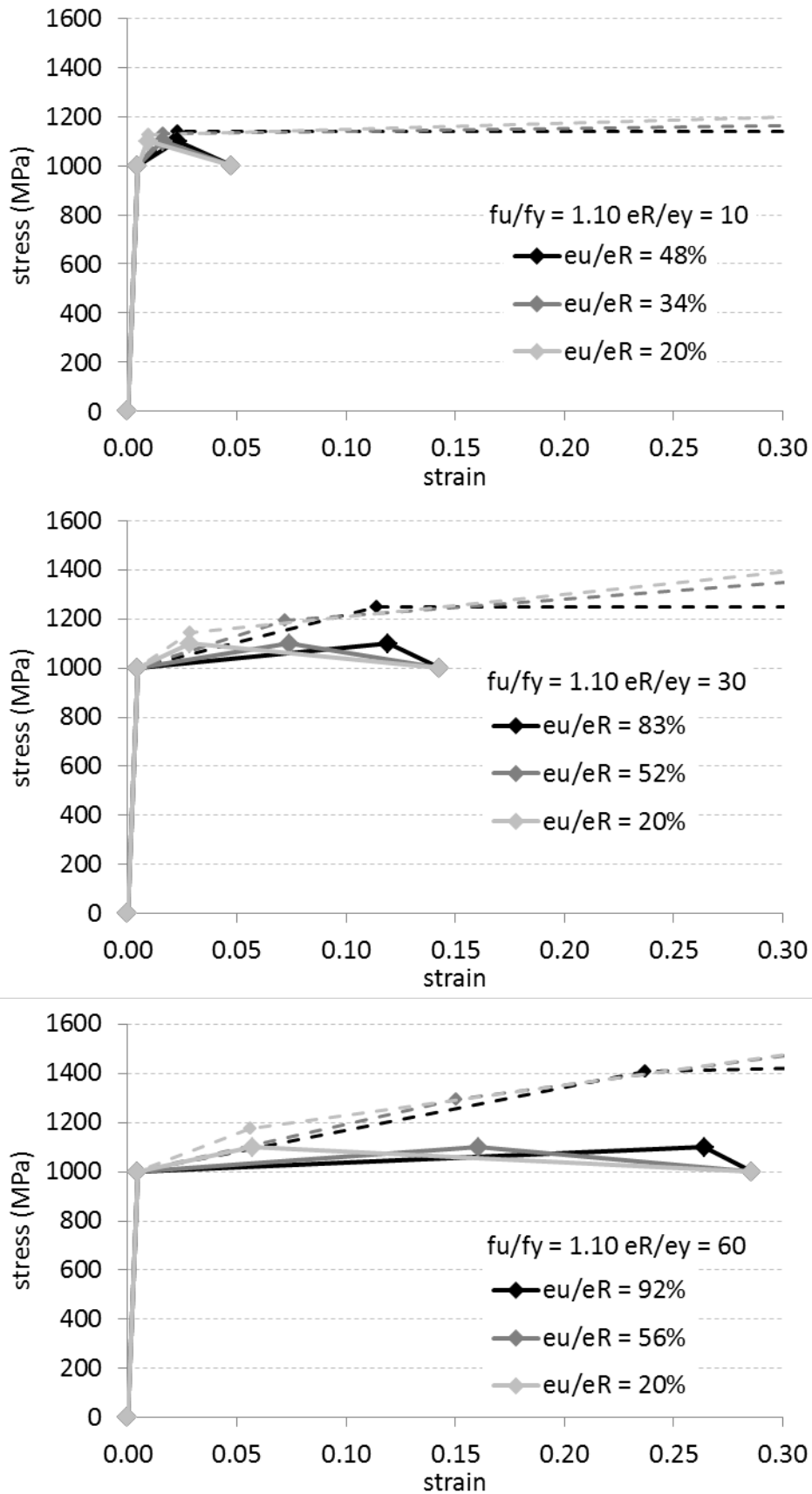


Figure 51 Stress-strain diagrams (solid – engineering values, dashed – true values) of selected simplified material models Group B

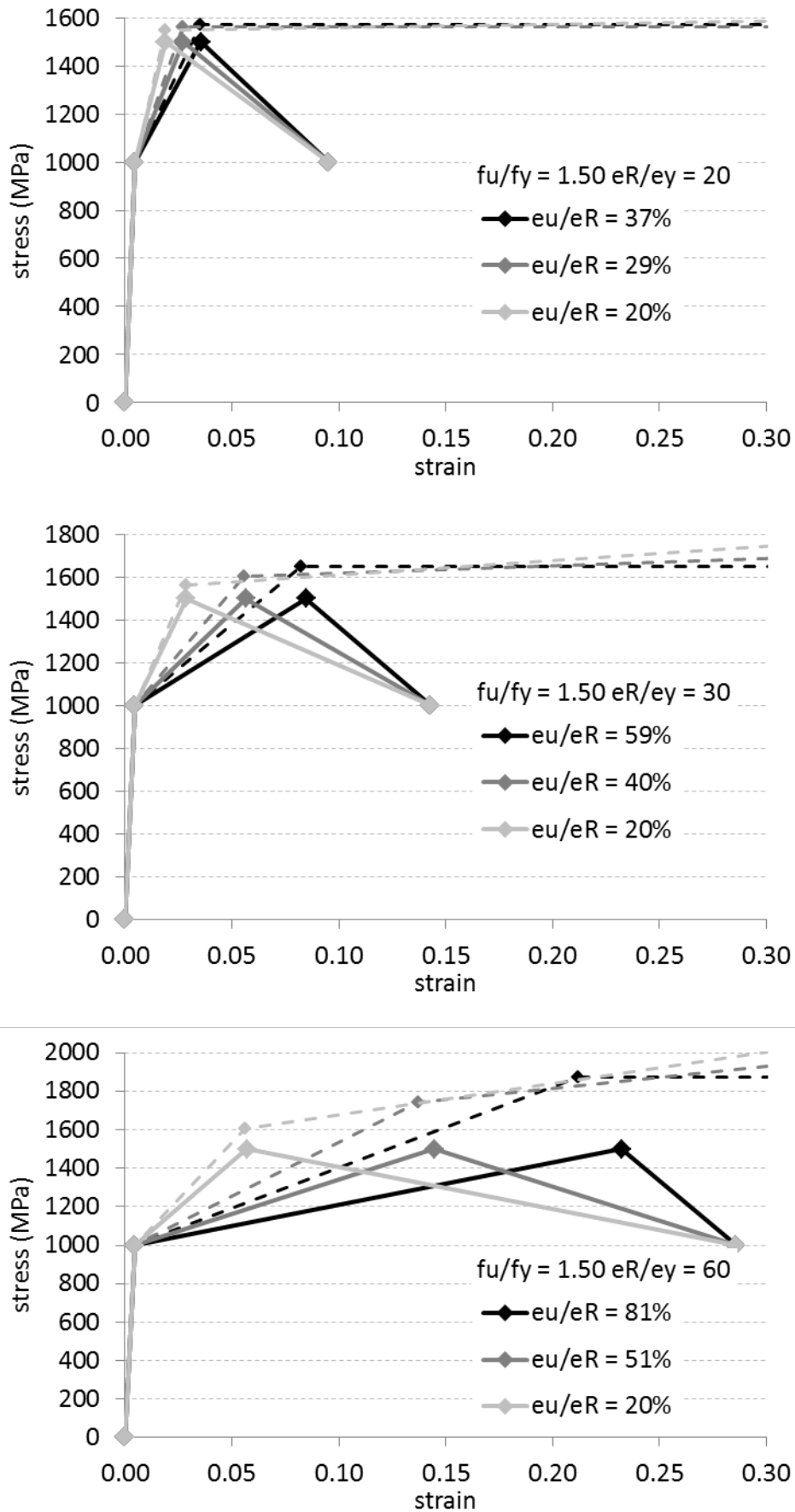


Figure 52 Stress-strain diagrams (solid – engineering values, dashed – true values) of selected simplified material models Group X



## Annex C: The upper limit of ultimate strain

The definition of the upper limit of ultimate strain is the highest possible value of strain at the ultimate load when the given limit strain  $\varepsilon_R$  can be reached at the yield stress level. This happens when the true stress is constant after the true strain reaches the value corresponding to the ultimate load. The additional material group called C was used in this study with  $f_u/f_y=1.2$ .

We have calculated the values of the limit strains from finite element simulations of coupon tests with cross-section 8 x 20 mm and the gauge length 71.5 mm (to obtain standard  $A_5$  value). The yield load was then 160 kN and the ultimate load was 168, 176, 192 or 240 kN for groups A, B, C and X respectively. To reach a given  $\varepsilon_R$  we had to interpolate between the results obtained for  $\varepsilon_u/\varepsilon_y$  ratio from 2 to 60 (see Figure 53).

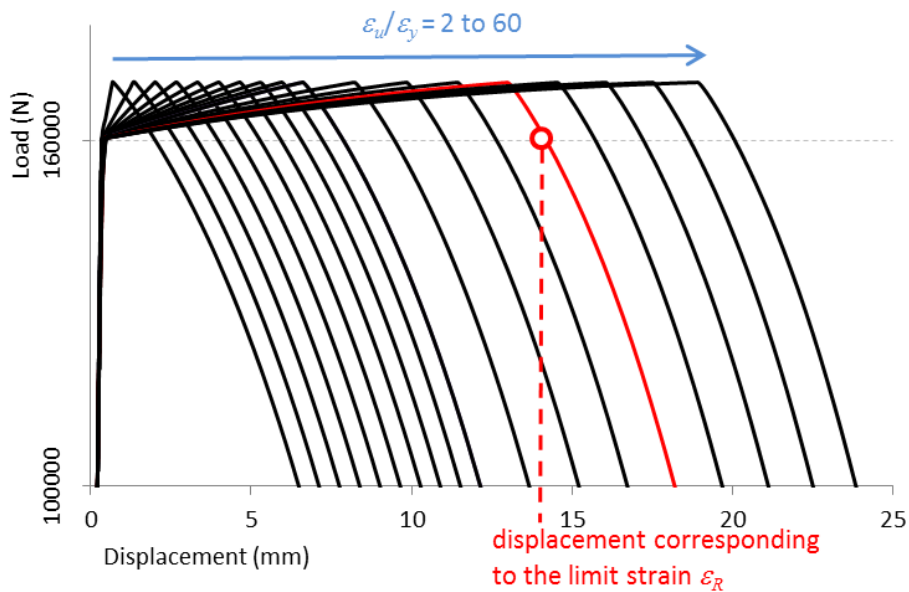


Figure 53 Finite element results for the limit strain search (group A)

The relationship between the maximum possible ultimate (uniform) strain and the corresponding limit strain is linear for all of the groups (see Figure 54).

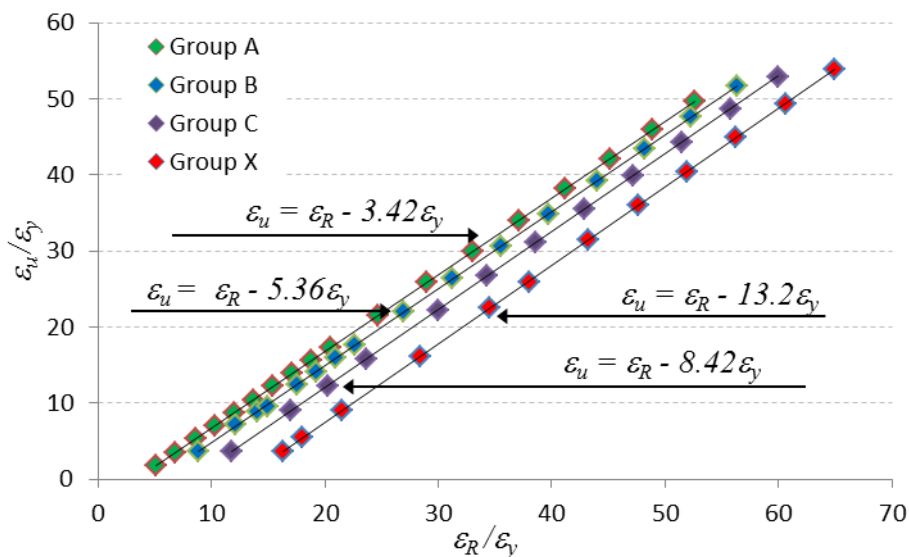


Figure 54 Interpolation of limit strains

This relation takes always the same form with the variable parameter  $A$ :

$$\varepsilon_u \leq \varepsilon_R - A\varepsilon_y \text{ or } \varepsilon_R \geq \varepsilon_u + A\varepsilon_y \quad (29)$$

Assuming that when  $f_u = f_y$  the strains will be equal ( $A = 0$ ) we can propose a simple exponential equation for the parameter  $A$ .

$$A = B(f_u/f_y - 1)^C \quad (30)$$

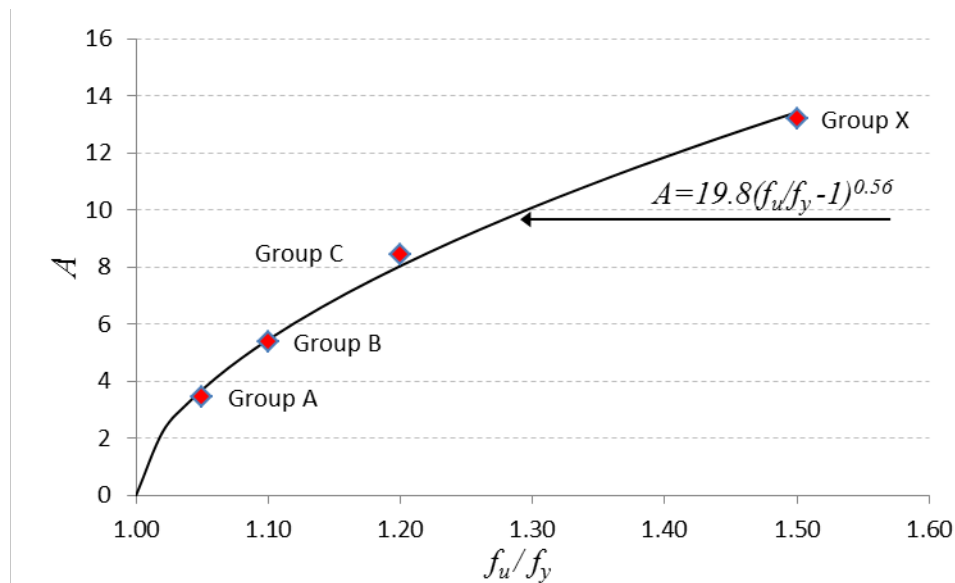


Figure 55 Calculation of parameter  $A$

The parameters  $B$  and  $C$  are approximated in Figure 55. Then the highest ultimate strain can be calculated as:

$$\varepsilon_u \leq \varepsilon_R - 19.8\varepsilon_y (f_u/f_y - 1)^{0.56} \text{ or } \varepsilon_R \geq \varepsilon_u + 19.8\varepsilon_y (f_u/f_y - 1)^{0.56} \quad (31)$$

This equation sets the lowest possible limit strain for steels fulfilling the ductility criteria of the Eurocodes. Particularly for normal steels according to EN 1993-1-1, where  $f_u/f_y$  is at least 1.1 and  $\varepsilon_u/\varepsilon_y$  at least 15 we can write:

$$\varepsilon_R \geq 20.5 \varepsilon_y \quad (32)$$

Similarly for high strength steels according to the EN 1993-1-12, the limit would be:

$$\varepsilon_R \geq 18.7 \varepsilon_y \quad (33)$$

## Annex D: CHT simulations of simplified material models

Table 24 Results of FEM calculations of CHT specimens

Model	$F_{max}$ (kN)	$F_{max}/A_{fu}$	$\Delta L_{Fmax}$ (mm)	$\Delta L_{\epsilon R}$ (mm)	$\Delta L_{\epsilon 10}$ (mm)	$\Delta L_{\epsilon R} / \Delta L_{Fmax}$	$\Delta L_{\epsilon 10} / \Delta L_{Fmax}$	
1	A1a-0	680	1.01	3.18	8.52	n/a	2.682	n/a
2	A1a-8	618	1.02	1.46	1.11	4.36	0.760	2.992
3	A1a-16	548	1.02	1.38	1.16	4.27	0.844	3.100
4	A1a-24	479	1.02	1.38	1.24	4.38	0.902	3.182
5	A1a-32	410	1.02	1.38	1.32	4.60	0.961	3.342
6	A1a-40	341	1.02	1.23	1.39	4.88	1.131	3.976
7	A1b-0	681	1.01	2.13	13.94	n/a	6.555	n/a
8	A1b-8	621	1.03	1.23	1.25	4.45	1.012	3.616
9	A1b-16	550	1.02	1.23	1.30	4.45	1.059	3.625
10	A1b-24	481	1.02	1.08	1.38	4.60	1.282	4.275
11	A1b-32	411	1.02	1.08	1.47	4.84	1.365	4.496
12	A1b-40	343	1.02	1.08	1.54	5.12	1.435	4.758
13	A1c-0	680	1.01	1.08	n/a	n/a	n/a	n/a
14	A1c-8	622	1.03	0.93	1.45	4.12	1.561	4.444
15	A1c-16	551	1.03	0.93	1.53	4.23	1.650	4.568
16	A1c-24	481	1.02	0.93	1.64	4.45	1.767	4.799
17	A1c-32	412	1.02	1.08	1.75	4.70	1.628	4.369
18	A1c-40	343	1.02	0.93	1.85	4.97	1.998	5.366
19	A3a-0	680	1.01	12.93	n/a	12.99	n/a	1.005
20	A3a-8	619	1.02	3.22	1.76	0.91	0.545	0.284
21	A3a-16	548	1.02	3.05	1.94	0.96	0.636	0.314
22	A3a-24	479	1.02	2.75	2.14	1.03	0.778	0.374
23	A3a-32	411	1.02	2.68	2.31	1.11	0.862	0.415
24	A3a-40	342	1.02	2.43	2.44	1.19	1.006	0.490
25	A3b-0	680	1.01	7.98	n/a	n/a	n/a	n/a
26	A3b-8	633	1.05	4.16	3.08	1.22	0.741	0.294
27	A3b-16	559	1.04	3.52	3.39	1.32	0.963	0.376
28	A3b-24	488	1.04	3.35	3.68	1.45	1.099	0.434
29	A3b-32	418	1.04	3.18	3.91	1.59	1.230	0.499
30	A3b-40	348	1.04	2.88	4.08	1.69	1.420	0.587
31	A3c-0	681	1.01	3.03	n/a	n/a	n/a	n/a
32	A3c-8	641	1.06	5.28	n/a	1.58	n/a	0.298
33	A3c-16	565	1.05	4.08	n/a	1.70	n/a	0.418
34	A3c-24	493	1.05	3.48	n/a	1.85	n/a	0.533
35	A3c-32	422	1.05	3.18	n/a	1.99	n/a	0.628
36	A3c-40	351	1.04	2.73	n/a	2.10	n/a	0.770

	<b>Model</b>	$F_{max}$	$F_{max}/Afu$	$\Delta L_{Fmax}$	$\Delta L_{\epsilon R}$	$\Delta L_{\epsilon 10}$	$\Delta L_{\epsilon R} / \Delta L_{Fmax}$	$\Delta L_{\epsilon 10} / \Delta L_{Fmax}$
37	A6a-0	670	1.00	15.00	n/a	n/a	n/a	n/a
38	A6a-8	634	1.05	6.37	3.42	1.60	0.537	0.251
39	A6a-16	558	1.04	5.30	3.87	1.78	0.731	0.337
40	A6a-24	487	1.04	5.00	4.33	1.99	0.866	0.399
41	A6a-32	418	1.04	4.63	4.67	2.20	1.007	0.474
42	A6a-40	348	1.04	4.38	4.87	2.35	1.113	0.538
43	A6b-0	678	1.01	15.00	n/a	n/a	n/a	n/a
44	A6b-8	652	1.08	12.97	n/a	1.48	n/a	0.114
45	A6b-16	573	1.07	7.70	n/a	1.64	n/a	0.212
46	A6b-24	498	1.06	6.95	n/a	1.82	n/a	0.262
47	A6b-32	426	1.06	6.28	n/a	2.01	n/a	0.319
48	A6b-40	354	1.05	5.58	n/a	2.15	n/a	0.386
49	A6c-0	684	1.02	15.00	n/a	n/a	n/a	n/a
50	A6c-8	658	1.09	11.43	n/a	1.62	n/a	0.141
51	A6c-16	578	1.08	6.97	n/a	1.80	n/a	0.258
52	A6c-24	503	1.07	6.05	n/a	2.02	n/a	0.333
53	A6c-32	430	1.07	5.43	n/a	2.21	n/a	0.407
54	A6c-40	357	1.06	4.83	n/a	2.34	n/a	0.485
55	B1a-0	713	1.01	2.28	11.04	n/a	4.851	n/a
56	B1a-8	646	1.02	1.38	1.58	5.56	1.145	4.037
57	B1a-16	572	1.02	1.38	1.64	5.22	1.189	3.794
58	B1a-24	500	1.01	1.23	1.74	5.23	1.417	4.266
59	B1a-32	428	1.01	1.23	1.85	5.43	1.505	4.424
60	B1a-40	356	1.01	1.23	1.94	5.72	1.583	4.667
61	B1b-0	713	1.01	1.68	12.83	n/a	7.654	n/a
62	B1b-8	648	1.02	1.08	1.61	5.68	1.495	5.275
63	B1b-16	574	1.02	1.08	1.68	5.35	1.556	4.969
64	B1b-24	501	1.02	1.08	1.78	5.35	1.655	4.973
65	B1b-32	429	1.01	1.08	1.90	5.54	1.763	5.149
66	B1b-40	357	1.01	1.08	2.01	5.84	1.863	5.427
67	B1c-0	713	1.01	1.08	n/a	n/a	n/a	n/a
68	B1c-8	649	1.02	0.93	1.68	5.67	1.816	6.121
69	B1c-16	575	1.02	0.93	1.76	5.41	1.901	5.836
70	B1c-24	502	1.02	0.93	1.88	5.44	2.027	5.869
71	B1c-32	429	1.02	0.93	2.01	5.63	2.165	6.077
72	B1c-40	357	1.02	0.93	2.13	5.92	2.294	6.393
73	B3a-0	713	1.01	12.03	n/a	12.19	n/a	1.013
74	B3a-8	638	1.01	3.63	2.37	0.92	0.653	0.253
75	B3a-16	565	1.00	3.37	2.63	0.97	0.780	0.287
76	B3a-24	494	1.00	3.20	2.89	1.05	0.902	0.328
77	B3a-32	424	1.00	3.03	3.08	1.15	1.017	0.378
78	B3a-40	354	1.00	2.88	3.21	1.23	1.115	0.427

	<b>Model</b>	$F_{max}$	$F_{max}/A_{fu}$	$\Delta L_{Fmax}$	$\Delta L_{\varepsilon R}$	$\Delta L_{\varepsilon 10}$	$\Delta L_{\varepsilon R} / \Delta L_{Fmax}$	$\Delta L_{\varepsilon 10} / \Delta L_{Fmax}$
79	B3b-0	713	1.01	7.53	n/a	n/a	n/a	n/a
80	B3b-8	656	1.04	4.16	3.90	1.65	0.938	0.396
81	B3b-16	581	1.03	3.63	3.77	1.84	1.039	0.506
82	B3b-24	507	1.03	3.35	4.04	2.05	1.207	0.612
83	B3b-32	434	1.03	3.18	4.27	2.23	1.345	0.703
84	B3b-40	361	1.03	2.88	4.44	2.36	1.545	0.819
85	B3c-0	713	1.01	3.03	n/a	n/a	n/a	n/a
86	B3c-8	662	1.04	3.78	4.21	2.72	1.114	0.721
87	B3c-16	585	1.04	3.03	4.28	2.80	1.413	0.925
88	B3c-24	511	1.04	2.73	4.62	3.04	1.694	1.116
89	B3c-32	438	1.04	2.43	4.94	3.26	2.035	1.342
90	B3c-40	365	1.04	2.28	5.22	3.43	2.293	1.507
91	B6a-0	691	0.98	15.00	n/a	n/a	n/a	n/a
92	B6a-8	646	1.02	6.48	3.80	1.66	0.586	0.256
93	B6a-16	570	1.01	5.15	4.28	1.88	0.830	0.365
94	B6a-24	499	1.01	4.85	4.74	2.13	0.978	0.440
95	B6a-32	428	1.01	4.78	5.07	2.37	1.060	0.496
96	B6a-40	358	1.02	4.53	5.27	2.56	1.163	0.565
97	B6b-0	709	1.01	15.00	n/a	n/a	n/a	n/a
98	B6b-8	675	1.07	13.01	11.98	1.18	0.921	0.091
99	B6b-16	594	1.06	7.72	8.39	1.29	1.087	0.167
100	B6b-24	518	1.05	7.10	8.87	1.43	1.249	0.201
101	B6b-32	443	1.05	6.48	9.27	1.58	1.430	0.243
102	B6b-40	368	1.04	5.88	9.45	1.70	1.608	0.289
103	B6c-0	714	1.01	10.53	n/a	n/a	n/a	n/a
104	B6c-8	682	1.08	9.93	9.62	1.26	0.969	0.127
105	B6c-16	600	1.07	6.18	7.98	1.39	1.293	0.225
106	B6c-24	523	1.06	5.60	8.45	1.54	1.509	0.276
107	B6c-32	447	1.06	4.98	8.89	1.70	1.786	0.341
108	B6c-40	372	1.06	4.38	9.12	1.81	2.083	0.413
109	X2a-0	974	1.01	3.63	n/a	n/a	n/a	n/a
110	X2a-8	880	1.02	3.18	6.09	5.64	1.918	1.775
111	X2a-16	773	1.01	2.73	5.32	4.94	1.950	1.813
112	X2a-24	674	1.00	2.58	5.37	5.02	2.085	1.948
113	X2a-32	576	1.00	2.58	5.68	5.33	2.206	2.068
114	X2a-40	479	1.00	2.43	6.02	5.64	2.480	2.324
115	X2b-0	973	1.01	2.88	n/a	n/a	n/a	n/a
116	X2b-8	881	1.02	2.43	5.55	6.01	2.287	2.478
117	X2b-16	776	1.01	2.28	4.96	5.33	2.179	2.343
118	X2b-24	676	1.01	2.13	5.03	5.37	2.366	2.527
119	X2b-32	578	1.00	2.13	5.33	5.67	2.505	2.664
120	X2b-40	481	1.00	1.98	5.66	6.02	2.865	3.044

Model		$F_{max}$	$F_{max}/A_{fu}$	$\Delta L_{Fmax}$	$\Delta L_{\epsilon R}$	$\Delta L_{\epsilon 10}$	$\Delta L_{\epsilon R} / \Delta L_{Fmax}$	$\Delta L_{\epsilon 10} / \Delta L_{Fmax}$
121	X2c-0	974	1.01	1.98	n/a	n/a	n/a	n/a
122	X2c-8	884	1.02	1.83	5.36	6.37	2.934	3.488
123	X2c-16	780	1.02	1.68	4.94	5.75	2.945	3.427
124	X2c-24	680	1.01	1.68	5.02	5.74	2.993	3.426
125	X2c-32	581	1.01	1.68	5.29	6.00	3.157	3.580
126	X2c-40	483	1.01	1.68	5.64	6.37	3.363	3.797
127	X3a-0	974	1.01	8.58	n/a	n/a	n/a	n/a
128	X3a-8	872	1.01	6.93	9.23	3.78	1.332	0.546
129	X3a-16	756	0.98	5.58	7.24	2.52	1.299	0.451
130	X3a-24	657	0.98	4.98	7.15	2.84	1.436	0.570
131	X3a-32	563	0.98	4.83	7.51	3.08	1.555	0.638
132	X3a-40	469	0.98	4.53	7.78	3.21	1.719	0.708
133	X3b-0	973	1.01	5.73	n/a	n/a	n/a	n/a
134	X3b-8	882	1.02	4.98	8.71	5.29	1.749	1.064
135	X3b-16	775	1.01	4.23	7.30	4.31	1.727	1.020
136	X3b-24	675	1.00	3.93	7.22	4.26	1.840	1.085
137	X3b-32	577	1.00	3.78	7.58	4.47	2.008	1.183
138	X3b-40	480	1.00	3.63	7.94	4.59	2.190	1.266
139	X3c-0	974	1.01	3.03	n/a	n/a	n/a	n/a
140	X3c-8	888	1.03	2.73	9.19	4.46	3.371	1.635
141	X3c-16	785	1.02	2.58	8.14	4.12	3.158	1.598
142	X3c-24	685	1.02	2.43	8.01	4.25	3.299	1.753
143	X3c-32	586	1.02	2.43	8.27	4.52	3.408	1.864
144	X3c-40	488	1.02	2.28	8.66	4.77	3.803	2.096
145	X6a-0	876	0.91	15.00	n/a	n/a	n/a	n/a
146	X6a-8	851	0.98	15.00	n/a	3.52	n/a	0.234
147	X6a-16	729	0.95	10.08	11.32	2.73	1.123	0.271
148	X6a-24	637	0.95	8.58	10.66	3.24	1.243	0.377
149	X6a-32	550	0.95	8.13	11.10	3.66	1.366	0.450
150	X6a-40	462	0.96	7.68	11.35	3.95	1.478	0.514
151	X6b-0	974	1.01	14.73	n/a	14.84	n/a	1.008
152	X6b-8	898	1.04	12.78	n/a	2.00	n/a	0.156
153	X6b-16	789	1.03	10.38	n/a	1.75	n/a	0.169
154	X6b-24	686	1.02	9.03	n/a	2.04	n/a	0.226
155	X6b-32	587	1.02	8.58	n/a	2.29	n/a	0.267
156	X6b-40	488	1.02	7.98	n/a	2.46	n/a	0.308
157	X6c-0	974	1.01	7.83	n/a		n/a	n/a
158	X6c-8	924	1.07	10.08	n/a	3.05	n/a	0.302
159	X6c-16	816	1.06	7.38	n/a	2.09	n/a	0.284
160	X6c-24	712	1.06	6.48	n/a	2.31	n/a	0.356
161	X6c-32	609	1.06	5.88	n/a	2.51	n/a	0.426
162	X6c-40	507	1.06	5.43	n/a	2.62	n/a	0.482

## **Annex E: True stress-strain relationship for finite element simulations of structural details under diffuse necking**

---

Paper presented at Nordic Steel Construction Conference 2015, Tampere, Finland , 23-25 September 2015.

Petr Hradil<sup>a</sup> and Asko Talja<sup>b</sup>

<sup>a,b</sup> *VTT Technical Research Centre of Finland*

**Abstract:** The paper presents an automated numerical method for acquiring true stress-strain relationship from the material test results of high-strength steels. The model beyond uniform load is iterated to produce load-displacement relationship matching the experimental results recalculated by finite element method. We have used this approach to evaluate coupon tests of high-strength grades S700 and S960, and extended the study to mild steels S275 and S355 for comparison. The results were validated against the tensile experiments of plates with central hole made from the same steel S960 as original coupons. The presented algorithm will serve as a basis for evaluation of ductility limits for different steel grades.

### **1 Introduction**

Steel structures are generally designed to the level of yield or ultimate strength of the material in the cross-section. However, certain structural details tolerate relatively high strains in the localized areas where the instability in tension called necking may occur. For instance the net section resistance in tension can involve diffuse necking near the drilled holes. Such details are critical especially for high strength steels where the ductile failure happens at relatively low deformations. To simulate such cases with finite element method (FEM), one needs the definition of material plasticity in terms of true stress and true plastic strain relation also in the range of necking. The material model would be most preferably obtained from the standardized coupon tests.

#### **1.1 Stress-strain characterization**

The definition of inelastic behaviour of materials in FEM analysis is usually based on the true stress and true plastic strain relation which is convenient for the finite element solver. On the other hand, loads and displacements produced by material testing correspond to the engineering stress-strain relation that is only slightly different as long as the deformation is uniform throughout the tested cross-section. FEM design is commonly limited until the plastic strains reach 5%, which is usually less than the uniform elongation in material testing. The small difference between uniform engineering and true stress-strain curves is often neglected in modelling mild steel grades, because the limit of uniform deformation is rarely reached. Utilization of high strength steels is thus introducing a new challenge. Diffuse necking introduces non-uniform deformation that in high strength steels is usually initiated at low tensile strains, and therefore the localized instability can occur more frequently than in mild grades. This means that constitutive models should be always based on true stress and strain values. The commonly used true stress-strain models were developed for the very high deformations simulation (e.g. car manufacturing, cold forming, brake pressing) of standard materials where the assumption of rigid-plastic material with strain hardening [1] was accurate enough. The effect of elastic deformation in high strength steels is, however, more pronounced because of



the high stress levels at relatively low total strains. The material elasticity cannot be simply neglected.

## 1.2 Existing studies

A great number of empirical methods to obtain true stress-strain curves were continuously developed since 1950s [2], and nowadays it is possible to predict the true stress-strain behaviour from tensile, compression, ball indentation, punch, torsion or notch tensile tests. ManSoo et al. presented an iterative method for predicting true stress-strain curves over large range of strains using FEM calculations of real tensile tests [3]. The steel used in their study was Japanese grade SWCH10A 3.125 mm wire for cold heading and cold forging with tensile strength 357 MPa. The material model for FEM calculations was rigid-viscoplastic and incompressible. The true stress values were corrected in each iteration step by the ratio between predicted and measured load at given displacement and corresponding true strain was calculated as the average strain in the minimum cross-section.

## 2 True stress-strain curves for Abaqus models

Our iterative approach for the true stress-strain characterization of measured tensile test data uses similar method than ManSoo et al. [3] when the true stress values are corrected by the ratio between predicted and measured load,  $P_{FE}$  and  $P_M$  respectively.

Unlike the referenced study, our material model is elastic and plastic because of the significant fraction of elastic deformations in high-strength steels, and we used rectangular cross-section (coupons cut from the metal sheet) as a reference. Unfortunately, the solution based on the average strain in the minimum cross-section was not fitting the real experimental data well and we selected the maximum equivalent plastic strain as the reference value corresponding to the given displacement for iterative corrections. It should be noted that either of the options was not providing exact position of true stress to be corrected but the iterations were converging much faster in the latter case (see Fig. 2).

The algorithm was implemented in the Abaqus finite element software [4] and it was used to predict the true stresses and strains beyond the ultimate load. The criterion was that the average difference between calculated loads and the measured ones  $r$  should be smaller than the limit value  $r_{lim}$  (see Fig. 1).

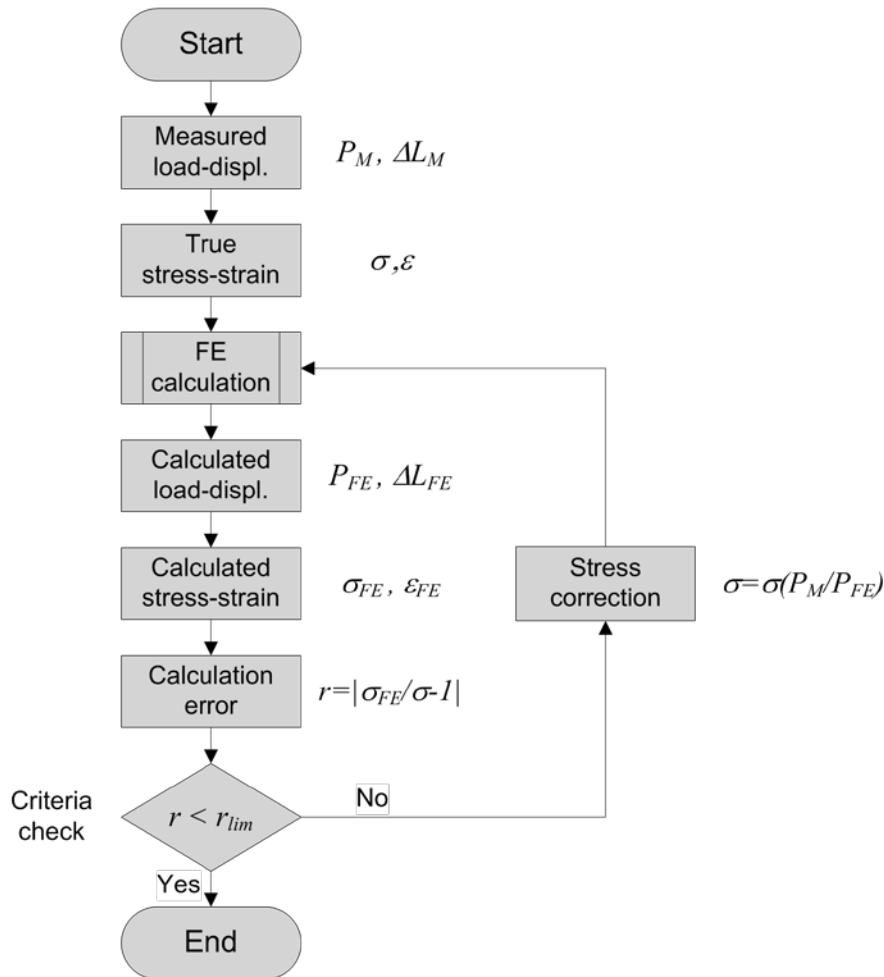


**Fig. 1:** Iterative procedure used for stress-strain characterization of measured data

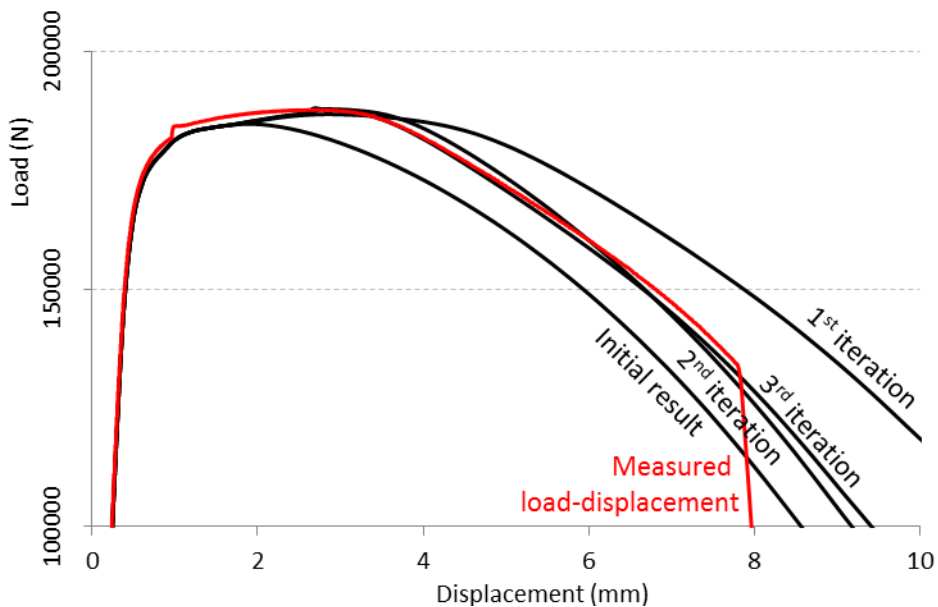


**Fig. 2:** Example of numerical stress-strain characterization (test S960-1)

## 2.1 Coupon tests

Since the focus of our study is on high-strength steels and especially on those grades not yet included in the Eurocode 3 [5], we have analysed test results from 16 coupon tests from S960 measured until the ductile failure with the gauge length 80 mm. Additionally we have used one

set of data for S700, S355 and S275 with the gauge length corresponding to A5 requirements of EN 10002-1 [6]. The basic coupon properties are summarized in Table 1.

## 2.2 Finite element models and scripts

For the simulation of coupon tests in Abaqus, we have used solid continuum 3D elements with reduced integration C3D8R and C3D6. Materials were elastic and plastic with the plasticity defined explicitly by iteration procedure. The distance between nodes was always less than 2 mm, in the necking area it was less than 0.2 mm. Due to the symmetrical nature of simulated experiments, only 1/8 of total volume of the coupon was modelled by using appropriate boundary conditions. Finite element models didn't have any failure criteria implemented, but provided results until pre-defined axial displacement with maximum step of 1% of this value. Small imperfection of 0.2 mm was needed in the middle of the specimen to initiate diffuse necking.

The models were generated using Python script and their selected results automatically evaluated and stored in spreadsheet files after the simulation. Moreover, the stress-strain and load-displacement charts were automatically generated in each iteration step. Then the whole procedure was repeated until the conditions of iteration method were met and the script switched to the next experimental data. This high level of automation enabled generating true stress-strain curves from the series of experimental results automatically without any user interaction.

*Table 1: Measured values of tested coupons*

Test		$t$ (mm)	$b$ (mm)	$f_y$ (MPa)	$f_u$ (MPa)	$\varepsilon_u (A_{gt})$	$E$ (MPa)	orientation
1	S275	7.97	19.8	300	418	0.179	172061	Rolling
2	S355	9.98	19.8	393	550	0.134	162137	Rolling
3	S700	10 <sup>1)</sup>	20 <sup>1)</sup>	708	792	0.095 <sup>2)</sup>	210000 <sup>1)</sup>	Rolling
4	S960-1	8.07	20.10	1060	1157	0.034	205142	Rolling
5	S960-2	8.08	19.98	1056	1167	0.039	206121	Rolling
6	S960-3	8.07	20.01	1061	1167	0.033	207249	Rolling
7	S960-4	8.07	20.11	1059	1157	0.038	207881	Rolling
8	S960-5	8.07	20.03	1061	1156	0.034	206614	Rolling
9	S960-6	8.10	19.96	1055	1158	0.032	204822	Rolling
10	S960-7	8.08	20.04	1062	1158	0.032	205123	Rolling
11	S960-8	8.09	20.13	1062	1162	0.034	204592	Rolling
12	S960-9	8.06	20.23	1062	1169	0.025	209650	Transverse
13	S960-10	8.05	20.15	1067	1174	0.022	207736	Transverse
14	S960-11	8.07	20.22	1061	1170	0.025	211583	Transverse
15	S960-12	8.06	20.16	1063	1167	0.024	208074	Transverse
16	S960-13	8.06	20.23	1061	1172	0.026	207249	Transverse
17	S960-14	8.08	20.15	1079	1194	0.030	209316	Transverse
18	S960-15	8.06	20.18	1058	1171	0.025	211805	Transverse
19	S960-16	8.06	20.20	1067	1174	0.024	210898	Transverse
Average S960		8.07	20.12	1062	1167	0.030	207741	-

<sup>1)</sup> Property was not measured, <sup>2)</sup> Value obtained additionally from the stress-strain curve

## 2.3 Predicted true stress-strain curves

The results of coupon tests evaluation are presented in Fig. 3, where the points of yield, ultimate and failure load are indicated. The true stress-strain curves didn't have any failure criteria and were linearly extrapolated beyond the last known experimental displacement of coupons.

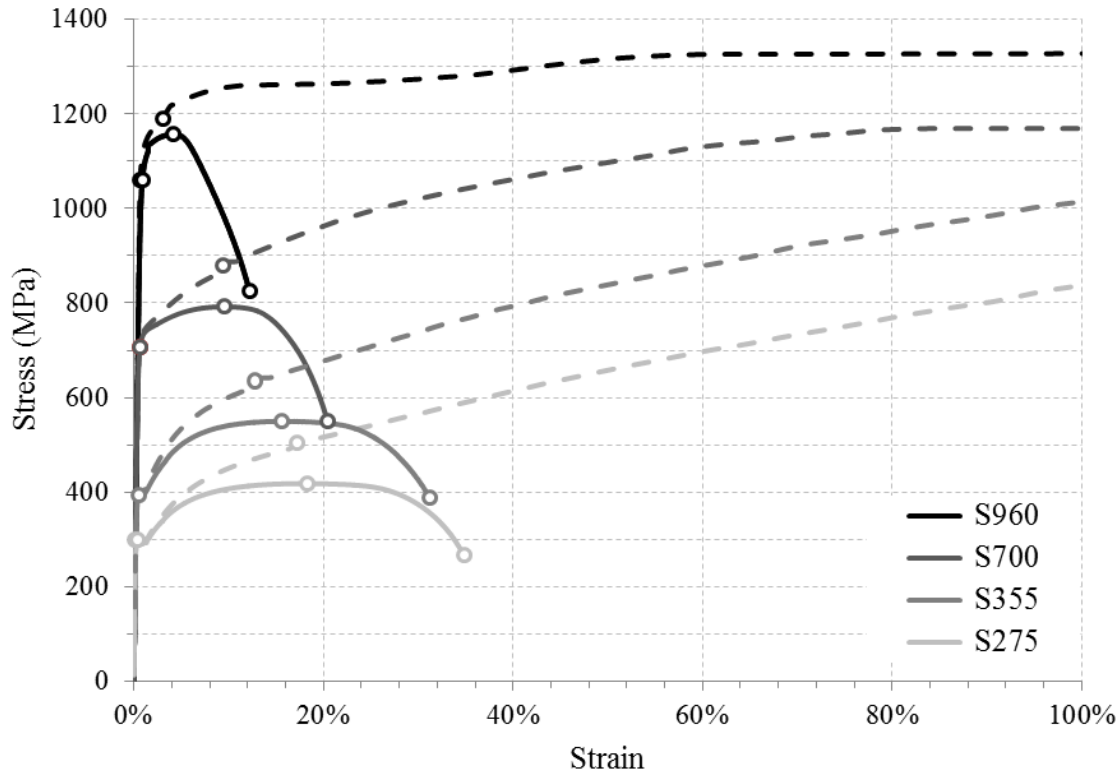


**Fig. 3:** Engineering stress-strain (solid lines) and calculated true stress-strain curves (dashed lines) for studied materials with indicated points of yield, ultimate load and fracture

Even though the ductile failure was not modelled in Abaqus, appropriate maximum (von Mises) equivalent strain and stress triaxiality (ratio of hydrostatic and equivalent stress) was recorded in each calculation step. These two values are governing parameters of common fracture models and will be used later in the investigation of ductility limits in different structural details. They were always located at the same place in the middle of necked cross-section. The maximum equivalent plastic strain at real coupon failure  $\varepsilon_{eq,C}$  was ranging from 98% (S960) to 188% (S275), and triaxiality  $T_C$  was ranging from 0.81 to 0.95.

### 3 Centre hole tests simulations

The average material model from sixteen coupons from S960 was used to predict the load-displacement of centre hole tension (CHT) tests. The numerical results were compared to the real experiments from the same material.

#### 3.1 CHT tests

Five specimens from high-strength steel grade S960 with the diameter of the hole ranging from 8 to 40 mm were calculated. Their geometry is illustrated in Fig. 4.

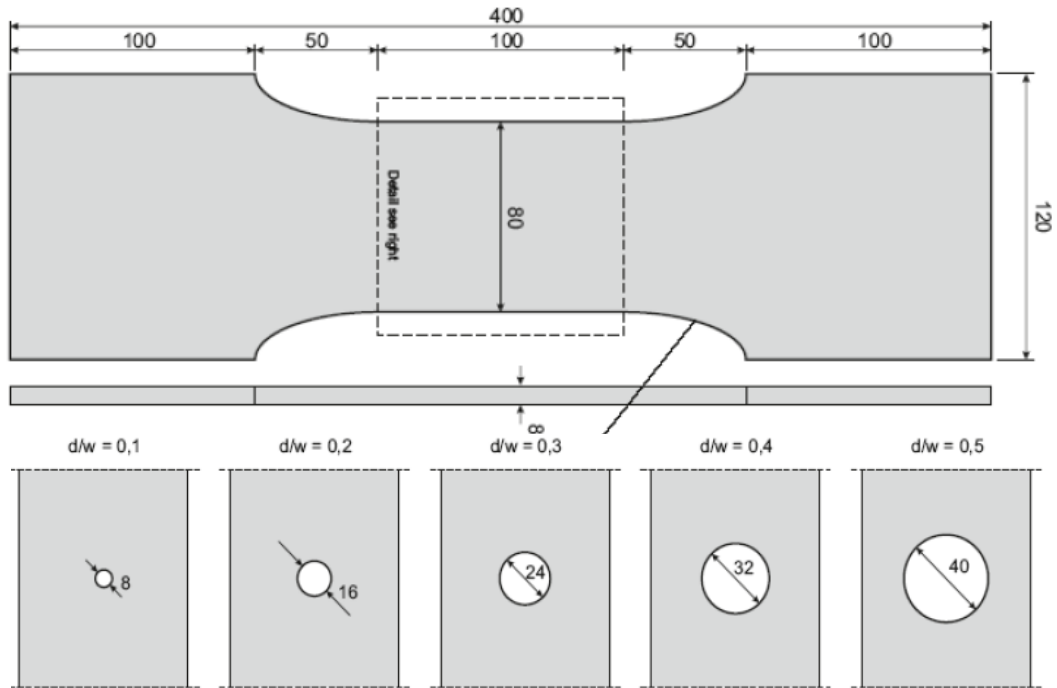


**Fig. 4:** Shape of CHT test specimen

### 3.2 Finite element models

Abaqus models used in CHT experiments evaluation were similar to those used in coupon tests with identical element types and maximum node spacing. The area of stress concentration around the hole was meshed so the number of elements around the hole was always the same regardless the diameter.

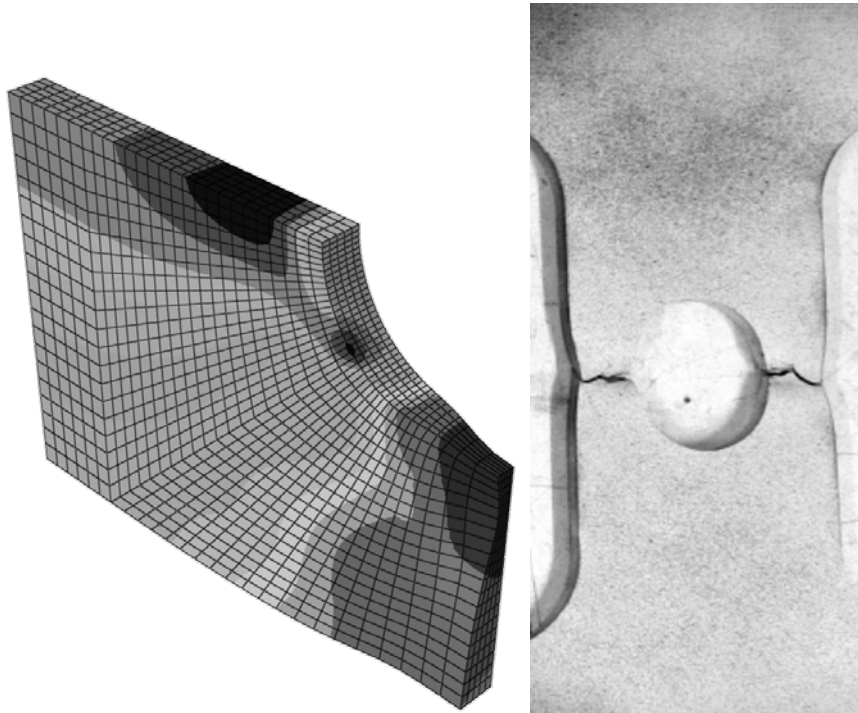


**Fig. 5:** Finite element model of CHT specimen and the real specimen [7] with symmetrical failure (von Mises stress distribution, S960 with hole diameter 40 mm)

From the observation of failure modes of real specimen, we decided to model symmetrically only diameters higher than 16 mm (see Fig. 5), and the smaller holes were always calculated

with the full length of the specimen as in Fig. 6. The asymmetrical cases required imperfection that was placed in distance  $a=(b-d)/2$  from the centre of the specimen.

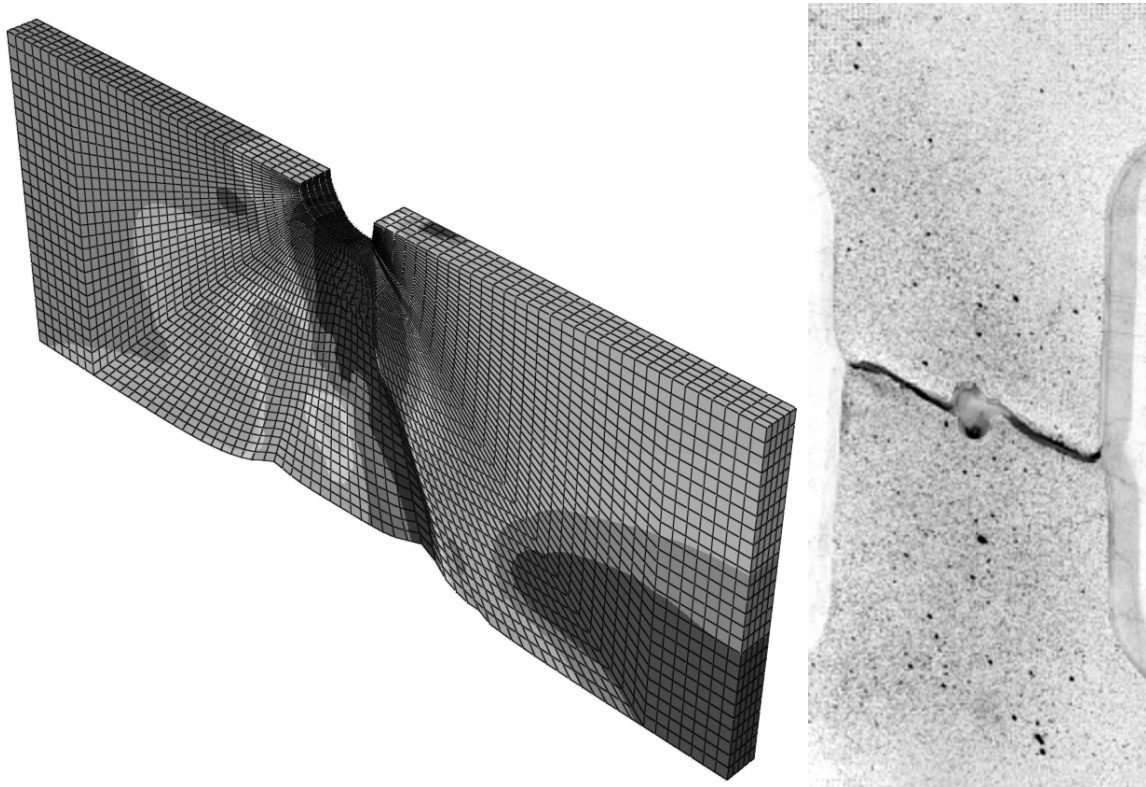


**Fig. 6:** Finite element model of CHT specimen and the real specimen [6] with asymmetrical failure (von Mises stress distribution, S960 with hole diameter 8 mm)

The same post-processing procedure was used for CHT simulations as for the coupon test, and therefore maximum equivalent plastic strains and maximum triaxialities were recorded automatically in the spreadsheet files after the simulation. The position of those values was, however, not the same. The highest strains were always at the hole edge in the middle cross-section, while the triaxialities reached the maximum slightly below the edge. Moreover, some specimen failed finally in shear which needs more investigation about the required ranges of stress triaxiality [8].

### 3.3 Predicted load-displacement and failure

As can be seen from Fig. 7 the predicted load-displacement is very close to the experimental results. Moreover, we have used simple method to estimate the failure of such specimens. Due to the complicated nature of failure mechanisms and models describing them, our goal was to predict safe value with the limited knowledge of model variables, ideally only the maximum equivalent plastic strain. For this purpose, we have selected SMCS failure model [9]. The method has been shown to make accurate fracture predictions for many practical conditions, such as the necked ligament between bolt holes, structural moment connection, material tension specimen and circumferential notch tensile (CNT) specimen. In these cases, fracture typically initiates internally, where the stress triaxiality is relatively high ( $T>0.75$ ) and then propagates outwards towards the surface of the material. However, there are other situations where fracture may initiate on the surface of the material, where triaxiality at failure is usually lower. Fracture initiation on the surface has been observed for example in large scale tests on structural braces and column base plate tests. Then more complicated models are often needed. SMCS model relies only on two parameters, equivalent plastic strain and stress triaxiality which are related according to Eq. (1) where  $\alpha$  is the parameter usually obtained by series of shear and tension



experiments with different triaxialities. The equation implies that higher triaxiality leads always to lower critical strain at failure.

$$\varepsilon_{cr} = \alpha e^{-1.5T} \quad (1)$$

We have further simplified the model with the assumption that the highest possible triaxiality would be 1 in the case of CHT details, and therefore only the knowledge of equivalent plastic strain in CHT is needed to assess the ductile failure as can be seen in Eq. (2) where  $\varepsilon_{eq,C}$  and  $T_C$  are known values of equivalent plastic strain and triaxiality at failure of tested coupon.

$$\varepsilon_{cr} = \alpha e^{-1.5} = (\varepsilon_{eq,C} / e^{-1.5T_C}) e^{-1.5} = \varepsilon_{eq,C} e^{1.5T_C - 1.5} \quad (2)$$

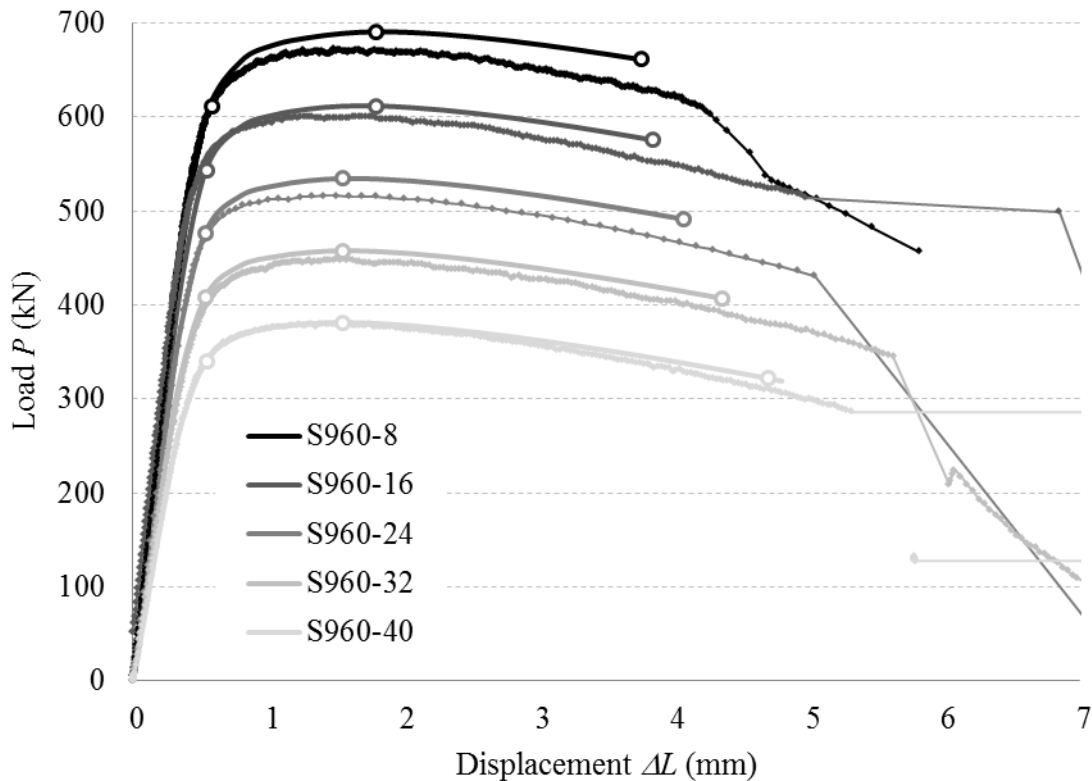


**Fig. 7:** Predicted load and displacement (thick lines) and measured values (thin lines) for CHT specimens with holes 8 to 40 mm and predicted values based on first yield load  $f_y A_{net}$ , ultimate load  $P_{max}$  and SMCS critical strain

The resulting critical plastic strain for CHT specimens was 83% which is smaller than the failure strain of coupons (98%), but it should be safe provided that the triaxiality doesn't exceed 1 in CHT specimens. The predicted failure occurs when the maximum equivalent strain reaches the critical value. This simple approach is very convenient for quick estimation of the ductile capacity of the studied details. The results are also included in Fig.7.

## 4 Conclusions

The main conclusions are

1. Developed procedure for assessment of true stress-strain relation in Abaqus is powerful tool to effectively obtain good quality material model for simulations of structural details with large strains.
2. The resulting models are intended to be used with the same finite element software and preferably the same meshing parameters.
3. Accurate prediction of ductile failure in details with high stress concentration is usually beyond the knowledge of common designer, but some estimation can be obtained using simple limits for equivalent plastic strains.

## Acknowledgments

The research leading to these results has received funding from Finnish Metals and Engineering Competence Cluster's (FIMECC) program BSA - Breakthrough steels and applications (2014-2018) and its project Design beyond present codes – enabling efficient utilisation of new materials. We would like to thank Ruukki Construction Oy for the experimental test results of coupons and CHT specimens.

## Notation

$b$	Coupon/CHT specimen width (mm)
$d$	Hole diameter of CHT specimen (mm)
$f_u$	Ultimate strength ( $R_m$ in testing standards, MPa)
$f_y$	Yield strength ( $R_{p,0.2}$ in testing standards, MPa)
$P_{FE}$	Predicted load (kN)
$P_M$	Measured load (kN)
$r$	Average difference between measured and calculated load (%)
$r_{lim}$	Minimum average difference between measured and calculated load (%)
$t$	Coupon thickness (mm)
$T_C$	Maximum stress triaxiality at failure of coupons
$\Delta L_{FE}$	Predicted displacement (mm)
$\Delta L_M$	Measured displacement (mm)
$\alpha$	SMCS fracture model parameter
$\varepsilon$	True strain (%)
$\varepsilon_{cr}$	Predicted critical equivalent plastic strain at failure of CHT specimen (%)
$\varepsilon_{eq,C}$	Maximum equivalent plastic strain at failure of coupons (%)
$\varepsilon_{FE}$	Predicted true strain (%)
$\varepsilon_u$	Ultimate uniform engineering strain ( $A_{gt}$ in testing standards, %)
$\sigma$	True stress (MPa)
$\sigma_{FE}$	Predicted true stress (MPa)

## References

- [1] Considère A. *Annales des Ponts et Chaussées IX9*, 6ème serie, p. 463, 1885.
- [2] Bridgman P.W., *Studies in Large Flow and Fracture*, McGraw-Hill, New York, 1952.
- [3] ManSoo J., Jea G.E., Min C.L. “A new method for acquiring true stress–strain curves over a large range of strains using a tensile test and finite element method”, *Mechanics of Materials*, 40, 586–593, 2008.
- [4] ABAQUS Documentation, ver. 6.13, Dassault Systèmes, 2014.
- [5] EN 1993 Eurocode 3 – Design of steel structures, CEN, Brussels, 2005.
- [6] EN 10002 Metallic materials – Tensile testing, CEN, Brussels, 2002.
- [7] Valkonen I., “20th European Conference on Fracture (ECF20): Ultimate limit loads in welded joints and in net sections of high strength steels with yield stress 960 MPa”, *Procedia Materials Science*, 3, 720-725, 2014.
- [8] Zhang Z.L., Hauge M., Ødegård J., Thaulow C. “Determining material true stress-strain curve from tensile specimens with rectangular cross-section”, *International Journal of Solids and Structures*, 36, 3497-3516, 1999.
- [9] Myers A.T., Deierlaine G.G, Kanvinde A. Testing and probabilistic simulation of ductile fracture initiation in structural steel components and weldments, Report No. 170, The John A. Blume Earthquake Engineering Center at Stanford University, 2009.

## Annex F: Ductility requirements for structural details with stress concentration and diffuse necking

---

Paper presented at Colloquium on Stability and Ductility of Steel Structures, Timisoara, 2016.

Petr Hradil<sup>a</sup>, Ludovic Fülöp<sup>b</sup>, Asko Talja<sup>c</sup> and Petri Ongelin<sup>d</sup>

<sup>a,b,c</sup> *VTT Technical Research Centre of Finland*

<sup>d</sup> *Ruukki Construction Oy*

**Abstract:** Structural steels need to demonstrate certain ductility in order to be used in buildings design. Fulfilling these criteria of design codes may be difficult especially for new high-strength steels where ductile fracture of tensile coupons appears at relatively low deformation. The goal of our study is to develop a calculation method of alternative ductility limits for structural details in a particular design situation. Such limits might be less demanding. Application of the method to a large variety of material models resulted in a simple criterion for the standard coupon test, the minimum distance between the uniform elongation and the coupon failure. This distance is called “necking capacity” of a tensile coupon in our paper.

### 1. Introduction

Material ductility is one of the most important requirements in structural steel design. It is implicitly used to alleviate stress concentrations in structural details and explicitly required in the plastic design and seismic design situations. Eurocode 3 [1] prescribes the ductility requirements in the form of minimum ultimate-to-yield strength ratio  $f_u/f_y$ , uniform elongation  $\varepsilon_u$ , and elongation at fracture  $A_5$  (see Table 1). When the material yield strength is increased in production by alloying or heat treatment, its ductility is generally decreasing. Therefore, more relaxed ductility requirements are applied to high strength steels (S500 to S700) in exchange for certain restrictions in plastic design and semi-rigid connections [2]. This trend continues with development of higher grades such as S960, which is often beyond the current limits.

The purpose of our study is to develop a more rational method to determine the ductility requirements for the structural detail in particular design situations. Such requirements may be easier to satisfy than the general ones. Additionally, design situations where high strength steel can be used without limitations are identified. The method relies on standardized material tests according to EN 10002-1 [3] and EN ISO 6892-1 [4] and properly calibrated finite element models (FEM). Numerical calculation is often able to generate acceptable solution for a given design case, but it is also powerful instrument to cover wide range of structural details and material parameters for the further generalization to design recommendations. An example of this approach is presented in the second part of this paper, where the developed method is applied in a large parametric study to formulate generalized ductility requirements for a structural detail.

### 2. Calculation of ductility requirements

The method presented in this section predicts the minimum required elongation at fracture ( $A_5$ ) of tensile coupon, for a given combination of  $f_u/f_y$  and  $\varepsilon_u$  to fulfil the selected design limit in a particular detail. It relies on a standard material coupon test and two numerical models, one of the selected structural detail and one of the coupon itself. The calculation is based on the assumption that strains larger than the uniform elongation of tensile coupon  $\varepsilon_u$  can be accepted in localized areas of statically loaded structures. However, the load should not cause ductile

failure in materials, and therefore the plastic strains and stress triaxiality should remain within acceptable limits. Unfortunately, it is impossible to describe the relation of stress triaxiality and plastic strain at fracture with data from commonly used coupon test, and therefore the present method generates conservative results. A more accurate solution requires a rather complicated testing programme.

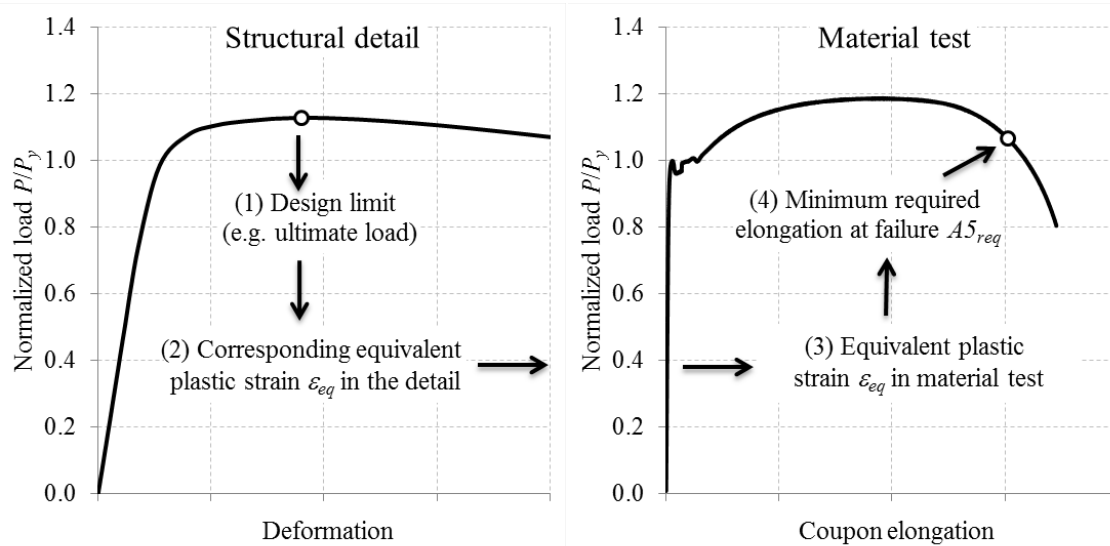


Fig. 1: Prediction of minimum required elongation at failure

The proposed method is based on a single parameter, the maximum equivalent plastic strain  $\varepsilon_{eq}$  in the critical cross-section of the structural detail. If a few conditions are satisfied, it is safe to assume as required coupon elongation  $A5_{req}$  the point when the same equivalent plastic strain  $\varepsilon_{eq}$  is reached in the coupon during the coupon test (Fig. 1). The required conditions are:

- (a) Stress triaxiality at the failure of the structural detail is smaller than the stress triaxiality of tested coupon. This condition is true on details with notches and holes in tension and plain rectangular coupons (see Fig. 2) except for the initial part of loading [5]. Similar findings were reported by Dunaud [6].
- (b) The relation between failure strain and stress triaxiality (the damage curve) of a material is monotonic non-increasing function as in Fig. 2. It has been observed that the fracture strains of non-notched specimens are always higher than those of notched samples with lower triaxiality [7], [8].

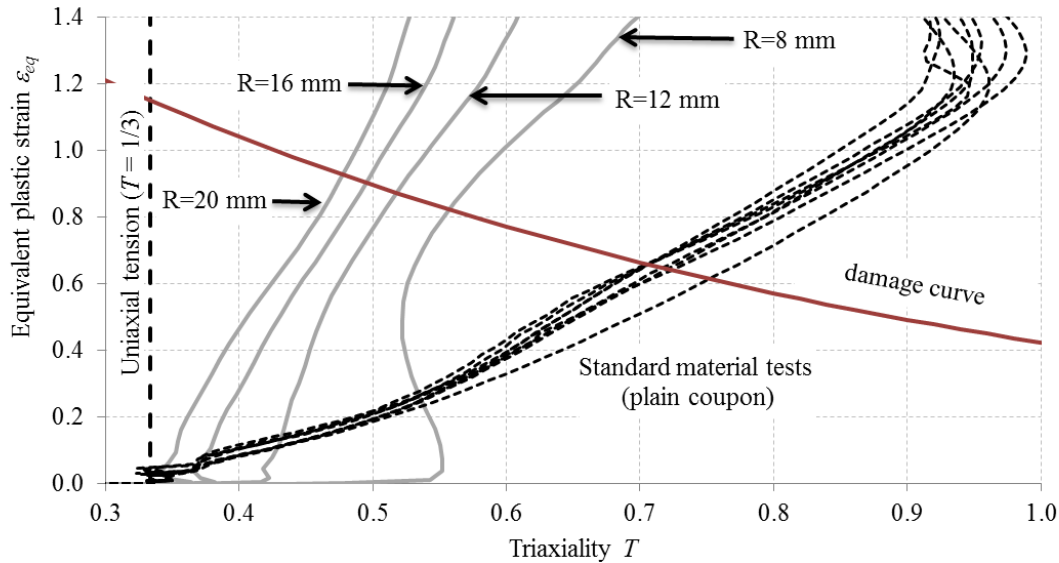


Fig. 2: Equivalent plastic strains and stress triaxiality observed in S960 models of specimens with hole in tension ( $R=8$  to  $20$  mm) and plain coupons, and example damage curve of the material.

The equivalent plastic strains were often found largest in the middle of the coupon cross-section and therefore hard to measure directly. For that reason, finite element models could be efficiently used. However, the numerical approximation brings additional uncertainties in the form of finite element mesh density and initial imperfections. We have observed that smaller elements at the stress concentration areas result in larger strains at the same load levels, and therefore two more conditions have to be satisfied when FEM is employed:

(c) The finite element mesh of the structural detail has at least the same density as the mesh of the simulated coupon test. It is recommended that the same software is used for both numerical models with the same element types and calculation settings.

(d) The surface imperfections of the real coupon are smaller than the imperfections implemented in FEM model of the coupon. This ensures higher stress concentration in the model, and therefore more conservative results.

### 3. Parametric study

#### 3.1 Material models

Our goal was to use in the parametric study a stress-strain relationship which creates the largest possible plastic strains at the given elongation. Therefore, we used, conservatively, ideally plastic material in true stress-strain terms beyond the ultimate load. This assumption excludes metal softening for instance due to micro-voids or dynamic recrystallization [9], but is still valid for the commonly used steel grades and their structural applications. The simplified true stress-true plastic strain models are tri-linear with strain hardening up until the true uniform strain.

The studied range was 1.0 to 1.5 for the  $f_u/f_y$  ratio, and 2% to 50% for uniform strain  $\varepsilon_{it}$ . Four series of such parametrical studies were carried out with the yield strength 250, 500, 750 and 1000 MPa. We observed that the highest strains at fracture elongation  $A_5$  were always achieved in the series with  $f_y = 1000$  MPa. As high strains correspond to the most conservative case, results presented in this paper relate to this group of materials only.



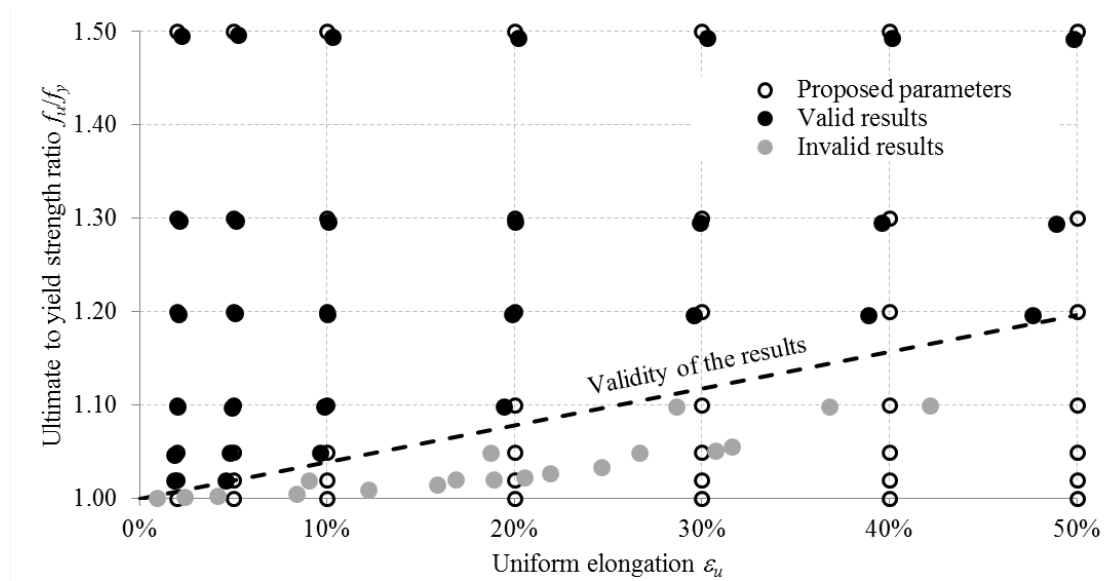


Fig. 3: Selection of material models based on proposed and calculated material parameters

The validity of the material models was verified by numerical simulation of the tensile tests with true stress-strain relation based on the selected range of material parameters  $f_u/f_y$  and  $\epsilon_u$ . It was observed that in materials with small  $f_u/f_y$  ratios and high  $\epsilon_u$ , the diffuse necking was initiated earlier than expected. Such materials were excluded from our calculations and the material models used in the parametric study are those, where the uniform elongation  $\epsilon_u$  is smaller than  $2.55(f_u/f_y - 1)$  as demonstrated on Fig. 3.

The numerical models were calibrated against real material tests of coupons and structural details as described in [5] with several additional steel grades. All of the experiments used in the present paper are summarized in Table 1.

Table 1 Measured material properties and ductility requirements of Eurocode 3 (EC3)

Material	$f_y$ (MPa)	$f_u$ (MPa)	$f_u/f_y$	$\epsilon_u$	A5	coupons tested	structural details tested	min $f_u/f_y$	EC3 min $\epsilon_u$	min A5
S275	300	418	1.39	18%	35%	1	-	1.15	2.1%	15%
S355(1)	393	550	1.40	13%	28%	1	-	1.15	2.8%	15%
S355(2)	396	473	1.19	18%	31%	2	5	1.15	2.8%	15%
S700	708	785	1.12	10%	20%	1	5	1.10	5.0%	10%
S960 <sup>1)</sup>	1062	1167	1.10	3%	9%	16	5	(1.10)	(7.6%)	(10%)

<sup>1)</sup> S960 is not in scope of current Eurocode 3

### 3.2 Structural details

The basic model selected for our study was tensile plate with 8x80 mm cross-section and central hole (CHT). For this detail we were able to validate finite element models against the real experiments with the hole diameter  $d$  from 8 mm to 40 mm [5]. Since the most critical strains were always related to the smallest diameter of the hole, we selected 8 mm for the entire parametric study (see Fig. 4).

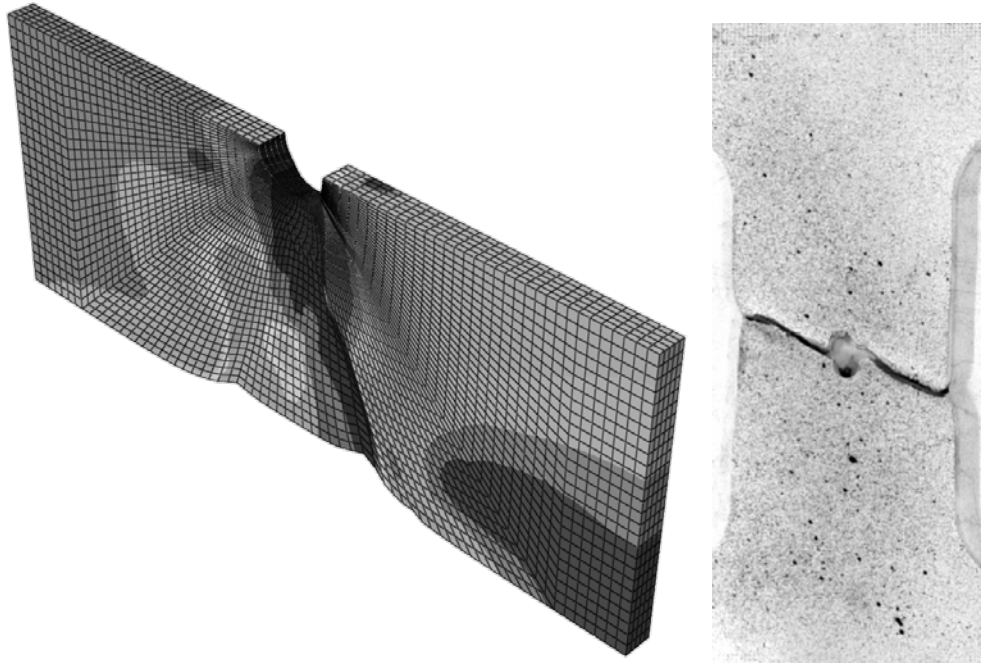


Fig. 4: Finite element model of CHT specimen and the real specimen [11]  
(von Mises stress distribution, S960 with 8 mm diameter of the hole)

Simple modification of our FEM models produced another common detail with stress concentration. Central hole was changed into circular side notch (SNT) of the same radius by applying symmetry boundary conditions to the opposite face than in CHT simulations. The results were added to the previously calculated CHT simulations.

### 3.3 Design criteria

The ultimate limit state resistance of cross-section reduced by holes or notches is related to the ultimate strength of material  $f_u$  and the area of net-section  $A_{net}$  in Eurocode 3. Therefore, our selected design criterion was that the cross-section has to resist the load equal to  $f_u A_{net}$ . On the other hand, if the elongation at the ultimate load is not considered, it would be possible that some of the materials would not fulfil minimum deformation requirements. For that reason, we have also studied elongation of details in tension. Since the Eurocode 3 does not explicitly state minimum allowable deformation, we have selected several levels of details' elongations on 100 mm gauge: 2 mm, 3 mm, 4 mm and 5 mm. The results from the extreme cases (2 mm and 5 mm) are presented herewith.

## 4. Results and discussion

The proposed requirement for minimum elongation at failure  $A_5$  of the coupon was obtained by the method described in Fig. 1 for 196 materials and 2 details. The results presented in this section are the envelope of the highest values interpolated between the calculation points. They are compared to real measured  $A_5$  values in four material tests with different steel grades. In most of the cases, the central hole in tension (CHT) was more critical than the side notch in tension (SNT). The results are further limited by the maximum yield strength 1000 MPa, the minimum diameter of the hole or notch  $d \geq 8$  mm, and  $\varepsilon_u \leq 2.55(f_u/f_y - 1)$  as described in the previous sections.

### 4.1 Ultimate load in the net-section

Some of the studied steel grades did not fulfil the material requirements given in Eurocode 3 (see Table 1). Nevertheless, all of the selected materials were able to reach the ultimate load  $f_u A_{net}$  in both geometrical configurations. This is also confirmed by experiments with CHT [5]. Therefore, we were always able to find such A5 that guarantees the corresponding level of equivalent plastic strain before ductile failure of the material. We would like to note that the design load according to Eurocode 3 is always more conservative because it is further reduced by several factors.

It can be observed that the results in Fig. 5 that all five tested materials have adequate elongation A5 to reach the desired ultimate load. E.g. S275 has available A5 elongation of 35% far exceeding the demand of  $\sim 25\%$ . The A5 limits form nearly vertical lines, and therefore are almost independent on the  $f_u/f_y$  ratio. Moreover, the values of minimum elongation at failure A5 differ from the uniform strain  $\epsilon_u$  by 0.3 to 5.7 percent. This indicates that the difference between A5 and  $\epsilon_u$  could be a suitable parameter to describe the new proposed ductility requirements. We call it the necking capacity of the material.

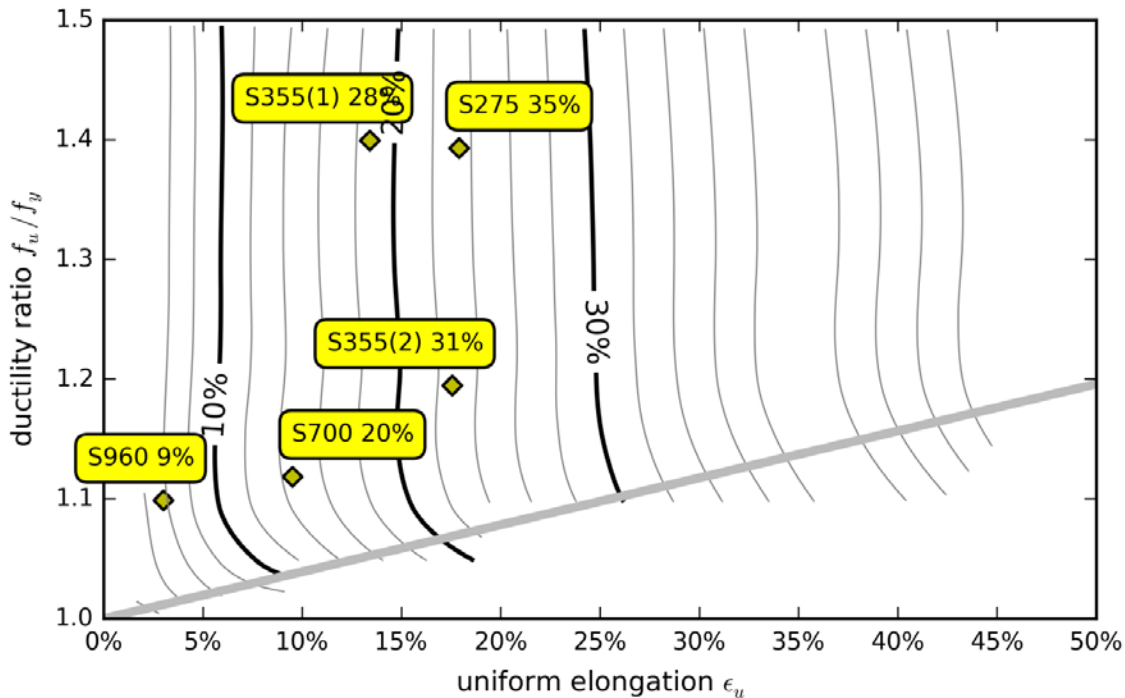


Fig. 5: Contour lines of minimum A5 to reach the ultimate load  $f_u A_{net}$  with measured values of A5 of five real materials in text boxes

#### 4.2 Elongation 2 to 5 mm measured on 100 mm gauge length

The same evaluation was performed using various deformation levels as the design criterion. Fig. 6 shows the results for the extreme case with 5 mm limit elongation measured on 100 mm gauge length. It can be observed that the measured coupon of S960 failed the 5 mm criterion on Fig. 6. All other materials fulfil the criteria from 2 mm to 5 mm elongation.

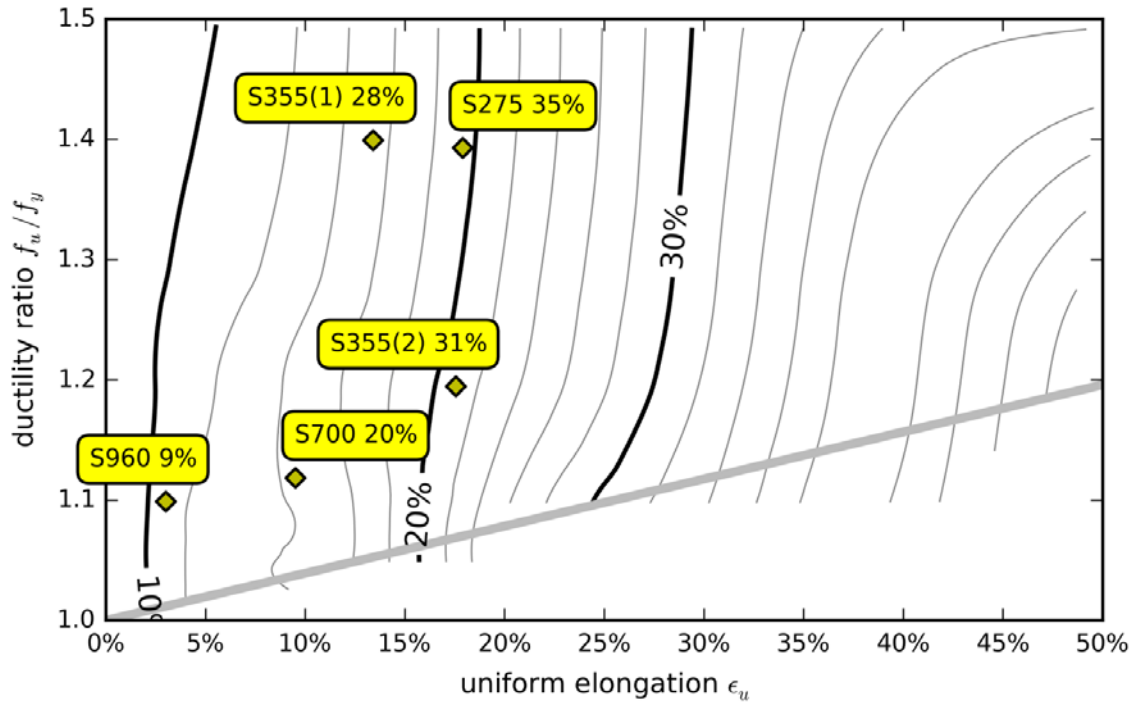


Fig. 6: Contour lines of minimum A5 to reach the elongation 5 mm

Table 2 shows the maximum difference between the required elongation at failure A5 and uniform elongation  $\epsilon_u$  that was observed for each of the design limits. Should those results be used in real design situation, the labour of finding the real deformation limit of the structural detail lays on the designer. Our intention is to investigate this problem further and propose a single requirement that would take implicitly the allowed deformation into account.

Table 2 Ductility requirements on CHT and SNT details

Allowed elongation on 100 mm gauge	Minimum necking capacity A5- $\epsilon_u$ required in coupon tests
2 mm	6%
3 mm	7%
4 mm	8%
5 mm	8%

## 5. Conclusions

The main conclusions are:

1. The ductility requirements prescribed in current Eurocode 3 in the form of minimum ultimate-to-yield strength ratio  $f_u/f_y$ , uniform elongation  $\epsilon_u$  and elongation at fracture seem to be questionable.
2. Based on our study, the ductility requirement to reach specific design load or deformation can also be expressed as a “necking capacity”, the difference between the elongation at coupon failure A5 and the uniform strain  $\epsilon_u$ .
3. The required necking capacity to reach ultimate load  $f_u A_{net}$  is 6% in the present study and the recommended levels of the necking capacity related to certain elongation are summarized in Table 2. Moreover, the required necking capacity seems to be almost independent on the  $f_u/f_y$

ratio. It should be noted that these values are only valid for selected CHT and SNT details (8x80 mm plate in tension with central hole or side notches diameter 8 mm).

4. The presented method may be used by designers to validate case-by-case the ability of particular material to reach specific design limits in a given detail.

5. The results can also be further generalized by calculating more structural details in different design situations. Then the necking capacity requirement may work as alternative limit to the existing ductility criteria.

### Acknowledgments

The research leading to these results has received funding from Finnish Metals and Engineering Competence Cluster's (FIMECC) program BSA - Breakthrough steels and applications (2014-2018) and its project Design beyond present codes – enabling efficient utilisation of new materials. We would like to thank Ruukki Construction Oy and SSAB Oy for the experimental test results of coupons and CHT specimens.

### References

- [1] EN 1993-1-1 Eurocode 3: Design of steel structures - Part 1-1: General rules and rules for buildings, European Committee for Standardisation, 2005.
- [2] EN 1993-1-12 Eurocode 3: Design of steel structures - Part 1-12: Supplementary rules for high-strength steels, European Committee for Standardisation, 2007.
- [3] EN 10002-1 Metallic materials - Tensile testing - Part 1: Methods of test at ambient temperature, European Committee for Standardisation, 2001.
- [4] EN ISO 6892-1 Metallic materials - Tensile testing - Part 1: Method of test at room temperature, European Committee for Standardisation, 2009.
- [5] Hradil P, Talja A. "True stress-strain relationship for finite element simulations of structural details", Proceedings of the 13th Nordic Steel Construction Conference (NSCC-2015), Tampere, Finland, 229-230, 2015.
- [6] Dunaud M. Ductile fracture at intermediate stress triaxialities: Experimental investigations and micro-mechanical modelling, Massachusetts Institute of Technology, 2013.
- [7] Hancock JW, Mackenzie AC. "On the mechanisms of ductile failure in high-strength steels subjected to multi-axial stress states", Journal of the Mechanics and Physics of Solids 31(1), 1-24, 1976.
- [8] Holland D, Halim A, Dahl W. "Influence of stress triaxiality upon ductile crack propagation", Steel Research, 61(10), 504-506, 1990.
- [9] Guo-Zheng Q. "Characterization for Dynamic Recrystallization Kinetics Based on Stress-Strain Curves" Recent Developments in the Study of Recrystallization (Ed.: P. Wilson), InTech, 2013.
- [10] EN 1993-1-3 Eurocode 3: Design of steel structures - Part 1-3: General rules - Supplementary rules for cold-formed members and sheeting, European Committee for Standardisation 2006.
- [11] Valkonen I. "20th European Conference on Fracture (ECF20): Ultimate limit loads in welded joints and in net sections of high strength steels with yield stress 960 MPa" Procedia Materials Science, 3, 720-725, 2014.